MICROMACHINED DISCRETE MASS RESONANT SENSORS

by

Steven Bruce Prescesky

B.A.Sc. (Honours), The University of British Columbia, 1989

A THESIS SUBMITTED IN PARTIAL FULFILLMENT OF
THE REQUIREMENTS FOR THE DEGREE OF
MASTER OF APPLIED SCIENCE

in the School
of
Engineering Science

SIMON FRASER UNIVERSITY

December 1992

Approval

Name: Steven Bruce Prescesky

Degree: Master of Applied Science

Title of Thesis: Micromachined Discrete Mass Resonant Sensors

Examining Committee: Dr. Shahram Payandeh, Chairperson

Dr. M Parameswaran
Senior Supervisor

Dr. John Dewey Jones
Supervisor

Dr. Andrew Rawicz
Examiner

Date Approved: December 15, 1992

PARTIAL COPYRIGHT LICENSE

I hereby grant to Simon Fraser University the right to lend my thesis, project or extended essay (the title of which is shown below) to users of the Simon Fraser University Library, and to make partial or single copies only for such users or in response to a request from the library of any other university, or other educational institution, on its own behalf or for one of its users. I further agree that permission for multiple copying of this work for scholarly purposes may be granted by me or the Dean of Graduate Studies. It is understood that copying or publication of this work for financial gain shall not be allowed without my written permission.

Title of Thesis/Project/Extended Essay

Micromachined Discrete Mass Resonante Sensors

Author: _____
(signature)

Steven B. Prescesky
(name)

Dec 15, 1992
(date)

Abstract

Micromachined resonant sensors detect the decrease in the resonant frequency of a micromachined structure with applied mass, force or pressure. Sensors employing micromachined resonators can be very small, very sensitive and provide versatile frequency output. This research uses a silicon dioxide structure for the novel application of measuring the mass of sub-nanogram discrete objects. The measurement of micron sized discrete particles opens various possibilities for biological research instruments.

Factors such as resonant characteristics, device mass, and ease of fabrication led to the choice of a silicon dioxide cantilever. Device configuration and dimensions were selected and modeled using finite element analysis. Cantilever structures were produced using thermally grown silicon dioxide on a <100> silicon wafer and in CMOS technology using CMOS compatible micromachining techniques. Prototype devices were resonated by external means and the resonance was detected optically.

Polystyrene spheres were used as calibration discrete masses. After individual spheres were loaded onto devices, the shifted resonant frequency was measured and compared to simulation results. First generation devices had a natural resonant frequency of 15.9 kHz and an experimental mass sensitivity of 1.9 kHz/ng. Results show the concept of sub-nanogram discrete mass measurement and the promise of increased sensitivity with refined device design.

to my beautiful wife Heather

Acknowledgements

I would like to thank my senior supervisor, Dr. Ash Parameswaran for his efforts in founding the Micromachining Group at Simon Fraser University, his ideas in this new microscopic realm, his enthusiasm and his belief in my abilities. My appreciation goes to members of the Micromachining Group especially those who have been an inspiration: Dr. Andrew Rawicz for his knowledge of vibration and engineering, Dr. John Jones for his clarifying perspective of finite analysis, and the wisdom of Dr. Marek Syrzycki. Thanks to Zi Wei Xie for his assistance with Quickchip.

I would also like to acknowledge the contribution of Dr. Robin Turner of the Biotechnology Laboratory of the University of British Columbia who together with Dr. Parameswaran first considered sub-nanogram discrete mass measurement. Thanks also to Dr. Turner for explaining microbiology to the uninitiated and to his group for preparing samples of cells on micromachined devices.

A special thanks to Shawn Brothers for work he performed in refining the experimental apparatus. Also, thanks to Jainming Chen for providing additional cantilever samples.

Table of Contents

LIST OF TABLES

LIST OF FIGURES

1. INTRODUCTION

> *"In addition, recent trends in the engineering literature indicate a growing interest in the use of silicon as a mechanical material with the ultimate goal of developing a broad range of inexpensive, batch-fabricated, high-performance sensors and transducers which are easily interfaced with the rapidly proliferating microprocessor."*
>
> - Kurt Petersen[1]

In 1982 Dr. Petersen predicted the importance of a new field now termed micromachining. Micromachining utilizes the single crystal silicon microchip as a platform on which to construct microscopic mechanical sensors and actuators which can be coupled with electronics either on the same or an adjacent chip. A complete sensor system can easily be designed using a single microchip.

The micromachining of mechanical devices employs many of the same process steps which are used to produce micron sized features in integrated circuits. Silicon and silicon dioxide are the fundamental materials used in integrated circuits and thus the primary candidates for micromachining. Both have very good mechanical properties[1] and single crystal silicon does not exhibit brittle properties because crystal dislocations are far apart on the micrometer scale. Thus it has been possible to produce microscopic replicas of mechanical structures typically built using steel in the macro domain of the civil engineer. Such static structures as cantilever beams, bridges, platforms [2], and actuators such as pumps [3], motors [4] and gear trains [5] have been produced.

Now more than just a curiosity, micromachined devices are finding commercial applications in sensors. Basic structures such as those listed above can be employed as part of the sensing transducer and can be used in sensing systems for a wide variety of mechanical, chemical and physical properties. A well developed system is the acceleration sensor [6]. A suspended platform is deformed due to applied acceleration force. The deflection is measured either by a change in capacitance between the platform and a fixed plate or by a change in resistance of piezoresistors placed directly

on the platform. Such sensors have considerable application due to their small size, low cost, accuracy and integrated signal processing circuitry.

Resonant sensors function by obtaining the shift in natural resonant frequency when mechanical measurands such as mass or pressure are added to the transducer. Typically the resonant frequency is measured both with and without the measurand and the shift is calibrated to the parameter of interest. One common sensor which employs these techniques is the quartz crystal microbalance (QCM). The QCM uses a quartz crystal oscillator operating at several MHz. When a mass, such as an evaporation deposited layer of metal, is deposited on the crystal surface the resonant frequency decreases. The resonant shift is correlated with the mass added to the crystal and knowing the density of the metal an estimate of the thickness of the layer can be made. Sensitivities of up to 10 ng/cm^2 have been reported [7].

The resonant sensing technique has been applied to micromachined devices as well[8]. Resonators have been employed in sensing systems for pressure [9] and deposited layer measurements [10]. Such micromachined devices measure a very small mass, but since the QCM also senses pressure or deposited layer mass over a larger surface area, the advantage of using the micromachined device over the QCM is limited. However, an extensive literature search suggests that up until now no one has used a micromachined resonator to measure discrete masses. The suitability of such microscopic devices for measuring minute objects is obvious. As the size of micromachined resonators can be reduced to tens of microns, the mass of a 1 ng object is comparable to the mass of the resonator itself. Large frequency shifts result from loading the object onto the micromachined resonator and high sensitivities can be obtained while operating at low frequency. This thesis will describe the development of a prototype mass sensor which can resolve better than 0.3 ng of mass in microscopic discrete objects.

1.1 Thesis Organization

This thesis discusses the design, fabrication, analysis and testing of the micromachined discrete mass resonant sensor. Chapter two describes the fundamental processes involved in constructing micromachined devices on a silicon wafer. Resonant sensor design parameters are investigated in chapter three. In chapter four, the experimental apparatus and testing procedures are presented. Chapter five provides testing and simulation results for several different device designs. Chapter six recommends possible design refinements. Chapter seven discusses possible applications of the discrete mass sensor and chapter eight summarizes conclusions reached in the thesis. Resonant mass sensor calculations, finite element analysis techniques and finite element analysis outputs are presented in appendices A, B and C respectively.

2. MICROMACHINING

The micromachining performed for this research used the anisotropic wet chemical etching technique. Mechanical structures were constructed of either silicon or silicon dioxide and were suspended above a cavity etched from the silicon substrate. The unique etching properties of anisotropic etchants are crucial to the formation of these microstructures.

2.1 Anisotropic Etching

Features such as pyramidal cavities with very smooth walls can be etched into single crystal silicon by anisotropic etching. Two anisotropic etchants that have been used in this work are Ethylene Diamine Pyrochatechol - water (EDPW), and Potassium Hydroxide (KOH) - water.

Anisotropic etchants perform preferential etching of crystalline material in the direction where the atomic packing density is the lowest. Single crystal silicon (Si) wafers have a diamond crystal structure, and the crystal plane with miller indices of <111> has the highest atomic density. This dense plane is etched at a much slower rate than any other plane. This work uses a standard silicon wafer of <100> orientation. The flat face of this wafer is a <100> crystal plane and the primary flat on the edge of the wafer corresponds to the <110> edge. This results in the <111> planes being parallel and perpendicular to the primary flat at an angle of 54.7° down from the wafer's surface.

In order to form a cavity, regions not to be etched must be masked. An effective mask for many anisotropic etchants is silicon dioxide (SiO_2). The SiO_2 is first grown on the surface of the Si with a thermal oxidation process. In order to etch a pyramidal pit, a rectangular region of SiO_2 is removed, leaving the underlying Si exposed. The anisotropic etchant attacks the exposed Si etching the <100> surface. The rectangular mask is aligned to the intersection of the <111> planes with the wafer surface. Etching proceeds until a region bounded by the oxide mask and its adjacent <111> planes is realized. Figure 2-1a shows an isometric view of such a pit. Once the etching has extended down to the bottom of the cavity so that all <111> planes meet,

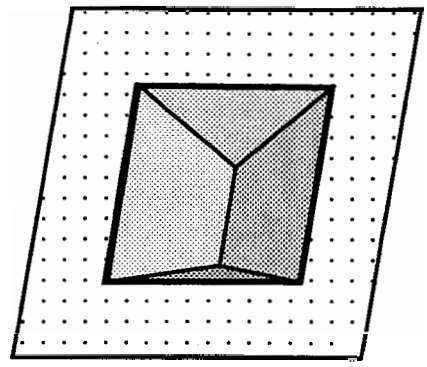

Figure 2-1a: Anisotropic Pit in <100> wafer

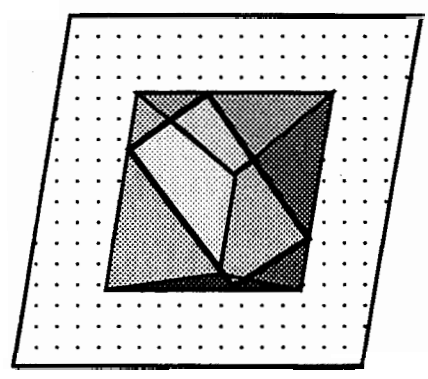

Figure 2-1b: Undercutting of misaligned mask

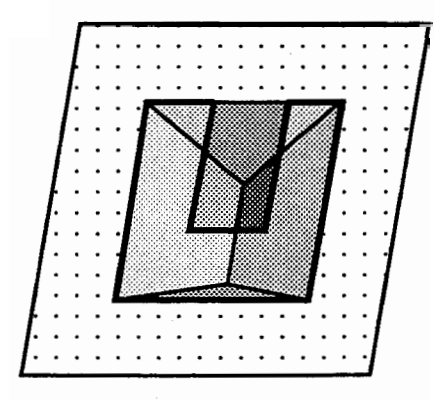

Figure 2-1c: Silicon dioxide suspended cantilever

Figure 2-1: Anisotropic Etching

the etchant will very slowly etch all <111> planes equally, undercutting the mask. Since the silicon wafer is monocrystalline and the etch is very anisotropic between crystal directions, the walls of the pit are mirror smooth.

Irregularly shaped masks may not be aligned to the <111> planes and thus undercutting will occur. Figure 2-1b shows a misaligned rectangular mask and the resulting pit. In can be seen that the pit is still pyramidal with surface dimensions equivalent to the greatest <111> area exposed by the mask. Figure 2-1c shows a suspended cantilever constructed of SiO_2 mask material. The SiO_2 cantilever is in effect an irregularly shaped portion of the mask which is undercut. The cantilever is freely suspended overhanging the pyramidal pit bounded by the <111> planes of the silicon substrate. Such a cantilever is an example of silicon dioxide micromachining where the desired device is part of the silicon dioxide layer used to mask the silicon substrate. Such micromachined SiO_2 devices are easily fabricated and yet are very strong making them suitable for many applications.

A second type of micromachining yields silicon devices which are bulk micromachined from the substrate material. The device depicted in figure 2-2 was produced by a shallow etch from the front followed by through etching from the back. Such bulk silicon devices require more process steps, are much more difficult to fabricate and are typically heavier and larger than micromachined SiO_2 devices. Bulk micromachined silicon devices offer the advantage of the stronger mechanical properties of single crystal silicon.

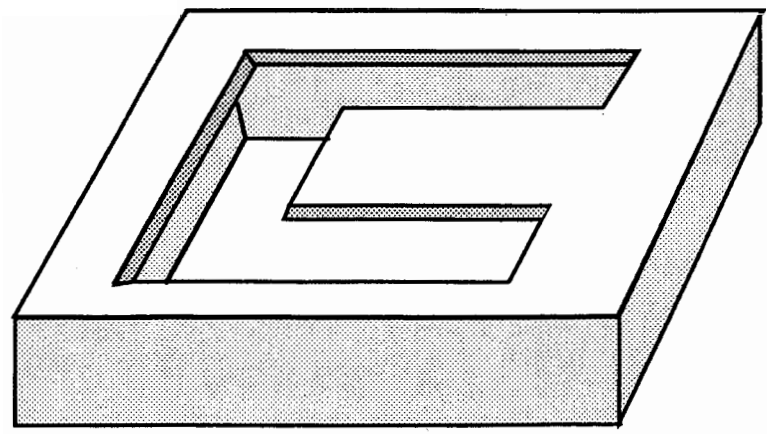

Figure 2-2: Silicon Bulk Micromachined Cantilever

The entire process necessary to produce an SiO_2 device is: wafer oxidation, photoresist application, soft baking of photoresist, patterning, developing photoresist, hard baking of the pattern, SiO_2 etch, stripping of photoresist, annealing of the oxide and an EDPW anisotropic etch to release the device. The key process step is the anisotropic etching of the Si to form the cavity above which the structure is suspended. All process steps except the final etch are found in the standard microelectronic fabrication process as described by Jaeger [11]. The following sections will briefly outline each fabrication process step.

2.2 Process Steps

2.2.1 Wafer Cleaning

The first step towards producing a micromachined structure was cleaning the silicon wafer in preparation for oxidation. The wafers were prepared with a standard cleaning process in order to remove contaminants from the surface allowing a more homogeneous oxide layer. The cleaning process consists of a basic bath, rinse in de ionized (DI) water, acidic bath and a further rinse. The cleaning is followed by degreasing in three solvents. Table 1 lists the process for the standard cleaning and degreasing procedure.

Table 1. Standard Cleaning & Degreasing Procedure

Process Step	Process	Time & Temp.
1	Immerse in Solution 1: 5:2:1 mix of DI H_20:H_20_2:NH_4OH	5 minutes @ 70-80°C
2	DI H_20 rinse	
3	Immerse in Solution 2: 5:2:1 mix of DI H_20:H_20_2:HCl	5 minutes @ 70-80°C
4	DI H_20 rinse	
5	Ultrasonic Agitate in: ClCH:CCl_2 (Trichloroethylene)	5 minutes
6	Ultrasonic Agitate in: $(CH_3)_2CO$ (Acetone)	5 minutes
7	Ultrasonic Agitate in: CH_3OH (Methanol)	5 minutes
8	DI H_20 rinse	

2.2.2 Oxidation

A layer of silicon dioxide (SiO_2) was grown on the surface of the <100> single crystal silicon wafer. This oxide serves as the structural material for silicon dioxide structures and as a mask for anisotropic etching of the silicon. Oxidization is performed by placing the wafers into an 1100°C furnace with

an oxygen and steam flow. The endothermic reaction:

$$Si + O_2 \Rightarrow SiO_2 \qquad (1)$$

occurs at high temperature resulting in a uniform layer of silicon dioxide covering the surface of the silicon.

The silicon dioxide layer is under compressive stress. Two oxygen atoms combine with the silicon atom and the newly formed silicon dioxide molecule must occupy more space than the silicon atom. The SiO_2 layer grows out from the original silicon surface and down into the silicon with a ratio of 54/46 respectively [11].

The cleaned and dried wafers were loaded onto a quartz furnace boat which supports them in an upright position. The furnace was heated to a stable 1100°C and a 1.9 l/s nitrogen flow was maintained. The boat was slowly inserted into the furnace, with the front surface of the wafers away from the flow, so that the wafers gradually increased in temperature. When the wafers had reached 1100°C, oxygen was pumped at a rate of 0.1 l/s through 95°C de ionized water and into the furnace inlet. The technique of adding steam to the oxygen is termed wet oxidation. After sufficient oxidation time, the oxygen flow was replaced with a neutral nitrogen flow of 1.9 l/s and the wafers were slowly removed. After sufficient cooling, the wafers were fully removed from the furnace, completing the oxidation process.

An oxide thickness of at least 1 μm was desired. Tables found in Jaeger [11] predict that a 3 hour wet oxidation will produce an oxide of 1.2 μm. Measurements of oxide thickness after 3 hours of wet oxidation using the lap and stain technique showed an actual oxide thickness of 1.0 ± 0.1 μm.

2.2.3 Patterning

The devices were patterned onto the surface of the silicon dioxide using photolithographic techniques. First, a layer of AZ 1312 SFD positive photoresist was coated on the oxide by spinning. The wafer was held in a vacuum chuck, and 15 ml of photoresist was pooled at the center. The wafer was spun at 4000 rpm for 30 seconds, resulting in an even layer of photoresist.

The photoresist was dried and semi-cured by soft baking at 90°C for 30 minutes.

The photoresist covered wafer was then selectively exposed to ultraviolet light. The photoresist is affected by the exposure and can then be removed by subsequent developing. The exposure method employed in this work was a prototype direct write laser lithography system. For this system, the desired patterns are designed in a CAD system and loaded into the direct write system. A HeCd laser was scanned and modulated across the wafer surface, selectively exposing the photoresist. The system has a resolution of 0.5 μm and can produce patterned regions of up to 4 x 4 cm.

The exposed wafer was developed in AZ 351 developer for 45 seconds and then rinsed in DI water. The developer removed the exposed photoresist leaving a photoresist mask layer where there was no exposure.

A coating of photoresist was spun onto the back of the wafer to protect the back from subsequent etching. The wafer was air dried and then cured in a hard bake oven at 110°C for 30 minutes.

2.2.4 Silicon Dioxide Etch

The photoresist serves as a mask for selective etching of the silicon dioxide layer to expose the silicon substrate. The oxide etchant is buffered hydrofluoric acid which is termed buffered oxide etchant (BOE). The wafer was floated in the BOE solution with the patterned side exposed to the etchant. The photoresist is hydrophobic and thus the coating on the back side of the wafer allowed it to float on the BOE. The BOE etches the silicon dioxide at a rate of approximately 6 μm/hour. A 15 minute etch was used to ensure clearing of the 1 μm oxide layer. The wafer was rinsed with DI water after etching. A rinse with acetone removed the photoresist layer and then a second DI water rinse and air dry are used.

Although the photoresist is not affected by BOE, the etchant undercuts the edges of the mask, rounding corners and reducing dimensions of the silicon dioxide structure. For a 15 minute etch, this undercutting was approximately 1 μm.

2.2.5 Annealing of Structures

After oxide etching, the silicon dioxide structures are resting on the silicon substrate. As mentioned previously, the silicon dioxide is under compressive stress. When the supporting silicon is etched, the structures tend to curl upward due to the larger stresses on the bottom surface of the oxide. A 200 μm cantilever was found to curl upward by approximately 12 μm at the tip. To minimize this curling, the oxide layer was annealed after oxide etching and before silicon etching. The wafer was placed in a furnace under nitrogen flow, heated to 1100°C, annealed for 30 minutes, and then cooled. The high temperature allows the SiO_2 to relax. Resulting 200 μm cantilevers curled upward by approximately 5 μm. After annealing, the wafer typically required a 15 second etch in BOE to remove the thin oxide layer formed over the exposed silicon during annealing.

2.2.6 EDPW Anisotropic Silicon Etch

The type of anisotropic etchant used was PSE-300 ethylene diamine pyrochatechol and water etchant (EDPW) produced by Transene Co. Inc.. 400 ml of EDPW was put into a 700 ml beaker under a fume hood. The freshly mixed solution is bright yellow and transparent. Figure 2-3 shows a diagram of the etching apparatus. A reflux is placed over the beaker with cold water circulating through it. The reflux condenses any vapour, maintaining the concentration of the solution and helping to contain toxic chemicals. The solution was slowly heated to 95°C with constant stirring using a Corning PC 351 heater/stirrer. The wafer was loaded into a quartz etching holder and immersed in the solution. The reflux was replaced, stirring was resumed and the temperature was maintained over the etching cycle.

As explained previously, the SiO_2 acts as a mask for the anisotropic etchant. The exposed silicon is etched in a two step oxidation reduction process [12]. First the silicon surface is oxidized:

$$Si + 2\,OH^- + 2\,H_2O \rightarrow SiO_2(OH)_2^{--} + 2H_2 \qquad (2)$$

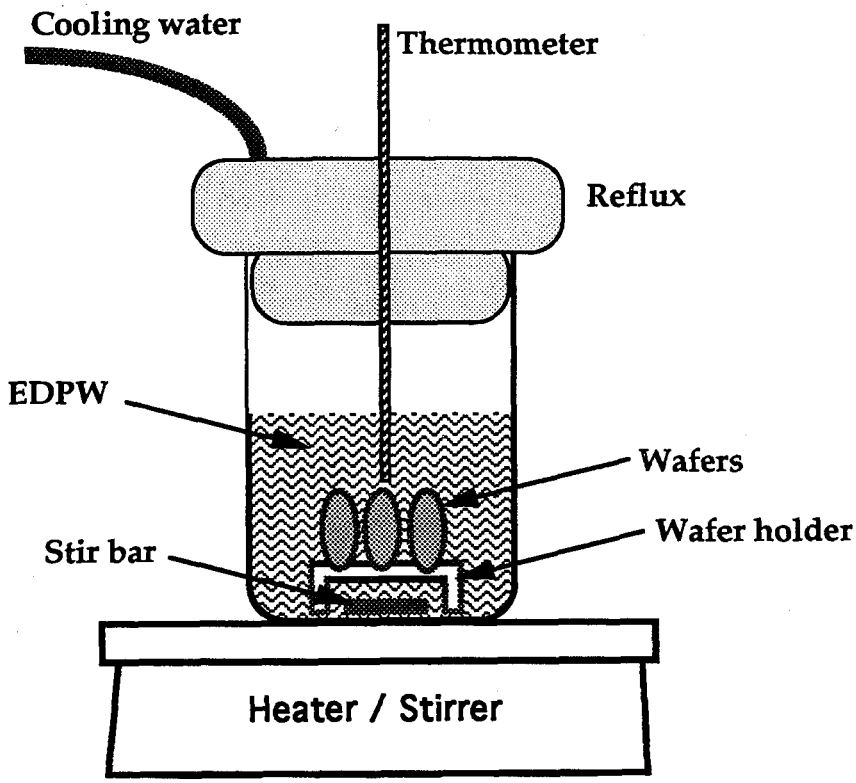

Figure 2-3: Etching Apparatus

Then the thin surface oxide is reduced:

$$Si(OH)_4 + 2\,OH^- + 3C_6H_4(OH)_2 \rightarrow Si(C_6H_4O_2)_3^{--} + 2H_2O \quad (3)$$

The product on the right side is soluble and is removed by the circulating etchant.

As mentioned previously, the etchant attacks planes which are loosely packed with atoms while the etching across the densely packed <111> plane is very small. Table 2 lists etching of the three most important planes <100>, <110>, and <111> as well as SiO_2 for fresh EDPW at several temperatures [12].

Table 2. Typical etching parameters for EDPW

Temperature	<100> etch rate [μm/hour]	<110> etch rate [μm/hour]	<111> etch rate [μm/hour]	SiO_2 etch rate [μm/hour]
70°C	12	18	0.2	0.0003
90°C	25	28	0.5	0.001
110°C	56	58	1.0	0.007

Potassium hydroxide (KOH) is another anisotropic etchant with slightly different properties. SiO_2 is etched at a significantly higher rate and thus a thicker oxide layer or another material such as silicon nitride must be used for a mask. Also the KOH etchant is more anisotropic, with the relative etch rate between <100> and <111> higher. This results in sharper defined pyramidal pits with smoother walls.

As the EDPW solution is used, it reacts with the air in the reflux and gradually changes color to a very dark brown. The etching rate for silicon also increases with time. Figure 2-4 shows etching depth as a function of time. This data was obtained by immersing small samples of silicon in freshly mixed 95°C EDPW solution and extracting them one at a time at 5 minute intervals. The etching depth was obtained using the focus adjustment of the Olympus BHMJL stereo microscope.

As the etchant removes the silicon surrounding the SiO_2 mask, the silicon underneath the convex corner of the mask is undercut. To fully release a 200 μm long cantilever, an etching depth of 100 μm was used. Figure 2-4 was used to select an etching time of 1.75 hours.

To avoid the formation of residues in the device cavity, the extracted wafer was immediately immersed in a heated water bath[12]. The wafer was then rinsed in DI water continuously for 5 minutes. Care was taken in the rinsing and drying procedure not to damage the SiO_2 structures. Devices were dried by rinsing with methanol and then placing them in a 90°C furnace to accelerate the evaporation of the methanol.

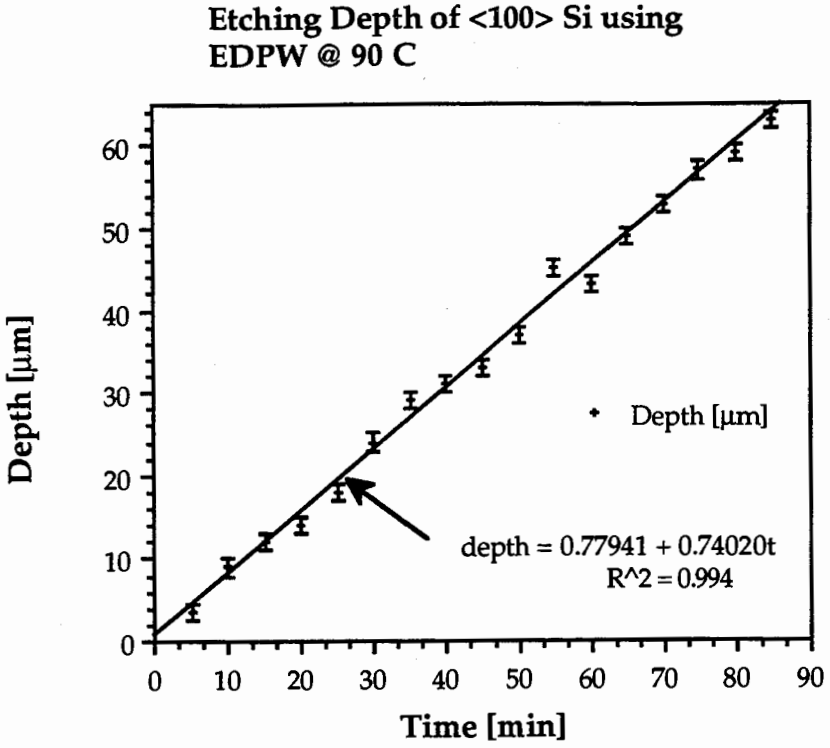

Figure 2-4: Experimental Etching Depth versus Time

2.3 CMOS Devices

Micromachined devices can be fabricated using integrated circuit (IC) chips produced using a commercial CMOS process. The micromachining of CMOS devices is termed CMOS compatible micromachining [13]. Such devices are composed of a sandwich of material layers available in the CMOS process. For the Canadian Microelectronics Corp. CMOS 3 process employed in this work, the sandwich layers from top to bottom consist of:

Passivation Silicon Dioxide
Second Aluminum Metal(optional)
Second CVD Silicon Dioxide
First Aluminum Metal (optional)
First CVD Silicon Dioxide
Polycrystalline Silicon (optional)
Field Silicon Dioxide
Substrate Silicon

The devices are primarily silicon dioxide similar to the ones described in the previous section. In addition, two aluminum layers and a polycrystalline silicon layer are available inside the sandwich. The metal layers are used in the CMOS for electrical connections. For micromachining the metal can perform other functions such as mirrored surfaces or capacitive plates. The polycrystalline silicon (poly) is a resistive layer which can be used for resistively heating devices.

Unconventional CMOS design rules are employed to expose the silicon substrate around the desired device. When designing the IC, a mask for each layer is designed. The silicon dioxide layers are masked out in the region around the mechanical device which will form the pit. As depicted in figure 2-5a, when the CMOS IC is fabricated the mechanical device rests on the silicon substrate and is surrounded by exposed substrate. The CMOS chips are then post processed using an EDPW anisotropic etching process as described in the previous section. This etching removes the exposed silicon and undercuts the structure as depicted in figure 2-5b.

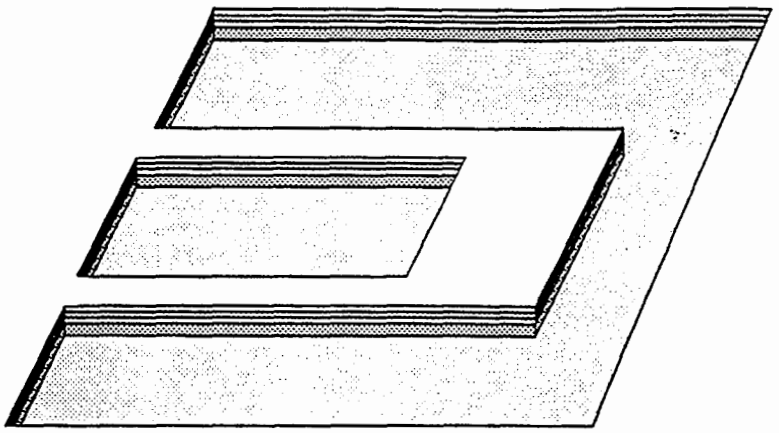

2-5a: CMOS Cantilever prior to Post Processing

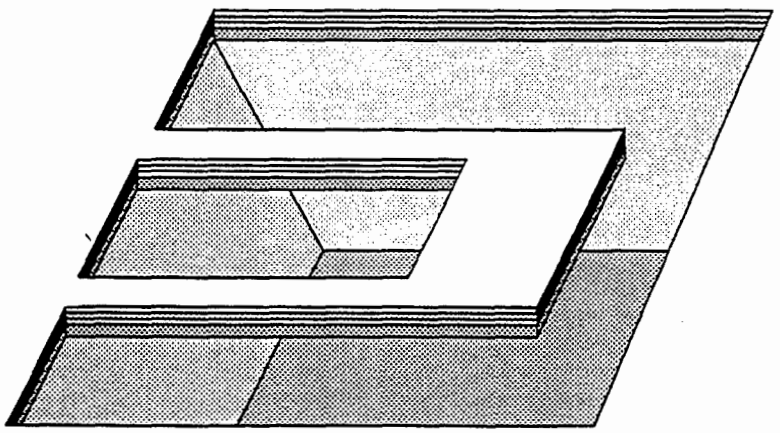

2-5b: CMOS Cantilever after EDPW Post Processing

Figure 2-5: CMOS Compatible Micromachining

3. RESONANT SENSOR DESIGN

Table 3 lists the primary design criteria of this discrete mass sensor. The high resolution and relatively large load capacity suggest the use of a resonant device.

Table 3. Mass Sensor Design Criteria

<<1.0 ng mass resolution
>2 ng mass loading capacity
repeatable device fabrication
feasible means of obtaining mass measurement from sensor

Resonant devices operate in the frequency domain. The measurand, in this case mass, affects the frequency of operation of the device. The resonant frequency can change over a large range and can be measured with great accuracy. This allows for a large ratio of load capacity to mass resolution.

Two resonant sensing schemes widely used for mass sensing are the quartz crystal microbalance (QCM) and the micromachined resonant device [10]. The QCM is a high frequency quartz oscillator whose resonant frequency is decreased by stress on the crystal due to surface force. The QCM has been used to measure film thickness and can detect distributed masses as small as 10 ng/cm^2 due to its 6 MHz oscillating frequency [7]. However, a relatively large surface area of the order of 10 mm^2 excludes its use in measuring sub-nanogram particles.

Micromachined resonant sensors have been used to measure the mass of distributed films and changes in film mass due to vapour interaction with distributed films [14]. Howe and Muller measured film thickness using a microbridge 180 μm long made from amorphous polysilicon. The bridge was actuated using electrostatic attraction and its resonant motion was detected by measuring the change in capacitance between the bridge and the substrate 2 μm below. The capacitance is detected by internal "on chip" circuitry.

The micromachined resonator approach lends itself to our design goal of accurately measuring micron sized particles as the size of a micromachined device is of the same order and its mass is in the nanogram range. Thus a micromachined device's resonant frequency will be significantly affected by a nanogram load. Micromachined devices are also surprisingly strong and are not excessively stressed by the large periodic forces of resonating with an added mass.

Micromachining also meets the third design goal of repeatable device fabrication. When all the fabrication process steps are controlled, very repeatable devices can be produced. As the EDPW etch does slowly etch the silicon dioxide structures, careful process control may be necessary to ensure repeatable devices from batch to batch. Experimental results provided in section 5.2.2 show that there is little variation in resonant characteristics within a single batch of devices.

To meet the fourth design goal, we must be able to determine the resonant frequency of the device and measure its shift when a mass is applied. There are two components required: actuation of the device and measurement of its resonant amplitude. The microbridge mentioned previously [14] shows that this goal can be met with the combination of electrostatic actuation and changes in capacitance between the device and substrate to indicate resonant amplitude. Other techniques for actuating and detecting will be discussed in sections 3.3 and 3.4.

The micromachined resonator approach meets the four primary design goals of this sensor application. To my knowledge, it is the only approach which has the immediate potential to meet all of these goals.

3.1 Frequency Shift due to Mass Loading

The resonant mass sensing approach relies on the fact that loading a device with added mass will reduce its resonant frequency by a predictable amount. The resonant frequency decreases to maintain energy equilibrium in the resonant system. The constant total energy is the sum of potential and kinetic energy at any instant. When the beam is fully deflected to assume the resonant mode shape, the potential energy due to strain energy in the beam is maximum and the kinetic energy is zero. When the beam moves through its rest position, the velocity and kinetic energy are maximum. At this instant the strain energy in the beam is zero and therefore so is the potential energy.

The resonant frequency of a uniform beam with an end load can be estimated using Rayleigh's method. This method equates the energy for the two states corresponding to maximum potential energy and maximum kinetic energy. When resonating, the beam is at maximum deflection where the kinetic energy is zero and the potential energy is [15]:

$$E_p = \frac{EI}{2}\int_0^L \left(\frac{d^2Y(x)}{dx^2}\right)^2 dx \qquad (4)$$

Where:
- $Y(x)$ is the maximum deflection profile
- L is the length of the beam
- I is the beam's moment of inertia
- E is the Young's modulus of the material

When the moving beam passes through its rest position, it has no potential energy and its kinetic energy is:

$$E_{k,beam} = \frac{S\rho\omega_n^2}{2g}\int_0^L Y^2(x)\,dx \qquad (5)$$

Where:
- S is the beam cross sectional area
- ρ is the density of the material
- ω_n is the natural frequency

The kinetic energy of the end mass is:

$$E_{k,mass} = \frac{M}{2}\omega_n^2 Y^2(L) \tag{6}$$

Where: M is the mass of the end load

Equating: $$E_p = E_{k,beam} + E_{k,mass} \tag{7}$$

Results in:

$$\omega_n^2 = \frac{EI\int_0^L \left(\frac{d^2Y(x)}{dx^2}\right)^2 dx}{\frac{S\rho}{g}\int_0^L Y^2(x)\,dx + MY^2(L)} \tag{8}$$

In order to solve equation (8), the deflection profile Y(x) must be estimated. If it assumed that the mass M does not affect resonant mode shape, the fundamental mode shape profile for an unloaded beam can be substituted. Proceeding under this assumption, Stokey [15] provides an approximate solution to equation (8):

$$\omega_n = \sqrt{\frac{3EI}{L^3}\left(\frac{1}{M + 0.23m}\right)} \tag{9}$$

Where: m is the mass of the beam
M is the mass of the end load

This result applies for the case of a simple clamped beam with an added tip mass. The resonant frequency decreases in proportion to the inverse square root of the sum of the added mass and a portion of the beam's mass.

For rigid structures the resonant mode shape is relatively insensitive to added mass. The potential energy of the deflected system, or the strain energy in the

fully deformed beam, is thus not a function of added mass. The maximum kinetic energy as the beam moves through the rest position is proportional to the masses of both the beam and the added mass. The kinetic energy is also proportional to the beam velocity squared which is a function of resonant frequency. Since potential energy is not a function of added mass, the resonant frequency shifts to reduce maximum kinetic energy and thus maintain constant energy.

The formula for the resonant frequency of a cantilever with added mass required the resonant mode shape to be known. For complicated device configurations the mode shape cannot be determined analytically. In this case finite element analysis must be employed to determine the resonant mode shape and resonant frequency. Finite element analysis is a mathematical method for solving problems with complicated geometries and boundary conditions by segmenting the domain into many finite portions and performing a solution which links them all together. This technique was used in section 5.2.1 to estimate various resonant parameters of an experimental device. A more complete explanation of finite element analysis is found in Appendix B.

3.2 Key Design Parameters

This section discusses important design parameters of discrete mass sensors based upon the micromachined resonator approach. The four most important mechanical parameters of a resonant device used for mass sensing are: resonant Q factor, resonant frequency, mass of the device, and resonant mode shape.

3.2.1 Resonant Q factor

As shown in figure 3-1, the resonant Q factor is defined as:

$$Q = \frac{f_n}{f_2 - f_1} = \frac{1}{2\xi} \tag{10}$$

Where: ξ is the damping factor

Q is a dimensionless parameter representing the ratio of the resonant frequency to the frequency width at half power or 70.7% of the maximum amplitude. The Q factor is a measure of the sharpness of the resonant response.

The Q factor is the most important parameter for resonant devices. This is because a smaller shift in resonant frequency can be resolved when the resonant frequency curve is very sharp. We can define an arbitrary criterion for resolution of two curves analogous to Rayleigh's criterion for optical resolution [17]. This criterion is that the peak of the first curve is not closer than the half power point of the second. Figure 3-1 also shows two resolved curves. Using this criterion, the resolution of a resonant system is:

$$R = \frac{f_{res}}{2Q} \text{ [hz]} \tag{11}$$

The Q factor is related to the damping of the system. Increased damping reduces the Q, making resonances less sharp and resonant amplitudes smaller for a given actuation. When the Q is reduced to 0.5, the device is said to be critically damped [16] and the device will not oscillate or resonate. The two

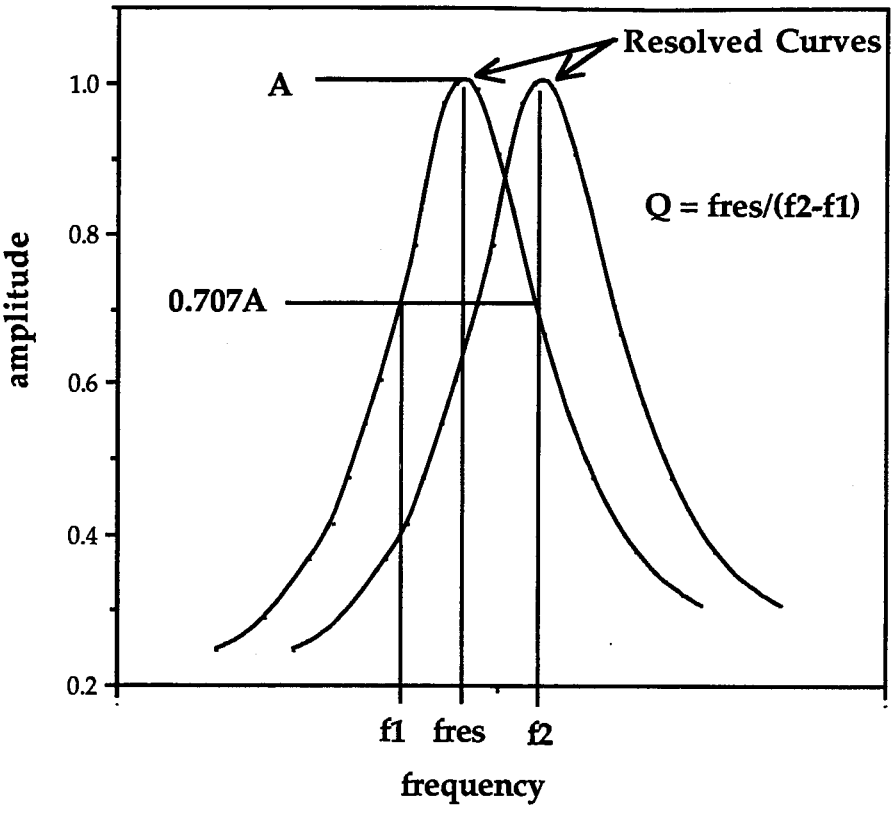

Figure 3-1: Q of a Resonant Curve

primary types of damping contributing to the Q factor are structural and viscous. The structural and viscous damping factors are additive.

Structural damping is the dissipation of energy when materials are cyclically stressed. Structural damping is a result of material parameters and device configuration. Structural damping is independent of frequency and proportional to the square of the amplitude of vibration. For a resonant system, structural damping can be minimized by selecting a device configuration so that the device is flexible. For torsional resonance, the torsional member should be made relatively thin. For angular resonance, the flexing member should be thin and any supports which resist this flexing motion should be minimized or eliminated.

Drag between a moving body and its surrounding fluid causes viscous damping. Increased viscosity of the fluid corresponds to more drag and therefore more viscous damping. If the fluid is very viscous and the device produces significant drag, resonance cannot be achieved. Viscous damping can be minimized by operating in inviscid fluids such as air or eliminated by operating in a vacuum.

For many discrete mass measurement applications, operation in a viscous fluid will be required. The viscous damping can be reduced by reducing the drag produced by the body. Drag can be reduced by reducing the frontal area pushed through the fluid. Drag can also be reduced by minimizing the drag coefficient through switching to a more aerodynamic shape. Blevins [18] has derived the value of the viscous damping produced by an oscillating cylinder

in a still fluid to be:

$$\zeta_{visc} = \frac{\pi \rho_{fluid} D^2}{2 \quad m_t} \sqrt{\left(\frac{\nu}{\pi f D^2}\right)} \tag{12}$$

Where:

$$m_t = \frac{\text{mass of cylinder \& displaced water}}{\text{length}}$$

$$= (\rho_{cyl} + \rho_{fluid}) \frac{\pi D^2}{4}$$

ρ_{fluid} is the density of the fluid

ν is the kinematic viscosity of the fluid

D is the diameter of the cylinder

ρ_{cyl} is the density of the cylinder

f is the oscillating frequency

This equation can be used to estimate the viscous damping factor for a cantilever of width D resonating in water with a frequency f. This will give a excessive estimate of the damping because the drag produced by a cylinder is less than that of a plate oriented perpendicular to the flow. Using equation (12) for a silicon dioxide cylinder of 50 μm in diameter oscillating at 15 kHz:

D $= 50\ \mu m$

f $= 15\ kHz$

ρ_{cyl} $= 2.5\ g/cm^3$

ρ_{fluid} $= 1.0\ g/cm^3$

ν $= 1\ mm^2/s$

results in a viscous damping factor of 0.053. The viscous damping factor for a flat cantilever will be higher than this value. Using equation (10) this corresponds to an in fluid Q factor of < 9.5 for a cantilever with no structural damping.

3.2.2 Resonant Frequency

The resonant frequency affects both the sensitivity of the device and the ease of actuation and detection. Devices with lower resonant frequencies can be actuated and detected more simply. At lower frequencies, vibrational amplitudes tend to be larger, making detection an easier task. However, increasing resonant frequency may increase the sensitivity of the device as the Q factor is increased.

The optimal resonant frequency is thus the highest Q resonance which is feasible. A feasible resonance is one at which the device can still be actuated and its resonance detected.

3.2.3 Mass of the Device

The mass of the device affects the frequency shift for a given test mass. The larger the device mass, the less the effect of loading with a small test mass. However, lighter, thinner structures are more fragile and are susceptible to damage, especially when being immersed or removed from liquid.

During manufacture of test devices produced for this research, silicon dioxide cantilever devices were observed to bend due to surface tension of evaporating water. As the rinse water evaporated, the tips of the cantilevers were pulled down by the water's surface. As the last of the water evaporated, the cantilevers were bending through approximately 45 degrees and their tips were touching the bottom of the cavity. Cantilevers with lighter, thinner support arms typically remained in this position while more robust devices would spring back to the horizontal position. This effect was assumed to be a combination of yielding of the cantilever and binding between tip and the bottom of the cavity.

In summary, the device mass must be minimized, subject to meeting performance criteria. The device must still resonate at the desired frequency, incorporate any structural features desired and be robust enough to withstand forces generated during fabrication and operation.

3.2.4 Resonant Mode Shape

When the device is resonating, the amplitude of oscillation varies across the structure. The resonant mode shape is the profile of the distorted device at the instant of maximum overall amplitude.

Different types of resonance include angular, linear, and torsional motion. Similar to a vibrating string, there are also different modes of resonance. The resonance with the lowest frequency is termed the fundamental and the subsequent ones of the same type are the first harmonic and second harmonic and so forth. The harmonics are at higher frequencies and have different mode shapes. A cantilever device can exhibit both angular motion and torsional motion resonance. As shown in figure 3-2a, the fundamental mode shape has the tip of the cantilever oscillating up and down like a diving board as the device flexes. Figure 3-2b shows a cantilever in first angular harmonic resonance. The 1st angular harmonic mode shape is an "S". Note that there is a resonant node, or location that does not oscillate, along the cantilever. Figure 3-2c shows a cantilever in first torsional harmonic resonance. This torsional mode has a node running along the length of the cantilever along its centerline.

The optimum device design utilizes a resonance with both high Q and a large resonant amplitude. The high Q allows very small shifts in resonant frequency to be determined and the large amplitude simplifies detection.

The test mass should be located at the maximum resonant amplitude region of the device. This is the region where the small test mass will most largely affect the resonant frequency of the more massive device. If the test mass is located over a resonant node, it will not affect resonant frequency. Linear motion resonance, where the whole surface oscillates with the same amplitude, is desirable because altering the location of the test mass changes the resonant shift negligibly.

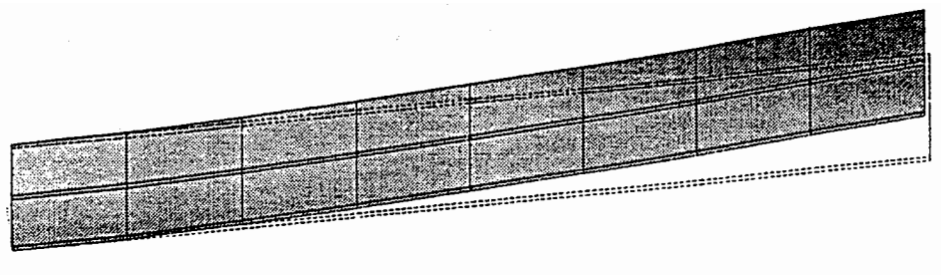

Figure 3-2a: Fundamental Mode Shape

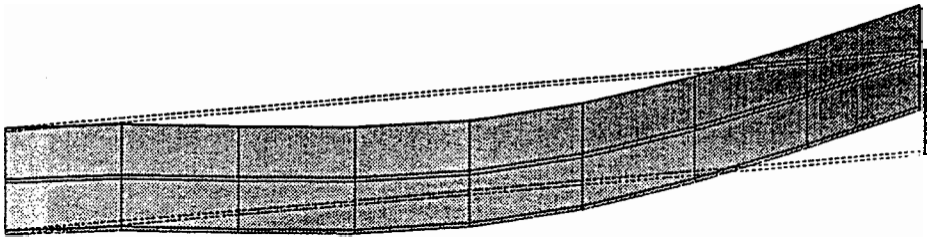

Figure 3-2b: 1st Angular Harmonic Mode Shape

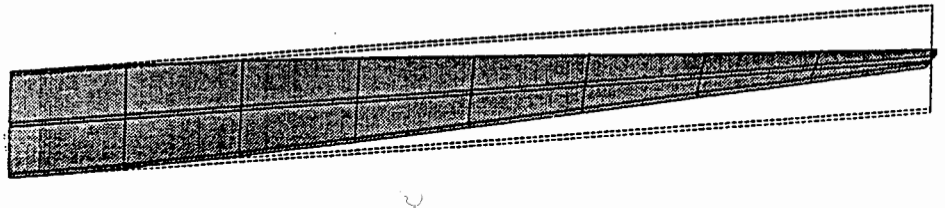

Figure 3-2c: 1st Torsional Harmonic Mode Shape

Figure 3-2 Resonant Mode Shapes

The resonant mode shape is also important for device detection. Mode shapes with large linear or angular amplitudes are easier to detect. As will be explained in section 3.4, angular motion resonance is particularly easy to detect using optical means.

3.3 Actuation Methods

The mechanically resonant structure must be actuated in order to excite a resonant response. A periodic energy source with a tunable forcing frequency is used to scan through frequencies near the device resonance. As the device nears resonance this small periodic force excites a relatively large amplitude response from the device.

Actuation methods can be grouped under the categories internal or external. Internal actuation is an actuation method which can be performed "on chip" utilizing support circuitry surrounding the device. External actuation employs components external to the micromachined chip which interact with the device.

3.3.1 External Actuation

External actuation methods allow the use of a simple device without any "on chip" electronics. Such an actuation method allows for quick testing of new device concepts. An example of external actuation is to oscillate the entire chip with small amplitude on a vibration table. This small amplitude base vibration of the cantilever will excite a resonance if the vibration frequency is similar to the resonant frequency of the device. Away from resonance, the entire cantilever will oscillate with small amplitude in unison with the substrate.

For resonant devices, the amplitude of sinusoidal base vibration required to excite resonance is small with respect to the resonant amplitude of the tip of the cantilever. If the base vibration amplitude varies with frequency the resonant response characteristic will not be accurate. An accurate characteristic requires that the vibration table maintain a constant acceleration over the entire frequency range.

3.3.2 Internal Actuation

Internal actuation methods offer the distinct advantage of small size, eliminated external components and a higher level of device integration. Two possible means of internal actuation are thermal and electrostatic actuation. Thermal heating of a CMOS cantilever device causes it to bend

upwards [19]. This bending is due to differential expansion of individual layers in the microstructure. The device which is connected to the relatively large silicon heat sink, cools rapidly and flattens out when heating is removed. CMOS devices can be resistively heated using the polysilicon layer and a current source. A pulsed current causes the cantilever's temperature and thus the whole cantilever to oscillate. When the heating frequency matches the cantilever's resonant frequency the cantilever will oscillate with large amplitude. Thermal actuation of a silicon dioxide cantilever at frequencies as high as 470 kHz has been reported [20].

Electrostatic actuation uses electrostatic force produced between two plates to move the device. A voltage V between two plates produces an electrostatic force:

$$F_e = \frac{\varepsilon A V^2}{2d^2} \qquad (13)$$

where:
- E is the gap's dielectric coefficient
- A is the area of the conducting plates
- d is the distance between plates

To produce sufficient force to actuate the device the square of the distance d must be kept small as compared to the plate area A. Electrostatic actuation is not compatible with standard CMOS as it is not possible to produce a conductive plate beneath the freestanding oxide structure.

3.4 Detection Methods

Methods to detect the amplitude of vibration of the cantilever include optical, capacitive, piezoresistive, and acoustic. Detection methods may also be classified as internal or external.

Optical detection involves reflecting a focused laser beam from the device and detecting the movement of the reflected beam. An effective detector for a moving beam is a quadrant photodiode. The quadrant photodiode consists of 4 separate photodiodes on a single substrate. The detector is centered in the optical beam so that the diode current is equal for all photodiodes. As the beam moves into one quadrant, that photodiode produces more current and the opposing one less. By calculating the portion of the beam falling upon each quadrant, the movement of the centroid is calculated. Such a system involves external components including the laser source and quadrant detector. This system requires that the source be aligned and precisely focused onto the test device. Devices with angular resonant modes work best with this type of optical detection because the reflected beam receives an oscillating angular shift. When placed at a distance, the quadrant detector sees this angular shift as a large positional shift. Linearly resonant devices would impart a small lateral shift in the beam corresponding to the resonant amplitude of the device. A small lateral shift in the beam is not easily detected using the quadrant detector.

It may be possible to employ integrated optics to produce an internal optical detection system, thus eliminating alignment. It is possible to build optical waveguide on a CMOS chip [21]. An integrated optical waveguide could be routed onto the cantilever and a pickup waveguide placed in close proximity to the end of the cantilever. As the resonating cantilever passes through the horizontal position, light would be coupled into the pickup waveguide. Optical fibers would be coupled to the two waveguides with one connected to the laser source and the second to a photodetector. The modulated output at the detector would indicate oscillation of the device.

Changes in capacitance between conducting plates on the moving structure and the substrate have been used for resonant sensor applications [14] as well

as accelerometers [22]. Due to the minute capacitances produced, the plates must be in very close proximity. On chip signal processing is required to reduce stray capacitance and gain an accurate measurement.

Changes in piezoresistivity may be usable for resonant detection. Piezoresistors placed at high strain areas of the device will periodically change their resistance due to the strain induced by flexing. Successfully employed in silicon accelerometers [23], this method is preferred over capacitive techniques for commercial applications. No references of high frequency piezoresistive pickup were found.

Sensitive acoustic microphones have been employed to measure audio emission from resonant micromachined structures at resonant frequencies of 10.4 kHz [20]. External microphones were employed at close range to maximize the signal to noise. There is significant effort to produce micromachined microphones [24], so the possibility of integrated acoustic pickup exists.

3.5 Actuation and Detection Methods Selected

The prime objective of this research was to show the concept of discrete sub-nanogram mass measurement using resonant micromachined structures. After preliminary experiments with silicon structures outlined in section 5.1, external actuation and detection methods were selected for use with silicon dioxide structures described in section 5.2. External means were advantageous because they allowed simple microstructures thus allowing quick fabrication of test devices using only in house processes. The entire chip was actuated on a vibration table and the motion of the device was monitored using the quadrant photodiode optical approach. As outlined previously, other methods offer distinct advantages but require additional process steps or CMOS micromachining techniques. The use of external actuation and detection allowed the fabrication of large batches of devices completely in house with a short manufacturing time.

3.6 Mass Positioning

For measurement, discrete masses of a diameter of 10 μm and less must be placed individually on the payload section of the device. Possible methods of locating such small masses include using micromanipulators, random placement and screened placement.

A micromanipulator which allows micron level movement in three dimensions can be used to move and place individual objects. Electrostatic force between the manipulator tip and the object proved sufficient to secure objects such as polystyrene spheres up to 20 μm in diameter. When such objects were drawn across the surface of a silicon dioxide device, the electrostatic force between the device and object was sufficient to remove the object from the manipulator. This force also proved sufficient to secure the object to the device during resonant testing with amplitudes in excess of 5 μm. This method of placement allows accurate positioning of the test object but is quite tedious.

Objects in a liquid suspension can be randomly placed over an array of cantilevers by allowing them to settle out of the suspension. Control over placement of the individual objects is purely statistical and the seeding density can only be coarsely controlled globally. One problem with this random technique is that it is probable that many devices will be loaded with more than one test object. As well, placement of the object on the device will be random.

A screened process would place a micromachined grid over the array of cantilevers as depicted in figure 3-3. The grid would interlock with the cantilever array and orient itself. The grid would have openings large enough for one object to fall through onto the center of the payload section of the device. The cantilever array and grid assembly would be placed into a suspension similar to the random process described above. After a sufficient time for objects to settle out of suspension, the assembly would be removed, excess test objects removed with compressed air and the grid removed.

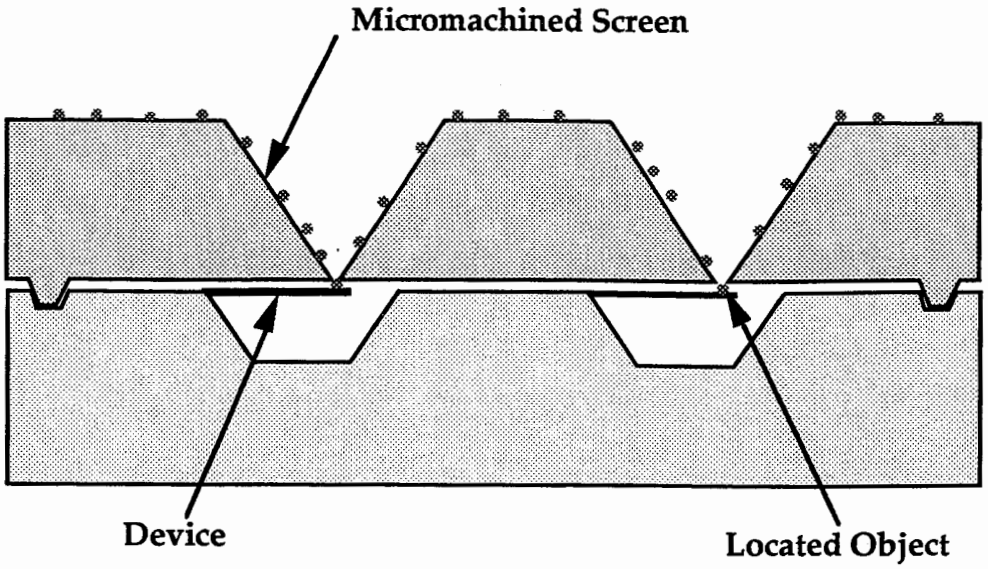

Figure 3-3: Screened Mass Placement Concept

4. EXPERIMENTAL APPARATUS

4.1 Experimental Setup

Figure 4-1 shows the experimental setup employed for external actuation and detection of silicon dioxide resonant microstructures. The setup can be broken into systems for actuating and detecting.

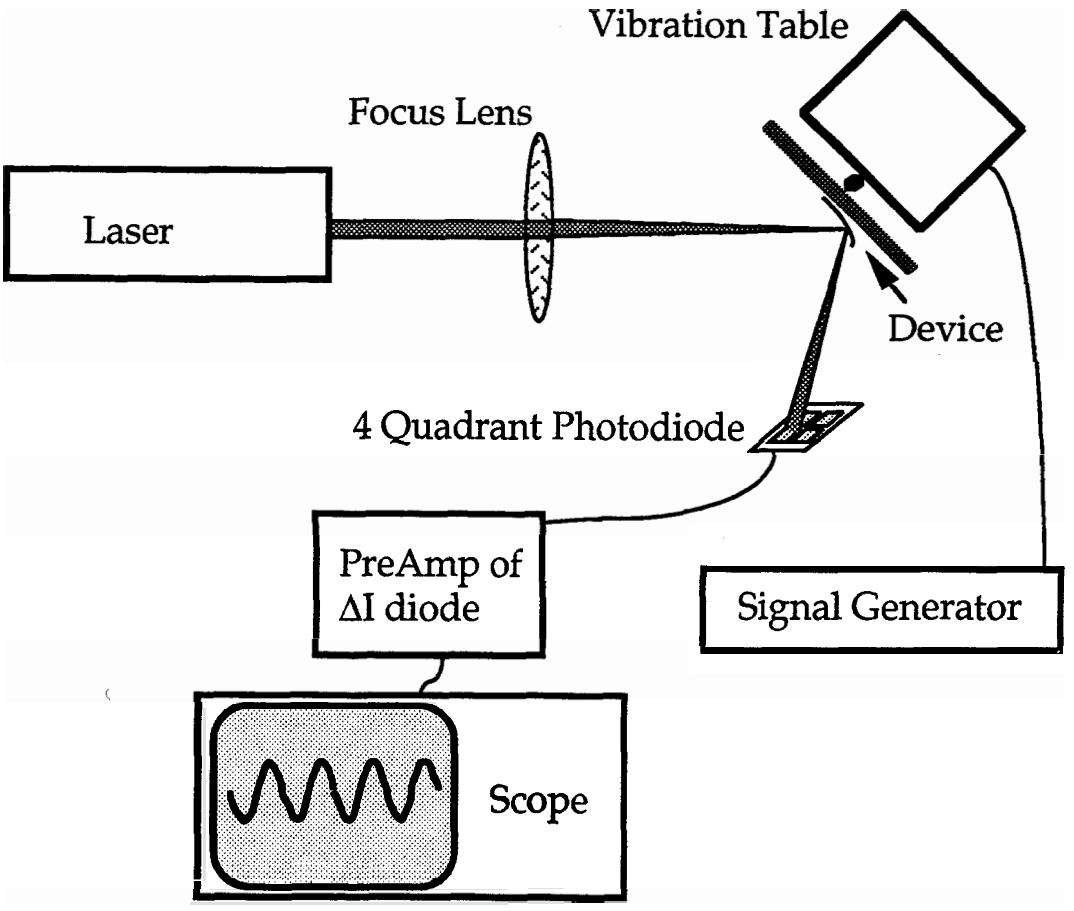

Figure 4-1: Apparatus Diagram

4.2 Actuating System

The actuation system consisted of a Wavetek model 145 function generator, MEI PA7220 audio amplifier and Global Specialties MAX-100A frequency counter to supply a sinusoidal actuating signal of known frequency. This

signal was fed to a Brüel & Kjaer model 4810 mini-shaker table. A 3/8" 10-32 setscrew was mounted onto the table and acted as a mounting post for the silicon substrate. The ~1 cm^2 substrate was rigidly connected to the setscrew by hard wax. The wax was applied by heating the setscrew, melting wax onto the tip and then positioning the substrate onto the liquid wax.

The shaker table was bolted to an aluminum fixture so that the actuation is in the horizontal plane. The microstructures were oriented so that their angular resonant movement was also in the horizontal plane. This maintains the optical detection plane horizontal as well.

The 4810 shaker has a working frequency range of DC to 18 kHz. In this frequency range, a fixed amplitude input signal produces a constant acceleration of the table and test device. As the frequency increases, the table's amplitude decreases as the acceleration is maintained constant. Above 18 kHz, there are one or more armature resonances of unspecified frequency. Such resonances would provide a larger forcing acceleration and thus, away from device resonance, would result in a larger linear amplitude of the substrate and possibly lead to erroneous results above 18 kHz.

4.3 Detection System

External detection of the resonant amplitude of individual devices was achieved by sensing of the deflection of a laser beam focused onto the surface of the device. As the device resonated in an angular motion, the reflected beam traversed an angle. The beam traversed periodically, and its energy was collected by alternate quadrants of a quadrant photodetector. The amplitude of the beam's angular traversal, and thus the device's resonance, was calculated. Section 4.3.1 analyses the optical principles employed in this system and section 4.3.2 discusses the quadrant detector and associated circuitry.

4.3.1 Optical Analysis

The laser source used was a Metrologic ML268 visible diode laser and collimating lens with power supply in a single package. This laser emits 1.0 mW at a wavelength of 670 nm. The laser is roughly collimated into a 1mm x 3mm beam with the integrated collimating lens. The laser was mounted on a Newport Research Corp. base attached to a Newport Research Corp. 12"x24"x1/2" aluminum optical breadboard. All other components including the fixture for the shaker table were rigidly attached to the same breadboard.

The laser beam was reflected by a beam steering mirror into a plano-convex focusing lens of focal length 30 mm. This lens focused the beam onto the plate portion of an individual cantilever. The dimensions of this plate were 50 μm x 50 μm. The minimum spot radius that can be achieved is governed by the diffraction limit [25]:

$$R_{min} = 1.22 \frac{f\lambda}{d_{beam}} \qquad (14)$$

For: $f = 30$ mm

$\lambda = 670$ nm

$d_{beam} = 1$ mm

The minimum achievable spot radius is:

$$R_{min} = 24.5\ \mu m$$

The diameter of the spot used is the smaller dimension of the rectangular beam. Equation (15) shows that a smaller incident spot is focused to larger radius. The observed spot illuminated the entire 50 μm x 50 μm square detection area of the cantilever as well as a portion of the 150 μm support arms. This larger experimental spot size is due to the focusing lens not performing to the diffraction limit.

As outlined in section 4.1, the cantilever device was mounted so that its angular degree of freedom is in the plane of the incident optical beam. The device was oriented so that the substrate is at an angle of approximately 45 degrees to the incident beam. The focused beam hit the 50 μm square silicon dioxide plate of the device. The transparent silicon dioxide first surface reflected a portion of the beam through approximately 90 degrees and the remainder passed through the device into the underlying cavity. The light entering the cavity reflected from the polished walls and exited the cavity in several directions including towards the detector.

After reflecting from the device and substrate, the reflected beam defocuses and its radius increases:

$$R(l) = \frac{d_{beam} l}{f} \qquad (15)$$

Where: d_{beam} is the incident beam diameter
l is the distance from the device
f is the lens focal length

In order to correctly align the quadrant detector, the reflection from the device must be discerned from the substrate and cavity reflections. This can be accomplished by identifying the Fraunhofer, diffraction pattern produced by the square plate on the device in the far field optical pattern of the reflected, defocused beam.

The 50 μm plate can be thought of as a square aperture for the beam. Portions of the beam outside of this area do not hit the device and are thus not reflected by it. Hecht [25] derives the intensity distribution far field Fraunhofer pattern due to a square aperture as:

$$I(Y,Z) = I(0)\left(\frac{\sin\ \alpha'}{\alpha'}\right)\left(\frac{\sin\ \beta'}{\beta'}\right) \tag{16}$$

with:

$$\alpha' = \frac{ka}{2}\sin(\theta_1) \tag{17}$$

$$\beta' = \frac{kb}{2}\sin(\theta_2) \tag{18}$$

Where:

I(0)	is the intensity along the optic axis
a	is the width of the aperture
b	is the height of the aperture
k	is the wave number of the light
θ1	is the horizontal angle between the optic axis and far field point
θ2	is the vertical angle between the optic axis and far field point

Figure 4-2 depicts the Fraunhofer pattern from a square aperture. This pattern was seen in the far field of reflections from the cantilever device and substrate. The plate section on the cantilever acted as a 50 μm square aperture to the incident laser beam. Other reflections are from larger planar surfaces and appeared as large diffused spots. In order to sense angular displacements of the cantilever, the square aperture Fraunhofer pattern was centered on the quadrant detector.

4.3.2 Quadrant Detector

The Silicon Detector Corp. SD 085-23-21-021 four quadrant detector was used to sense the position of the reflected beam. The detector consists of four 0.55 mm^2 photodiodes set in a 2x2 square pattern. The photodiodes are on the same substrate and are separated by a gap of 10 μm. The unit is enclosed in a

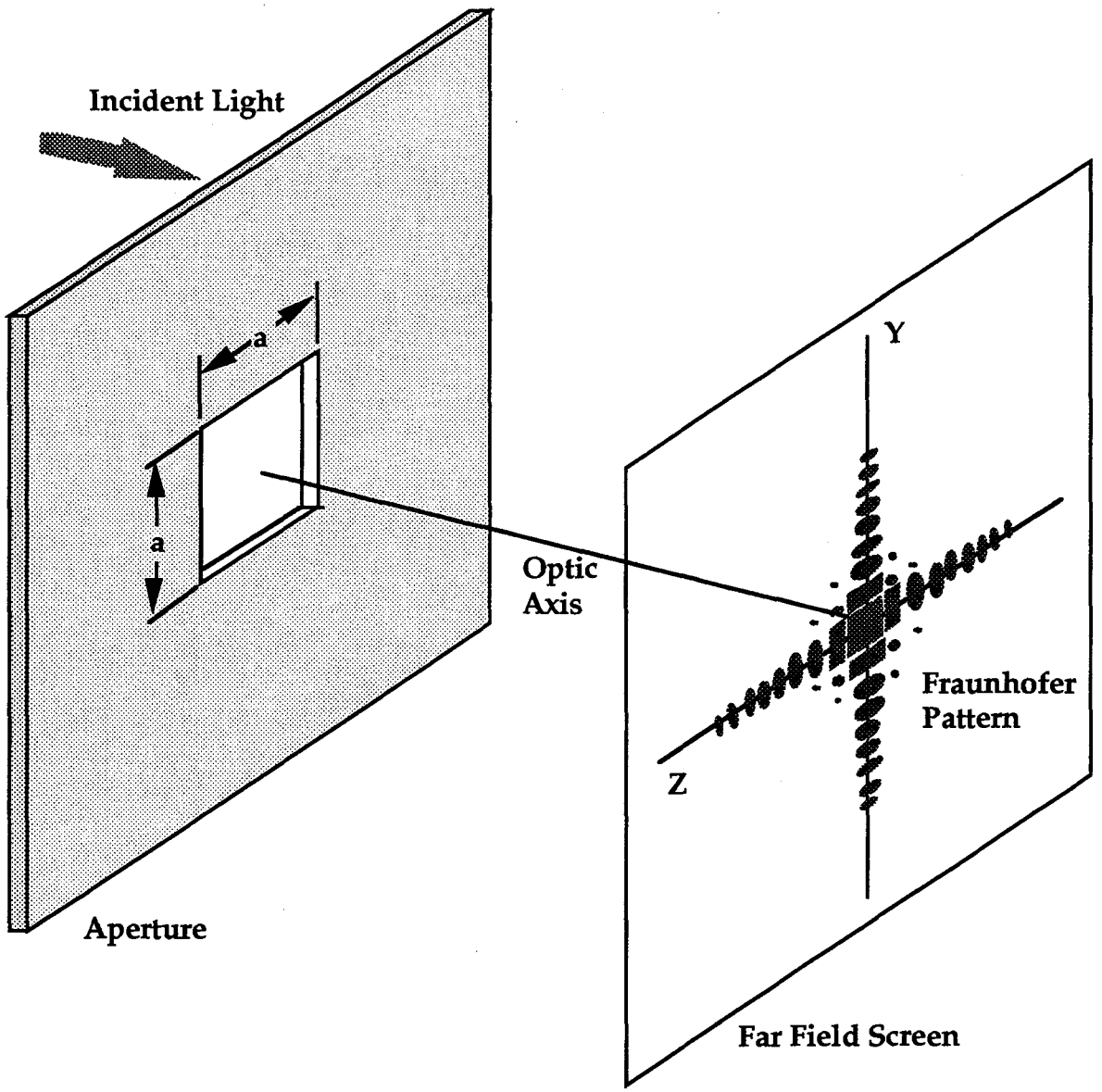

Figure 4-2: Fraunhofer pattern due to Square Aperture

TO-5 package with a glass cover window. The package has five pins, one for each diode and a common ground. Each photodiode produces a current of 0.35 amperes per watt of light at a wavelength of 633 nm.

This application requires the one dimensional sensing of the traversing beam. The four quadrant detector has the ability to sense motion of the beam in two dimensions. Only two of the four quadrants were used in sensing the lateral position of the beam. With adaptation to the amplification circuit, the

detection system can be made to sense the XY position of a beam reflected from a device with two dimensional angular movement.

The amplification circuit used with the two quadrant detector is shown in figure 4-3. An LM 324 four operational amplifier package was used along with discrete components. To reduce noise, the circuit was enclosed in a metal box so that the quadrant detector is protruding and was powered by a 12 volt battery with a 5 volt voltage regulator. The circuit amplifies each photodiode current with a pre-amplifier. The outputs from each pre-amplifier are put into a summer and a divider section. The summing output is a voltage proportional to the sum of the two photodiode currents. The dividing output is a voltage proportional to the difference between the two diode currents.

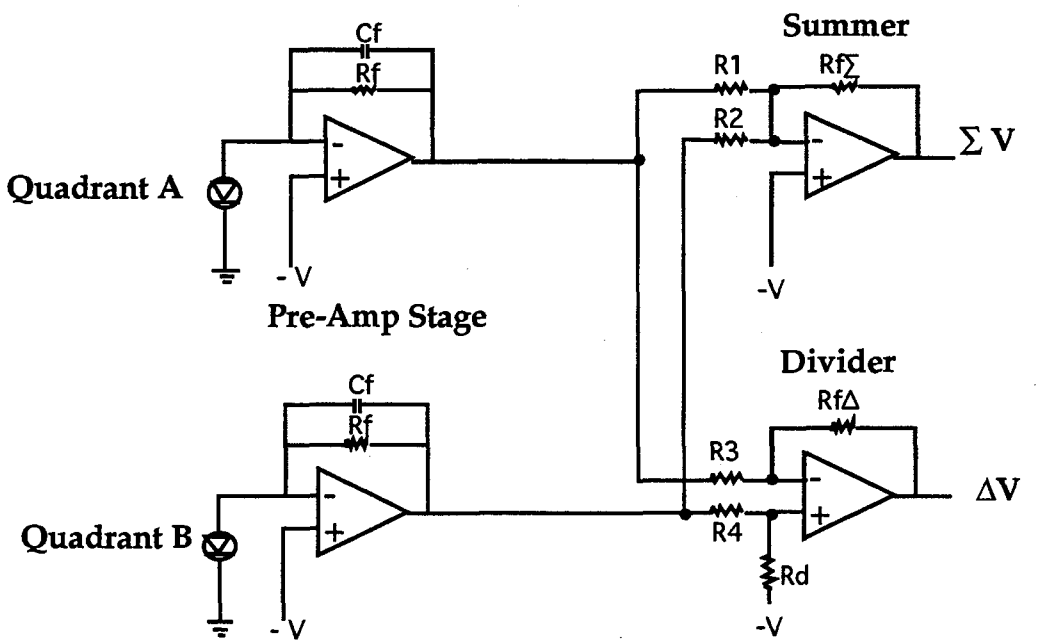

Figure 4-3: Two Quadrant Amplification Circuit

The summing and dividing signals were passed to a Tektronix 2232 digital storage oscilloscope. The oscilloscope was used to obtain the traces of the summing and dividing outputs, measure their amplitudes and verify the frequency of oscillation.

4.4 Optical Alignment

Coarse alignment of the focused laser beam onto the cantilever device was performed by observing the device through a 210x stereo microscope while adjusting the beam position using the beam steering mirror. After this alignment, the Fraunhofer pattern was observed on a white screen placed 50 mm from the device. A fine alignment of the beam was performed by maximizing the observed intensity of this pattern using the beam steering mirror.

The quadrant detector is placed in the path of the reflected beam at a distance of 50 mm from the device. Equation (16) can be used to estimate the size of the Fraunhofer pattern at this distance. Simplifying equation (16), the distance Y between the optic axis and the n^{th} subsidiary maximum of the Fraunhofer diffraction pattern is [25]:

$$Y = n\frac{\lambda d}{a} \tag{19}$$

Where
- d = distance between the device and detector plane = 50 mm
- λ = 670 nm
- a = device dimension = 50 μm

Table 4. Locations of Diffraction Maxima at the Detector Plane

n	Y
0	0 mm
1	0.67 mm
2	1.34 mm
3	2.01 mm
4	2.68 mm
10	6.76 mm

The radial distances to the subsidiary maxima of the diffraction pattern are

given in table 4. The Fraunhofer pattern is thus large enough for use in aligning the quadrant detector.

The quadrant detector and amplification circuit were mounted on a miniature XY stage which allows the quadrant detector to be centered onto the diffraction pattern. Coarse alignment of the quadrant detector was performed by observing the position of the pattern while moving the quadrant detector. Final alignment of the detector was performed by jointly maximizing the summing signal while zeroing the dividing signal. After the quadrant detector was aligned it was periodically adjusted to remove the DC offset of the dividing signal.

4.5 Data Analysis Procedure

The actuating frequency was scanned in increments of approximately 100 Hz in the region of interest. For each frequency setting, the peak to peak voltage of the dividing signal was obtained from the oscilloscope. The oscilloscope was used in digital mode with 8 sample averaging to filter noise. The DC voltage of the summing signal was recorded using the same digital oscilloscope capture. As the frequency neared the device's resonance, the sinusoidal amplitude of the dividing signal increased dramatically. The amplitude of the summing signal was relatively constant. Further increases in frequency resulted in decreased amplitude of the dividing signal while the summing signal remained relatively constant.

The resonant frequency of the device was estimated as the frequency which maximized the ratio dividing signal to summing signal:

$$f_{res} = f\left(MAX\left(\frac{V_{div}}{V_{sum}}\right)\right) \tag{20}$$

This corresponds to the frequency which resulted in the largest angular amplitude of the reflected optical beam.

The angular amplitude of the device resonance was estimated by calculating the linear amplitude of the reflected beam at the detector. This calculation assumes the beam to have a circular profile with uniform density. Figure 4-4 shows a circular beam incident on a two quadrant detector. The beam is shifted to the right by x. The illuminated area of quadrant 1 and 2 that is illuminated is A_1 and A_2 respectively. The total illuminated area A is a circle of radius R_{det}. R_{det} is given by equation (15) and corresponds to the beam radius at the detector plane.

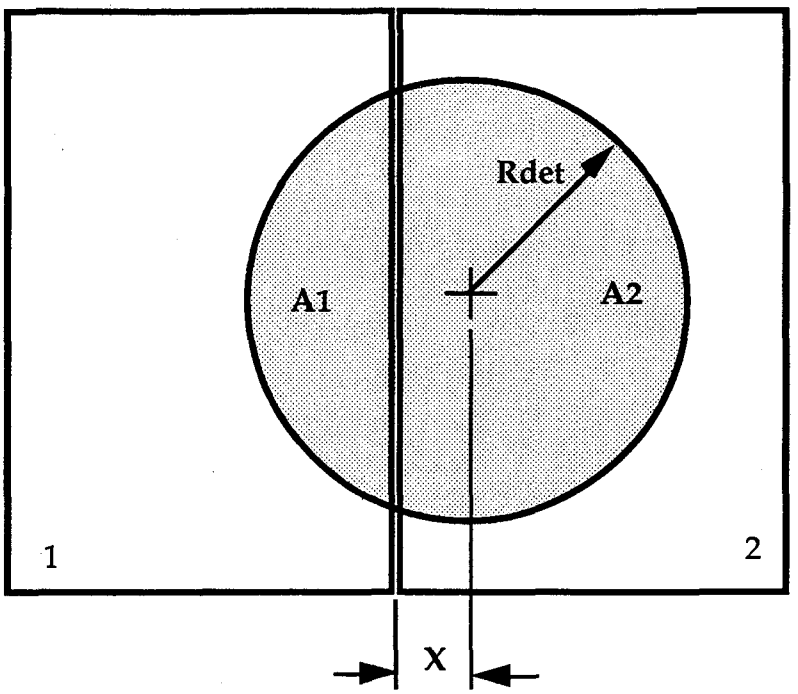

Figure 4-4: Two Quadrant Detector with incident beam

The summing and dividing signals are related to the area as follows:

$$V_{sum} = k\,(A) = k(A_1+A_2) \tag{21}$$

$$V_{div} = k\,(A) = k(A_2-A_1) \tag{22}$$

Where k is a constant proportional to the circuit gain and detector efficiency

The areas A and A_1 can be expressed:

$$A = \pi(R_{det})^2 \tag{23}$$

$$A_1=\frac{1}{2}R_{det}^2\left(2\,\text{acos}\left(\frac{x}{R_{det}}\right) - \sin\left(2\,\text{acos}\left(\frac{x}{R_{det}}\right)\right)\right) \tag{24}$$

An expression for x as a function of the summing and dividing signals and the beam radius is obtained by combining equations (21) through (24) and

simplifying:

$$1 - \frac{1}{\pi}\left(2\,\mathrm{acos}\left(\frac{x}{R_{det}}\right) - \sin\left(2\,\mathrm{acos}\left(\frac{x}{R_{det}}\right)\right)\right) = \frac{V_{div}}{V_{sum}} \qquad (25)$$

Figure 4-5 shows the relationship between x and the full angular amplitude of the device ϕ.

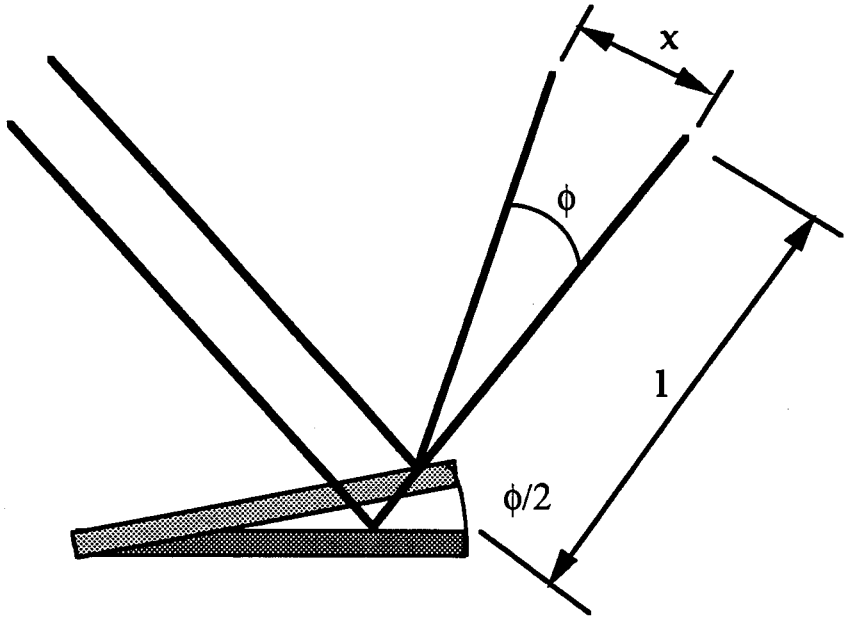

Figure 4-5: Relationship between x and ϕ

For small ϕ, the relationship is:

$$\phi \cong \frac{x}{l} \qquad (26)$$

Thus the full angular amplitude of the device can be found as a function:

$$\phi = \phi\left(\frac{V_{div}}{V_{sum}}, R_{det}, l\right) \qquad (27)$$

This technique was employed in finding the angular amplitude of the device for the amplitude frequency characteristic.

5. DEVICES AND RESULTS

5.1 Bulk Micromachined Silicon Platform

Due to silicon's excellent mechanical properties [1], it was selected for the first attempt of a resonant sensor. The concept was to construct a thin silicon platform with flexible support so that the platform could be actuated [26]. The actuation method chosen was electrostatic attraction between the platform and an adjacent electrode. Devices were bulk micromachined from <100> silicon. A 28 μm thick cantilever platform was fabricated, consisting of a 1000 μm x 1000 μm platform connected to a 1000 μm x 225 μm beam. Figures 5-1 and 5-2 are photo micrographs of the front and back surfaces of the cantilever platform device.

This type of bulk micromachining involves anisotropic etching from both sides of the wafer. This process differs from the process used for silicon dioxide structures outlined in section 2.2 in that the silicon dioxide acts as a mask to protect the silicon device which will be formed beneath the oxide.

Figure 5-3 shows the process steps employed in producing a bulk micromachined silicon device. First, the device was patterned on the front surface of a square piece of <100> single side polished wafer using the process as outlined in section 2.2. Care was taken to align the pattern square to the wafer and the distance between the start of the pattern and the corner of the wafer was noted. The silicon dioxide was etched to selectively expose the substrate silicon. The device was anisotropically etched 60 μm down using an 85°C EDPW solution. Corner compensation was employed to the convex corners of the plate. This compensation followed the methods outlined by Wu and Ko [27] and allows sharp convex corners to be realized after anisotropic etching.

After front surface etching, the front and side walls of the silicon device are fully defined. Etching through from the back surface of the wafer defines the back surface of the device and the device thickness. To protect the exposed silicon on the front surface from further etching, the wafer was cleaned and reoxidized in an 1100°C wet oxidation for 2 hours. After this oxidation the back surface of the device was patterned with 3mm x 3mm square openings

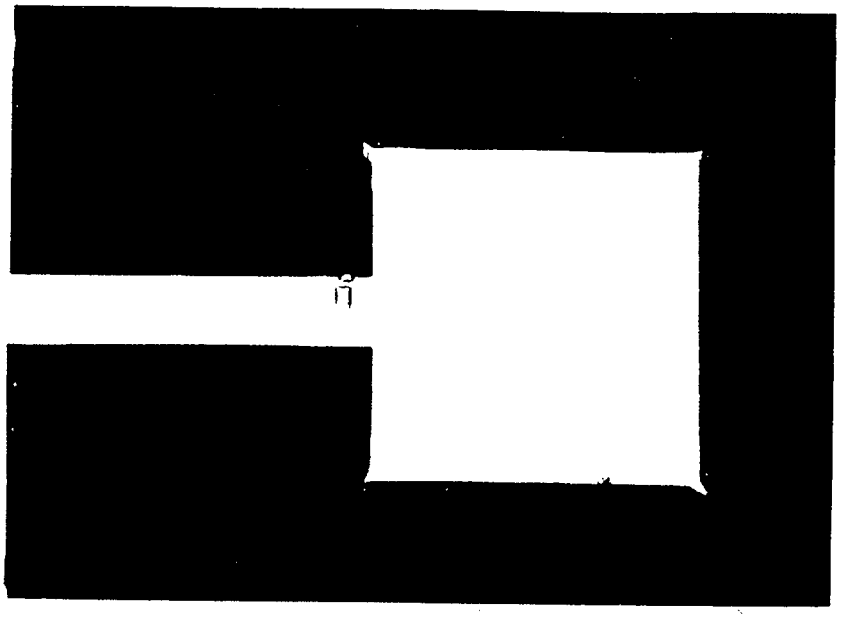

Figure 5-1: Photo Micrograph of Front Surface of Silicon Cantilever

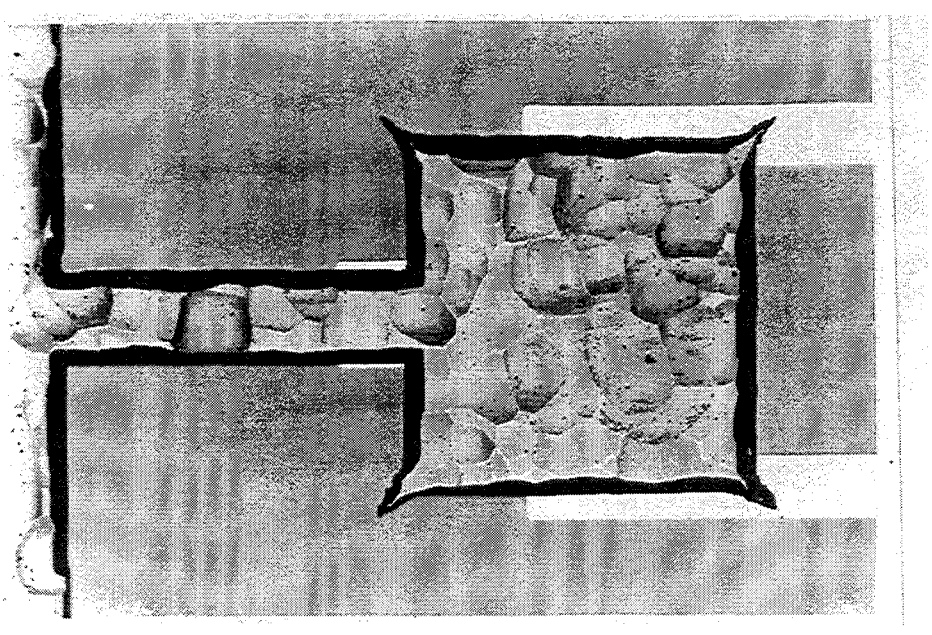

Figure 5-2: Photo Micrograph of Back Surface of Silicon Cantilever

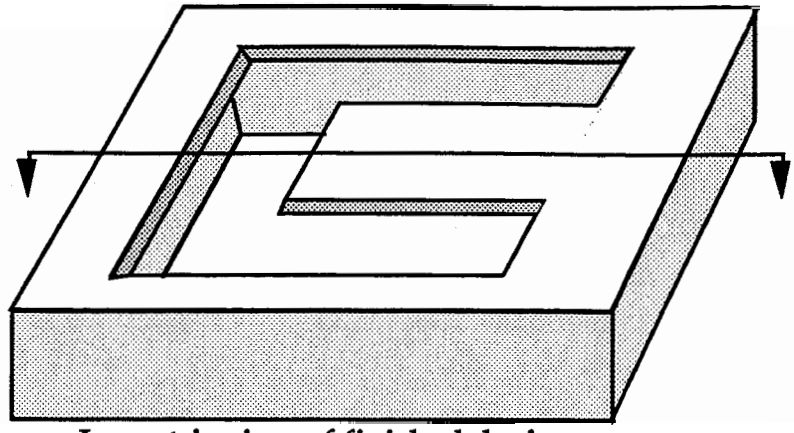

Isometric view of finished device

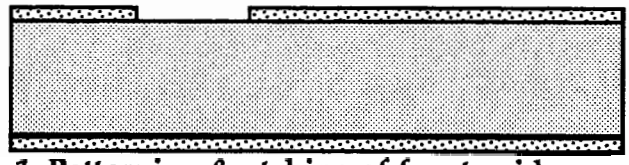

1. Patterning & etching of front oxide

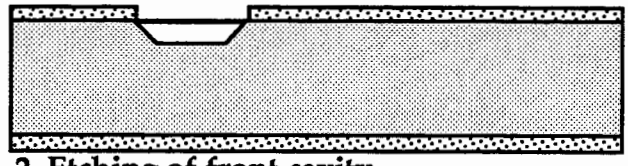

2. Etching of front cavity

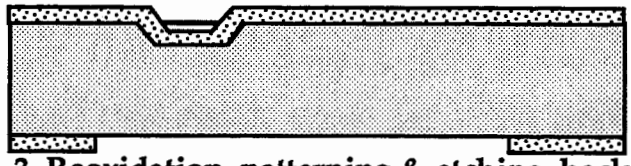

3. Reoxidation, patterning & etching back side

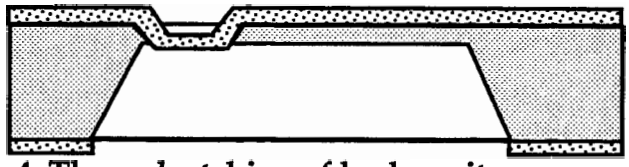

4. Through etching of back cavity

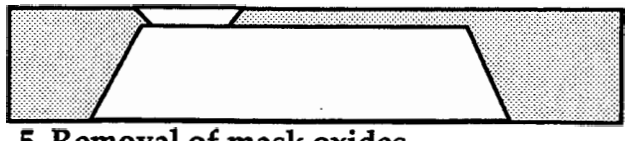

5. Removal of mask oxides

Figure 5-3 Bulk Micromachining Process Steps

which were aligned to the openings on the front surface of the wafer using the pattern offset for the front surface.

After silicon dioxide etching to remove the oxide from the square back surface openings, the wafer was rinsed and then etched in the 85°C EDPW solution. The etching was performed until the back surface cavities etched through the wafer at the bottom of the front surface cavities. There was no etch stop to prevent the etching from attacking the device silicon so a manual inspection was performed every 5 minutes nearing the end of the 6.5 hour etch.

The rough back surface visible in figure 5-2 is a result of the rough etching of the bottom of the back surface cavity. The <111> sidewalls of the back surface cavity are very smooth but the bottom surface is etched preferentially due to differing rates of etchant exchange at different locations of the cavity. It was also noted that such back surface etching produced devices with non uniform thicknesses. The thickness of this cantilever varies by 10 μm over the area of the device.

5.1.1 Electrostatic Actuation

The cantilever device was actuated electrostatically by grounding the device wafer and placing it in close proximity to a positively charged electrode. The electrode can be seen in the background of figure 5-2. The gap between the cantilever and electrode was produced by patterning the cantilever area on the front side and etching down 12 μm. The electrode pattern was produced by patterning a second aluminum coated wafer and then etching the excess aluminum with an aluminum etchant.

The square actuation pad and the aluminum bottom electrode form an air gap capacitor. The capacitance of this device is given by the expression:

$$C = \frac{\varepsilon_0 A}{D} \tag{28}$$

where ε_0 = permitivity of free space
A = area of actuation pad
D = gap between plates

Substituting for various terms, the capacitance was calculated to be ≈ 0.7 pF. Application of an electrostatic force on the plate will flex the cantilever resulting in an increase in the value of the capacitance. Such forces can be assumed to act at the center of the plate and thus put a load and a bending moment on the flexing section of the beam. Using superposition and assuming that the actuation region is stiff to bending, the deflection to a given force can be expressed as [28]:

$$Y = \frac{19FL^3}{12EI} \tag{29}$$

where E = Young's modulus
I = Moment of inertia
$= \frac{wt^3}{12}$ for rectangular X section

The cantilever can be actuated by applying a voltage to the aluminum electrode and grounding the cantilever. This produces an electrostatic attracting force between the electrode and the plate, which is expressed by:

$$F = \frac{\varepsilon_0 A V^2}{2D^2} \tag{30}$$

where A = area of actuator's capacitive plate
V = applied voltage
D = gap between electrodes

With sufficient voltage, the deflection of the cantilever is governed by equation (29). This deflection reduces the gap between the plate and the electrode thereby increasing the electrostatic force. The gap becomes (D-Y) at the tip and (D-y(L_1)) in the middle of the cantilever. Assuming that the plates remain parallel, the force due to the average of the reduced gap is given by:

$$F = \frac{\varepsilon_0 A V^2}{2(D - \frac{13}{19}Y)^2} \tag{31}$$

where Y = deflection of cantilever tip

As shown by equation (31), when the gap decreases, the force increases quadratically. Hence, past a critical threshold voltage, the beam should snap shut. Substituting (31) into (29), the applied voltage for a given displacement reaches a maximum at

$$Y_{crit} = \frac{19}{39} D \tag{32}$$

This threshold should occur at ≈45.5 volts. For voltages higher than the threshold, the model predicts that the gap will be zero.

5.1.2 Electrostatic Actuation Results

The same cantilever was actuated using an electrostatic force by applying a voltage to the aluminum electrode and grounding the plate. The applied voltage was varied from 0 to 80 volts. The deflection of the tip of the cantilever was measured using an optical microscope. The amount of deflection was measured at 4 volt intervals between 32 and 78 volts and this is plotted in Figure 5-4. The theoretical deflection, outlined in section 3.2 is also included in the figure. At 60 volts, the tip had deflected the entire gap. However, the electrical short was observed only at 77 volts.

The device did not exhibit the expected threshold closing after deflecting 6μm that was predicted in theory. Rather, the cantilever had deflected through most of its range between 35 and 40 volts and continued to deflect further up to 60 volts. Either some debris was constraining the device or the force was not increasing as drastically as predicted by the theory. Fringe fields and weakened forces result from the non-parallelism of the capacitive plates as the cantilever bends. This behavior accounts for the observed softer deflection characteristic. Attempts to achieve resonant response by applying a

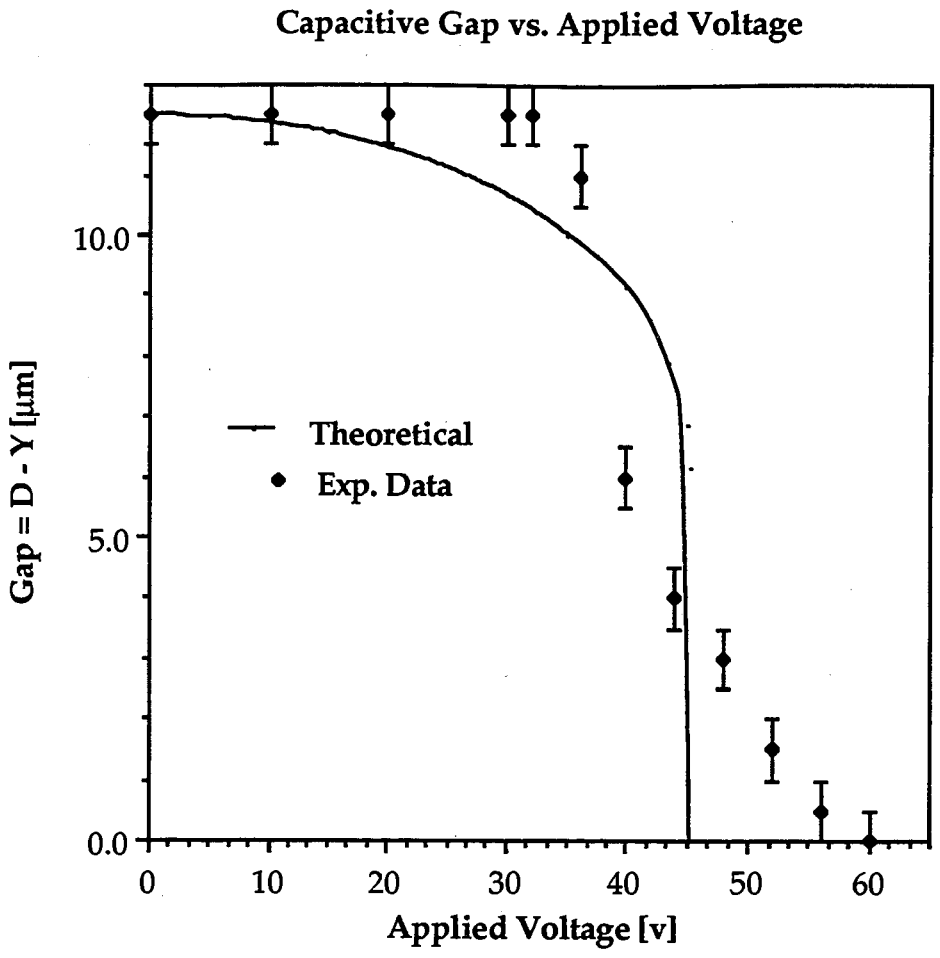

Figure 5-4: Experimental Electrostatic Actuation Characteristic

periodic voltage to the device were not successful.

The silicon cantilever design illustrates the concept of electrostatic actuation. Even with a 12 μm gap, voltages of the order of 40 V are required for actuation.

5.1.3 Linear Motion Platform

For discrete mass resonant sensing, a device with lower mass and more flexibility is required. The limits of bulk silicon micromachining without etch stops were examined with a second, more flexible device. Figures 5-5 and 5-6 are electron micrographs of a 225 μm x 225 μm plate supported at four corners by folded arms which are 1000 μm long and 20 μm wide. The average thickness of the structure is 15 μm. The linear motion platform was produced with a similar process to the silicon cantilever except that this device was produced with the anisotropic etchant KOH.

Although KOH etches the silicon dioxide layer at a significantly higher rate than EDPW [12], it is advantageous for bulk structures because of the sharp silicon edges it produces. A solution of 132 g of KOH and 300 ml of water at 70°C was used. The front surface KOH etch was performed for 32 minutes at which time the etching was 35 μm deep. As with other anisotropic etchants, the KOH undercuts convex corners, such as the corners of the platform, thus corner compensation was again used.

After front surface etching, the device was reoxidized and back surface openings were patterned. Back surface etching required 8.5 hours to release the structures. Due to the non-uniformity of the back surface etch, this device was made as thin as possible without risking etching through one of the arms. The symmetry of the support arms restricts motion of the platform to linear, normal to the face of the platform.

The linear motion device was very flexible and when a force was applied to the platform using a micromanipulator tip, the platform would move into the cavity 340 μm without fracturing the support arms. When the force was removed, the platform would spring back to its original position.

The thickness required for fabrication of these bulk silicon devices contributed to a relatively large device mass. Given a silicon density of 2.3 g/cm^3, the mass of the linear motion platform device is 2.3 μg. The uncontrolled process of back surface etching results in an uniform thickness across the device and a corresponding large uncertainty in the device mass and resonant characteristics. The purpose of the research was to produce a

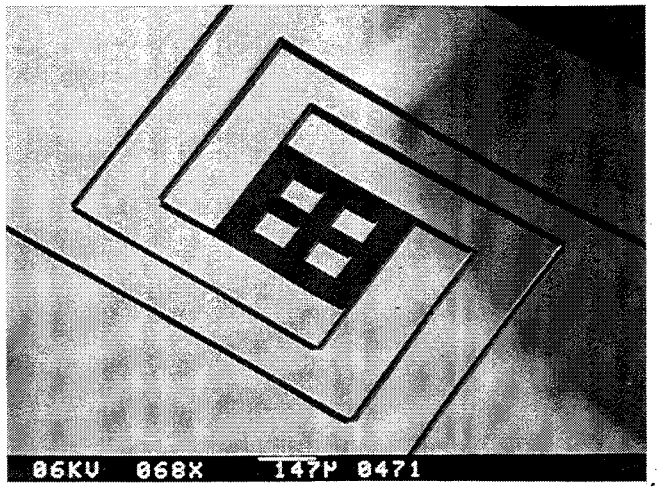

Figure 5-5: Electron Micrograph of a Linear Motion Platform

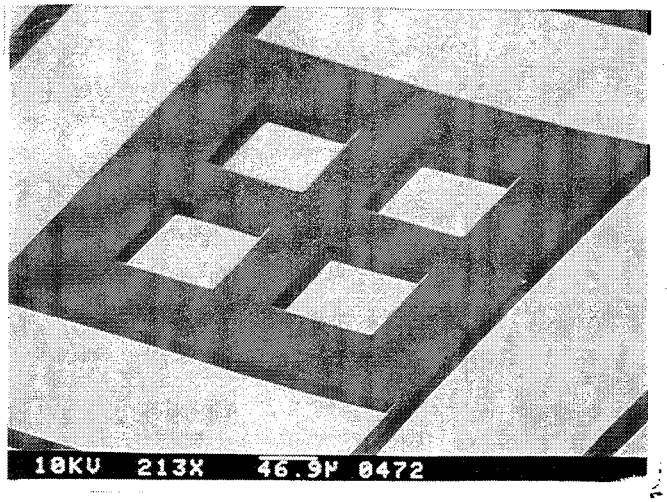

Figure 5-6: Close-up View of a Linear Motion Platform

resonant mass sensor capable of measuring less than one nanogram. Although the concept of actuating silicon devices was shown, the bulk silicon micromachining concept was abandoned due to the exceedingly large and uncertain mass of the devices.

5.2 Silicon Dioxide Cantilever

As outlined in section 2.1, silicon dioxide devices are micromachined from silicon dioxide which is grown on the silicon substrate. The EDPW anisotropic etchant does not etch the silicon dioxide significantly, thus the device can be made very thin. As compared to silicon devices described previously, the reduced thickness of silicon dioxide structures significantly decreases their mass. Silicon dioxide devices were repeatably constructed with a thickness of 1 μm. Compared to a minimum of 15 μm for silicon devices constructed using the technique outlined in section 5.1, the mass reduction is greater than 92%.

This mass reduction, along with the flexibility and strength of such thin structures, made the concept of a resonant device sensitive to small added masses possible. A design was devised which minimized device mass, while allowing adequate angular resonant amplitudes for detection.

A cantilever configuration was selected because the top face of the cantilever resonates in an angular motion. Since the cantilever is only pinned by the base, the amplitude of the motion possible is large and the amplitude can increase with the length of the cantilever. In order to reduce weight while retaining torsional rigidity, a cantilever consisting of two support arms and a large plate section was chosen. The plate serves as a test mass support and as a reflector for the optical detection system.

The plate dimensions were chosen as 50 μm x 50 μm in order to provide an ample reflector area for the optical detection system. The length and width of the arms were optimized to allow for a fundamental resonance of less than 18 kHz, which was required for reliable actuation by the shaker table. A simplified resonant model outlined in appendix A was used to determine the length and width of arms required to obtain the required resonant frequency. The arms were designed 150 μm long and 10 μm wide. 5 μm slots 10 μm apart were put onto the plate perpendicular to the arms. These slots were intended to locate test masses longitudinally along the cantilever. Each device has a volume of 4700 μm^3. The density of silicon dioxide is 2.5 g/cm^3 and thus the approximate mass of each device is 11.7 ng.

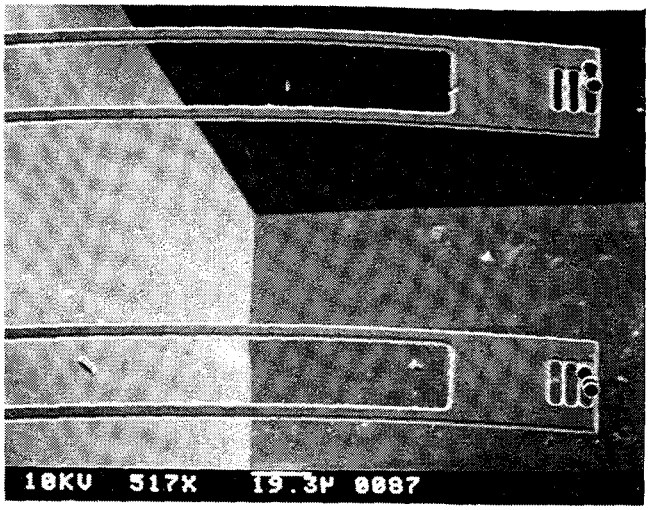

Figure 5-7: Electron Micrograph of Two Silicon Dioxide Cantilevers

The devices were fabricated using the procedure outlined in section 2. Figure 5-7 shows an electron micrograph of two finished devices. Three test masses can be seen at the tip of each cantilever. The rounding of the corners and slots in the device are a result of the wet etching of the oxide using BOE. The etchant undercuts the photoresist mask by 1 µm resulting in corners being rounded with a 1 µm radius and all device dimensions diminished by 1 µm. The annealed devices curve upward at the tip by ~5 µm.

The devices were removed from a water rinse following the wet anisotropic etch and the water was allowed to evaporate. It was noted that as the water filling the cavity evaporated, these relatively long and thin devices would bend under the surface tension of the water. As the water level decreased, the cantilevers would bend further until their tips would touch the bottom of the cavity. When the water had completely evaporated, most of the devices would spring back to the horizontal position. Some devices would remain touching the bottom. It was assumed that these devices became jammed

against the rough surface of the bottom. Shorter devices and subsequent ones with deeper sloped bottom cavities did not exhibit this failure.

5.2.1 Finite Element Analysis Results

To estimate the resonant characteristics of this device with and without loading, finite element analysis (FEA) was used. The commercial finite element package ANSYS was used for this and subsequent finite element analysis. Appendix B briefly outlines the concepts of FEA as well as describing in detail the model used for this analysis. Appendix C provides ANSYS outputs for this model.

A three dimensional finite element model with 274 nodes and 91 8 node linear brick elements was used to model the cantilever. The base of the cantilever was clamped in all 6 degrees of freedom. This model was used in a modal analysis to determine the resonant modes of the device. The fundamental, first angular harmonic and first torsional harmonic resonant mode shapes are shown in figure 5-8. The resonant frequencies are 15.5 kHz, 126.2 kHz, and 122.4 kHz respectively. The angular fundamental mode has a diving board motion with most of the curvature in the arms due to the relative rigidity of the plate section. The tip of the cantilever has the maximum fundamental resonant amplitude. The first angular harmonic has a node 172 μm from the base. The maximum first harmonic resonant amplitude is located 100 μm from the base and the maximum amplitude on the plate section is located at the edge of the plate nearest the base. The torsional mode has a node running down the symmetry axis of the cantilever. Due to the torsional stiffness induced by having two support arms, the torsional mode would probably resonate with low Q and small amplitude.

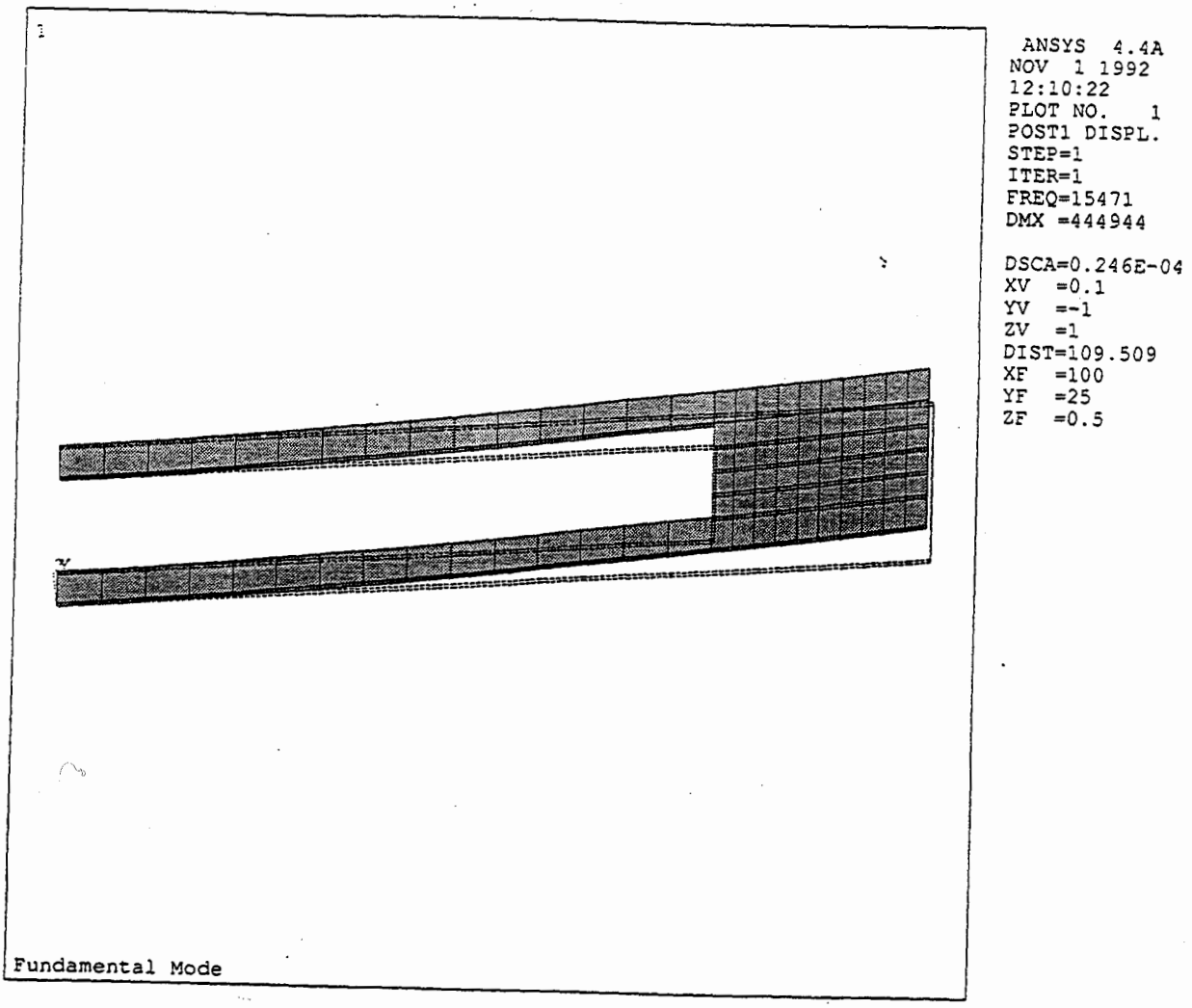

Figure 5-8a: Fundamental Mode Shape

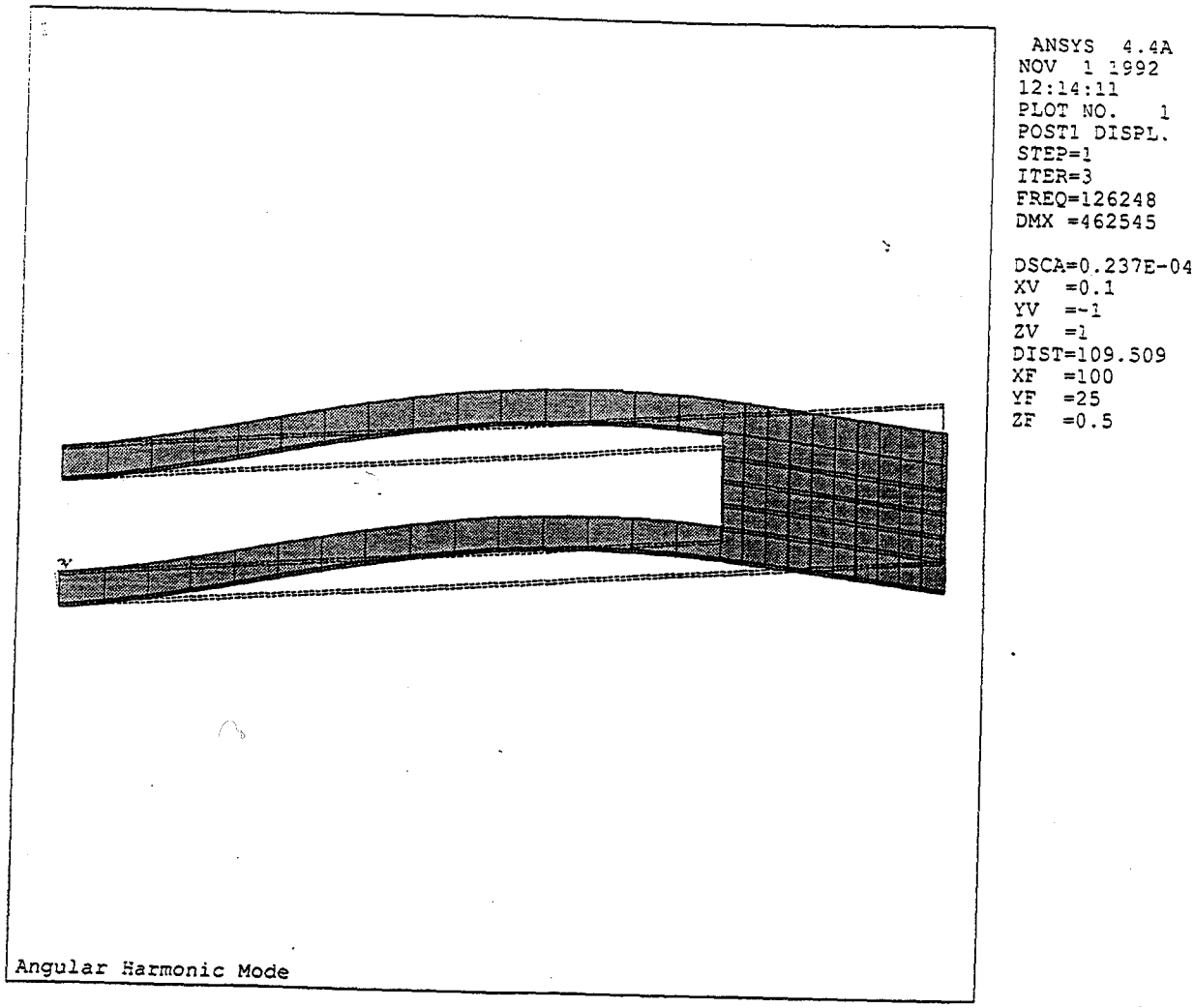

Figure 5-8b: 1st Angular Harmonic Mode Shape

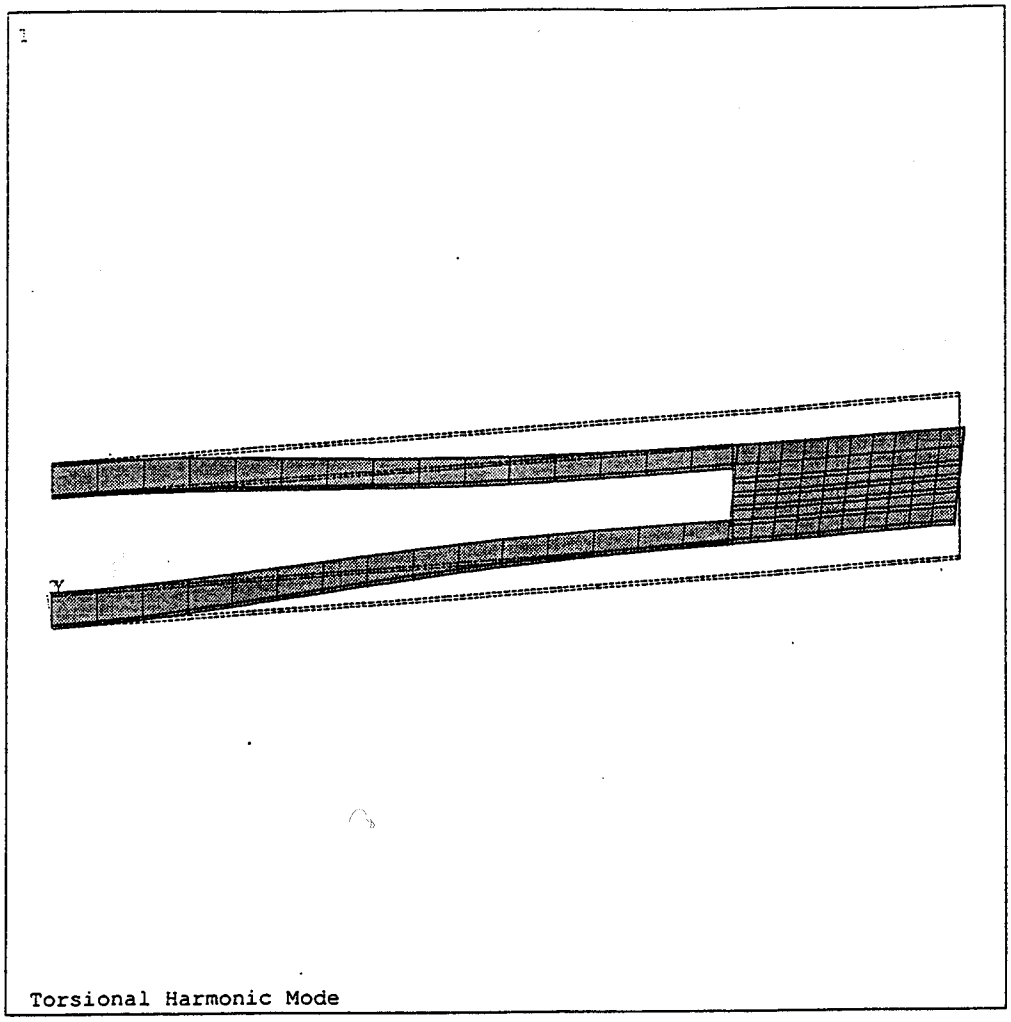

Figure 5-8c: 1st Torsional Harmonic Mode Shape

Figure 5-8: Silicon Dioxide Cantilever Mode Shapes

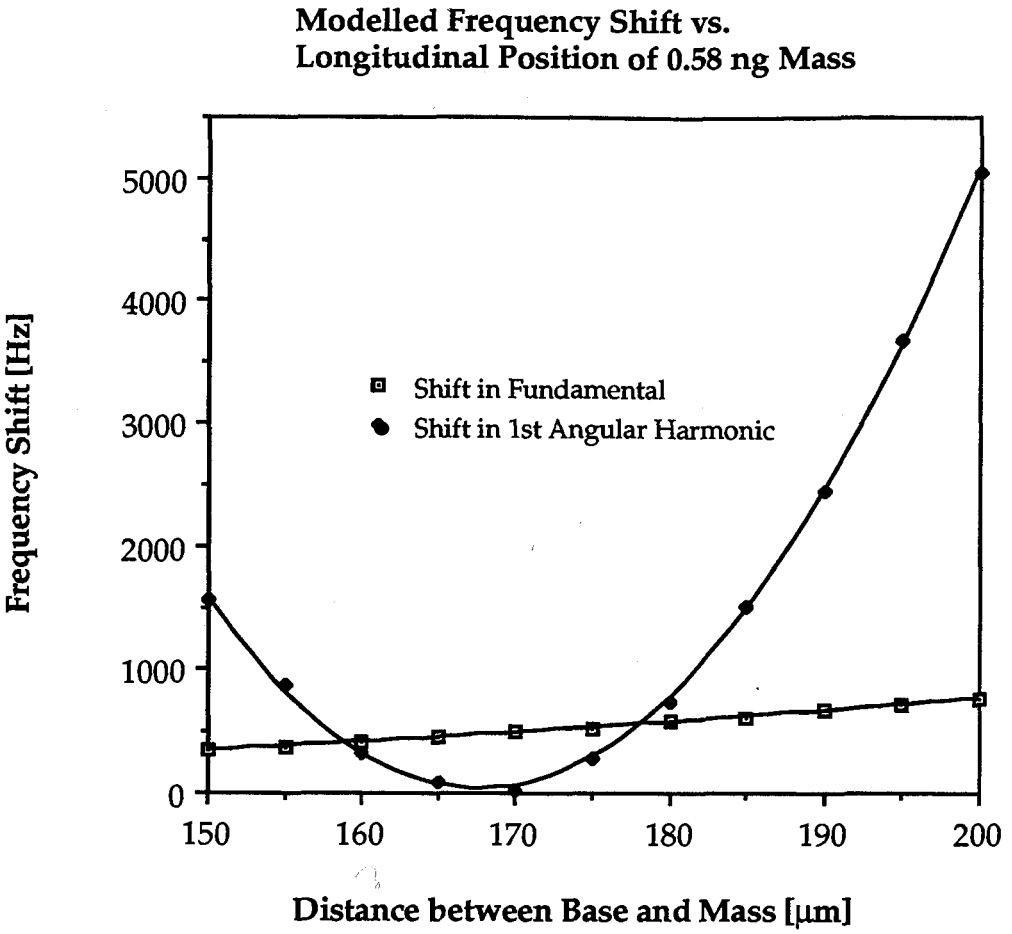

Figure 5-9: Resonant Shift vs. Longitudinal Mass Position

A point mass was put in the model at various locations on the plate section. A value of 0.58 ng was selected since it corresponds to the mass of a calibration sphere used in experimentation. The shift in resonance longitudinally along the plate for the fundamental and first angular harmonic resonant modes is shown in figure 5-9. The maximum shift for the fundamental of 0.8 kHz occurs when the mass is placed at the tip of the cantilever. The first angular harmonic has a larger 5.0 kHz shift when the mass is near the tip but no shift occurs when the mass is placed over the resonant node. Lateral movement of the mass changes the resonant shift by $< 0.3\%$ for the fundamental and $< 53\%$ for the first angular harmonic. The first torsional harmonic is sensitive to the lateral position of the mass and has a shift of 9.3 kHz when the mass is at the corner of the cantilever.

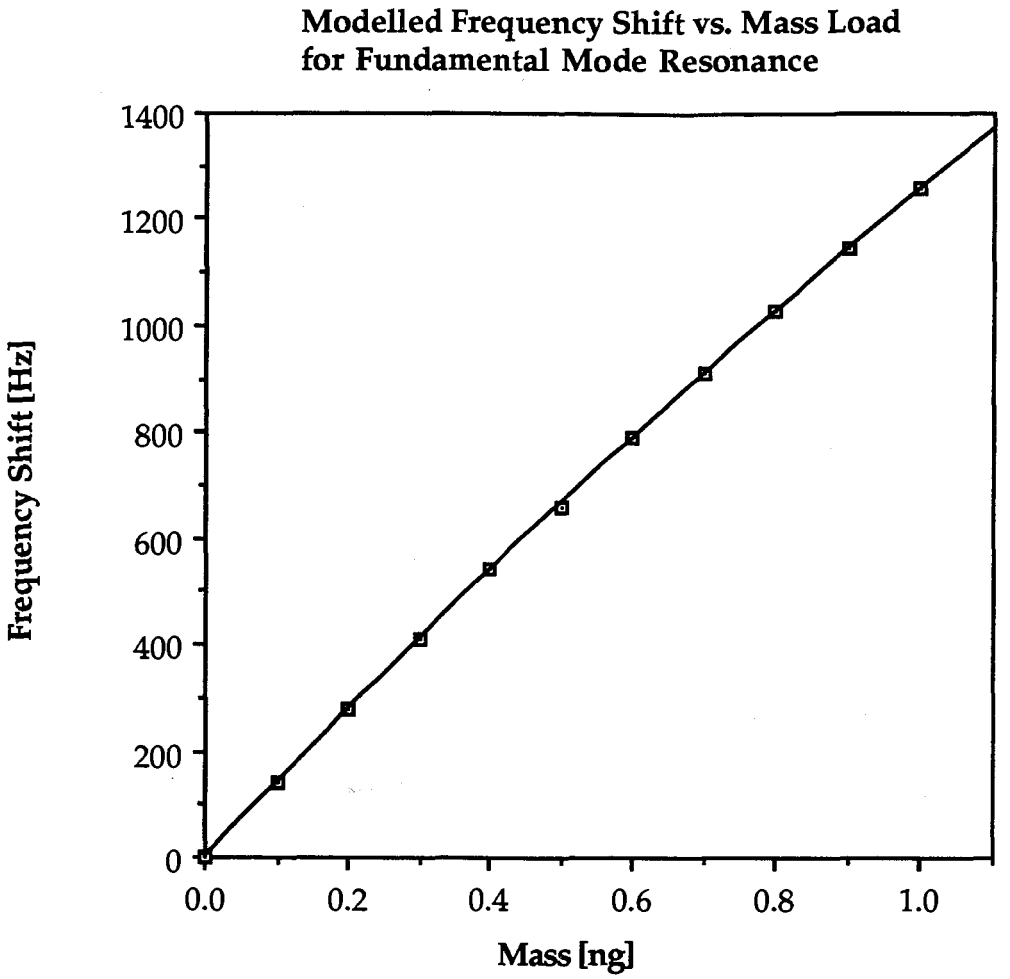

Figure 5-10: Modeled Frequency Shift vs. Mass

The first angular harmonic produces a large shift only if the mass is located at the edge of the cantilever. The harmonic is also very sensitive to lateral and longitudinal placement. The torsional mode is too rigid to achieve significant resonant amplitude. The relative insensitivity of the frequency shift exhibited by the fundamental mode makes it the most attractive for sensor application. The graph in figure 5-9 can be used for calibrating the mass position to the frequency shift of the device.

The modeled characteristic of frequency shift versus loading 5 μm from the tip for the fundamental mode is shown in figure 5-10. The curve is nonlinear

and the resonant frequency has the form:

$$f_n = \sqrt{\frac{1.296}{M + 0.394m}} \qquad (33)$$

Where f_n is the resonant frequency [hz]
M is the applied mass [g]
m is the beam mass [13.75e-9 g]

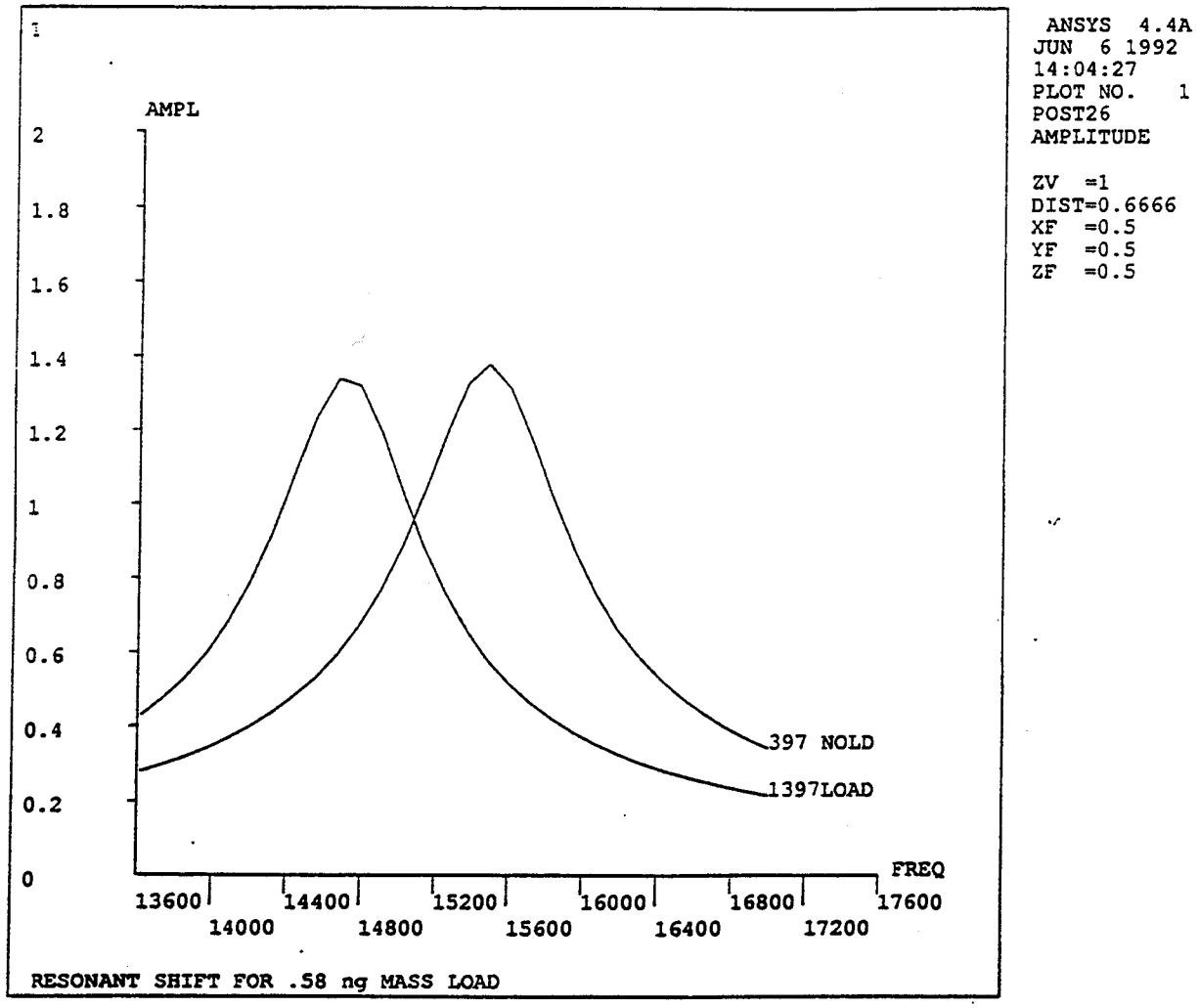

Figure 5-11: Modeled Frequency Amplitude Characteristics

The finite element model was used in a reduced harmonic analysis to determine the amplitude versus frequency graphs for loaded and unloaded devices. An experimentally determined damping factor of 0.1 was added to the model. The actuation was modeled by oscillating the base of the cantilever with an amplitude of 0.1 μm. Figure 5-11 shows the modeled amplitude versus frequency characteristic of an unloaded cantilever and the shifted characteristic of a cantilever loaded with a 0.58 ng mass 5 μm from the tip. The two curves are easily resolvable.

The modeled fundamental, first angular harmonic resonant frequencies, as well as the shifted frequencies as a result of a 0.58 ng mass placed 5 μm from the tip of the device are found in table 5. The 0.58 point mass causes a shift of 0.77 kHz in the fundamental frequency and thus the modeled sensitivity is 1.32 kHz/ng.

Table 5. Modeled resonant characteristics of 200 μm cantilever

Mode	Unloaded Frequency [kHz]	0.58 ng Load Frequency [kHz]
Fundamental	15.47	14.70
1st Angular Harmonic	126.2	122.4

5.2.2 Experimental Results

5.2.2.1 Device Resonant Response and Yield

40 cantilevers each 200 μm x 50 μm x 1 μm were fabricated on one substrate over an area of 1 cm^2. The resonant frequencies for both the fundamental and first angular harmonic were measured using the experimental apparatus outlined in section 4.1. The resonant frequencies as well as the resonant Q, are listed in Table 5. The ~0.9% variation in resonant frequency between cantilevers is largely due to differences in device dimensions attributed to the in-house fabrication process. The deviation from modeled natural frequency is +2.3% for the fundamental and +0.2% for the second harmonic. The experimental Q factor was determined using equation (10) by estimating the resonant frequency and half power points of the amplitude frequency characteristic.

Table 6. Resonant characteristics of cantilevers

Mode	f_{theory} [kHz]	f_{expt} [kHz]	Q_{expt}
Fundamental	15.47	15.8 ± .15	20.5
2nd Harmonic	126.2	126.5 ± .4	206

This fabrication batch exhibited a device yield of 95%. One of the two failures was a result of a severed support arm and the second a result of a filament of wax used for mounting the chip resting on top of the device. Other fabrication batches in which the etching depth was less than 150 μm exhibited yields of less than 50 % due to the tips of the cantilevers touching the bottom of the cavity after air drying. As explained previously, the cantilevers bend downwards as a result of surface tension of the evaporating water. This failure phenomena was probably the result of the tip of the cantilevers binding against the rough bottom of the cavity.

5.2.2.2 Mass Measurements

Mass sensing calibration was performed using polymer spheres produced by Duke Scientific Corp. The spheres having a diameter of 10.2 ± 0.3 μm, and a density of 1.05 g/cm^3 have a mass of 0.58 ± 0.06 ng. One such sphere was placed on the payload platform of the 50 μm x 200 μm cantilever using a

micromanipulator. Friction induced electrostatic force was sufficient to secure the sphere to the platform. Figure 5-12 shows an electron micrograph of one such sphere attached to a cantilever sensor. Notable in the figure are lateral slots machined into the platform. These are used to longitudinally locate the mass in order to increase the accuracy of the measurement.

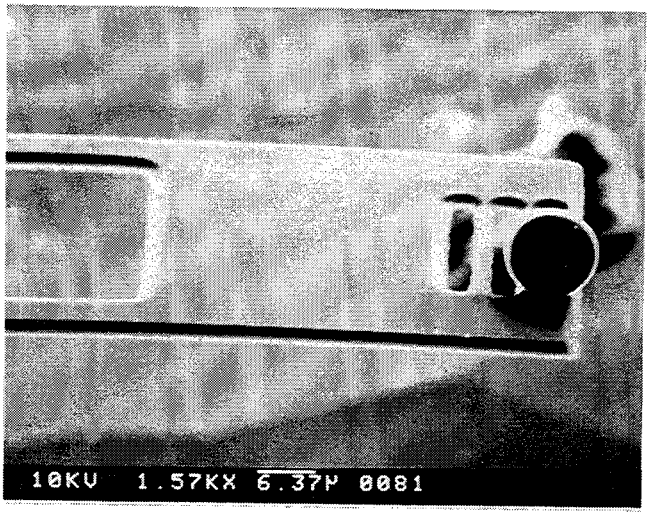

Figure 5-12: 0.58 ng Sphere attached to Cantilever

Figure 5-13 shows experimental resonance characteristics for an unloaded device and one with a 0.58 ng sphere located 5 μm from the tip. The 0.58 ng load is clearly resolvable in the figure. The sensitivity and resolution of the system can be calculated from figure 5-13. The fundamental resonant shift is 1.05 kHz and thus the sensitivity is:

$$S = 1.9\,\text{kHz/ng} \tag{34}$$

Using equation (11), the resolution of the system is:

$$R = 550\,[\text{hz}] \tag{35}$$

Due to the low Q of the system, shifts of less than 550 hz cannot be discerned using the resolution criterion as defined. Combining (34) and (35), the system can resolve a mass difference of:

$$M_{min} = 0.29 \text{ ng} \tag{36}$$

M_{min} represents the minimum added mass which can be reliably detected by the system. M_{min} does not represent the error in mass measurement as the peaks of the resonant amplitude curves in figure 5-13 were detected to a higher precision than 550 Hz.

Comparing the resonance characteristic in figure 5-13 with the simulated one in figure 5-11, it is notable that the shapes of the characteristics are very similar, however the measured shift of 1.05 kHz is larger than the simulated value of 0.77 kHz. This disagreement of 36% can be attributed to several factors including uncertainty in the actual density (and hence calculated mass) of the sphere. Sources of error due to the modeling include possible error in the bulk values for the material properties and the addition of the slots to the experimental device which were not included in the simulation model.

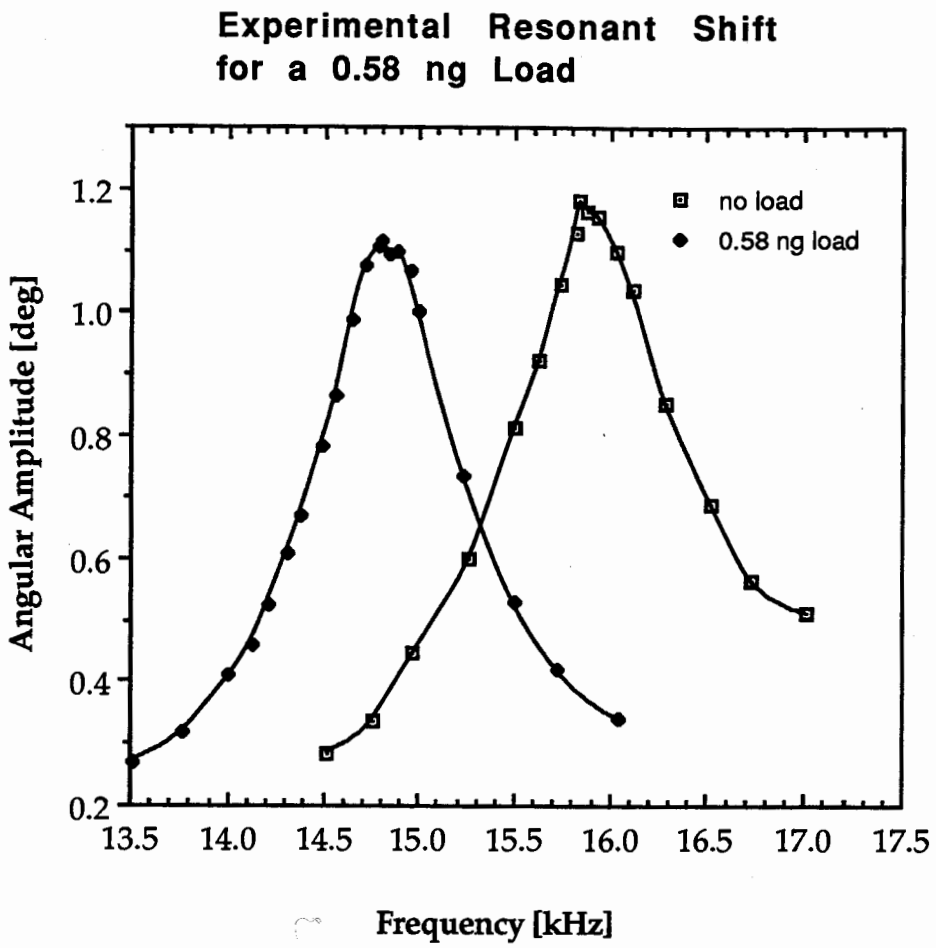

Figure 5-13: Experimental Frequency Amplitude Characteristics

The frequency shift versus applied mass characteristic was also investigated. A new batch of cantilevers with similar configuration to those specified in section 5.2.1 was used. The dimensions of the cantilever were:

arms: 120 μm x 8 μm x 1 μm
plate: 60 μm x 60 μm x 1 μm

Due to the larger plate area, the cantilever had a fundamental resonant frequency of 13.15 kHz. Spheres having a diameter of 9.87 ± 0.057 μm and thus a mass of 0.528 ± 0.009 ng were loaded one by one onto a payload slot 5 μm from the tip of one cantilever. The resonant frequency was measured for 0 through 5 spheres. The experimental frequency shift versus applied mass characteristic is shown in figure 5-14.

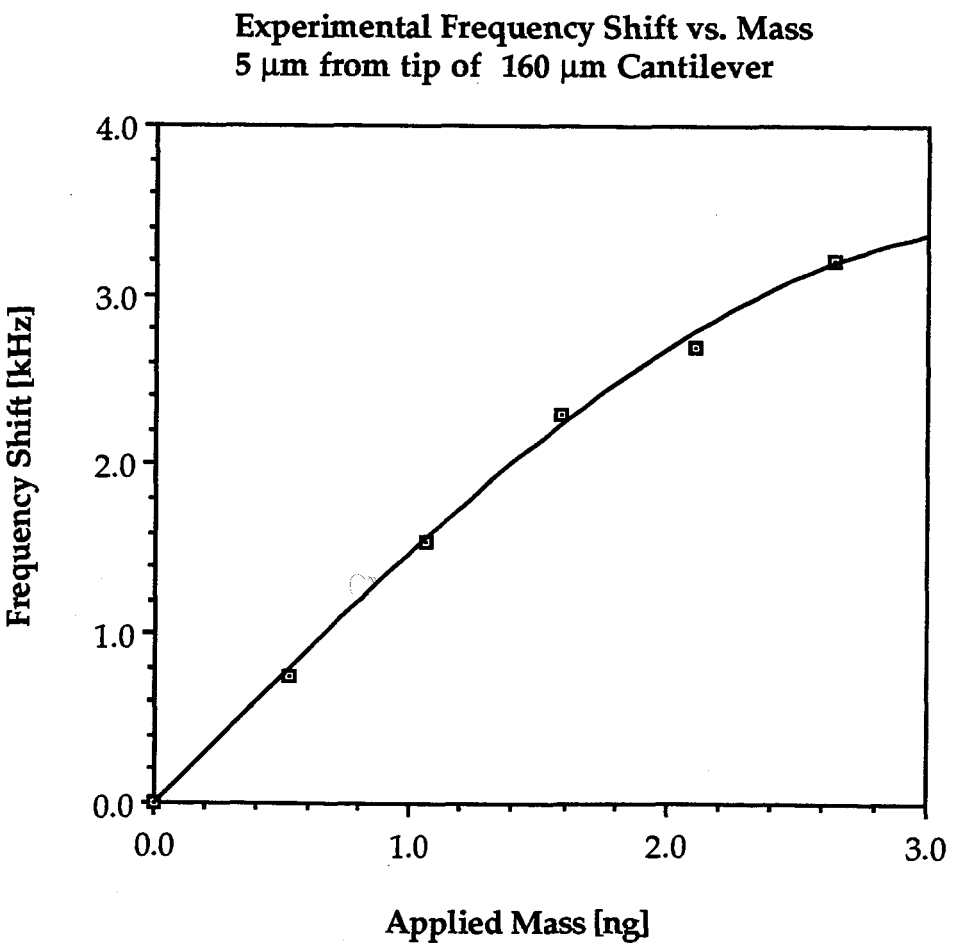

Figure 5-14: Experimental Frequency Shift versus Mass

As anticipated the curve is non-linear and the resonant frequency has the form:

$$f_n = \sqrt{\frac{0.612}{M + 0.256m}} \qquad (37)$$

Where f_n is the resonant frequency [hz]
M is the applied mass [g]
m is the beam mass [13.75e-9 g]

Equation (37) is of the same form as the derived equation (9) and equation (33) calculated from finite element analysis. Differences in equation constants between equations (37) and (33) are due to the differences in geometry and resonant frequency between the two devices.

The micromachined silicon dioxide cantilever has been shown to function as a resonant mass sensor in air. The conversion of frequency shift to mass requires that the longitudinal position of the mass be known and a calibration equation of the form (37) be applied. With repeatable processing, such as CMOS compatible micromachining, such an equation would apply for the entire batch of thousands of devices.

6. RECOMMENDED REFINEMENTS

The performance of the silicon dioxide resonant sensor system could be improved in the following areas:

- Fabrication accuracy and repeatability
- Ease of actuating and detecting resonances
- Ease of loading test devices and reduced sensitivity to load position
- Improved resonant characteristics include higher Q and lower viscous drag

Cantilevers produced in CMOS would improve fabrication and allow for improved actuation and detection schemes. Optimized cantilever designs would improve resonant characteristics while new resonator configurations could reduce load position sensitivity.

6.1 CMOS Cantilevers

Poor accuracy and repeatability of the fabrication process is largely a result of the in house techniques employed in patterning and especially in wet etching of the silicon dioxide. The BOE etchant used undercuts the photoresist mask with time, leaving devices with reduced dimensions and rounded corners which are not repeatable from batch to batch. The thickness of the devices is a function of the oxidation process used and variations in the in-house process can also result in non repeatable devices.

Cantilevers produced using CMOS compatible micromachining techniques have accurate dimensions as a result of the dry etching processes employed by the commercial foundry. Device thickness is also well controlled as a result of the stringent tolerances required for CMOS circuitry.

CMOS cantilevers may improve actuation by allowing internal techniques to be employed. Figure 6-1 shows an array of 200 μm cantilevers produced with CMOS compatible micromachining techniques. These cantilevers each have a polysilicon resistor which runs up each arm. The resistors can be used to

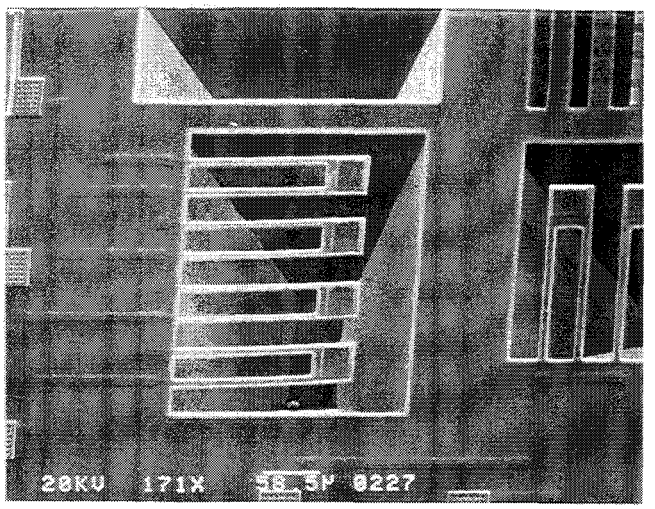

Figure 6-1: CMOS Cantilevers

thermally actuate the devices. The internal thermal actuation method would eliminate the vibration table and audio amplifier from the experimental apparatus making the system more compact.

CMOS cantilevers may also improve detection performance. The cantilevers in figure 6-1 have 44 μm x 44 μm aluminum mirrors covering the plate area. These mirrors reflect more of the focused laser beam, simplifying the alignment of the detector. Internal detection methods, such as the integrated optical detection approach described in section 3.4, could be added to CMOS designs. Designs with internal detection would eliminate the need of an optical bench and manual alignment.

In summary, resonant sensors produced using CMOS compatible micromachining offer the promise of accurate, repeatable devices. These devices could be made with sophisticated internal actuation and detection systems resulting in increased system portability.

6.2 Refined Resonator Designs

The cantilever resonator could be refined to improve its resonant characteristics. A higher Q device would increase measurement accuracy and allow smaller masses to be measured. One method of increasing Q is to increase device resonant frequency while maintaining the frequency width of the response curve. The resonant frequency for a cantilever can be increased by reducing the mass of the tip and by shortening its length.

Figure 6-2 shows the finite element analysis model of a higher frequency cantilever in fundamental resonance at 49.2 kHz. The three dimensional finite element model consisted of 356 nodes and 130 8 node linear brick elements. The model configuration is identical to the one outlined in appendix B. The two arm cantilever structure uses 75 μm x 10 μm x 1 μm arms which support a plate which is 40 μm x 50 μm x 1 μm. The modeled fundamental and first angular harmonic resonant frequencies of this device as well as the shifted frequencies as a result of a 1 ng mass placed 5 μm from the tip of the device are found in table 7.

Table 7. Modeled resonant characteristics of high frequency cantilever

Mode	Unloaded Frequency [kHz]	1 ng Load Frequency [kHz]
Fundamental	49.2	43.3
1st Angular Harmonic	440.0	410.0

The fundamental frequency shift due to the 1 ng load is 5.9 Hz. Thus the modeled sensitivity of the device is:

$$S = 5.9 \text{ kHz/ng}$$

This sensitivity is 4.4 times higher than that modeled for the 200 μm device. The Q factor and resolution of this device would have to be determined experimentally.

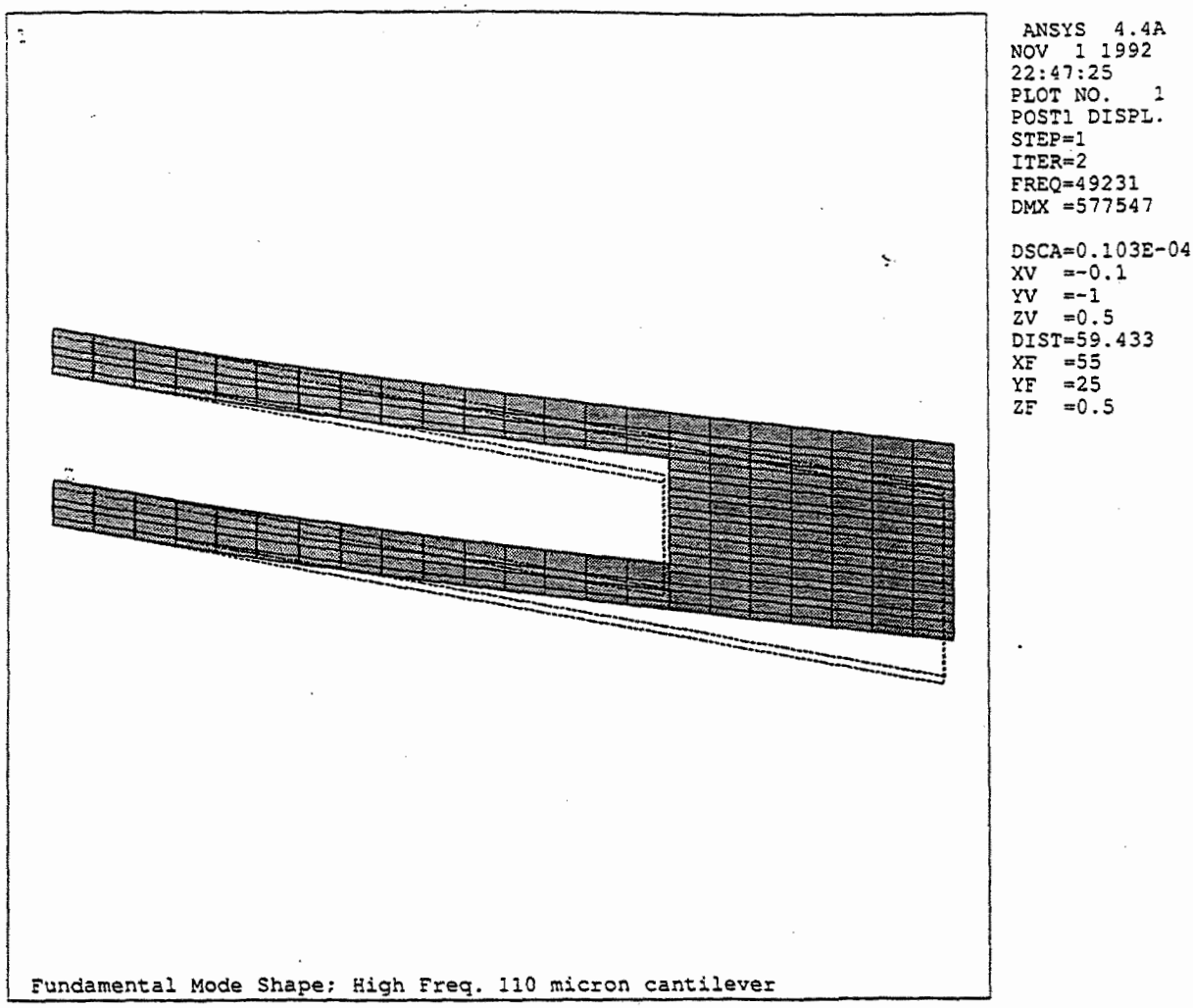

Figure 6-2: FEA Model of High Frequency Cantilever

Other resonator configurations would be less sensitive to the location of the load. A linear resonator similar to the linear actuation platform described in section 5.1.2 would be relatively insensitive to the position of the load on the platform. All locations on the platform resonate with equal amplitude, thus due to symmetry the frequency shift due to applied load will be location independent.

7. APPLICATIONS

The micromachined discrete mass resonant sensor has application in measuring individual discrete masses of less than 10 μm in diameter. Currently a resolution of 0.29 ng has been achieved. Recently, extremely high Q devices have been demonstrated which have a Q of $6x10^5$ at a resonant frequency of 26.7 kHz. These silicon devices are relatively large at 800 mm^2 in size. If a comparable Q is achievable in a low mass silicon dioxide device extremely small masses could be resolved.

At present, the study of single cells of biological material is the most promising application for such small discrete sensors. Microbiologists and biomedical engineers are interested in how cells live and grow under various conditions. Studies of cell growth and division and the reaction of cells to toxic substances are only two of many possible applications. Currently the cell mass is determined using bulk measurement of dehydrated cells [30]. This is a destructive test which is statistical in nature. Another approach proposed by Kilburn et al. [31] suggested the use of acoustic resonance densitometry to measure the total mass of cell cultures with in excess of 10^6 cells per ml. The discrete mass sensor will have advantages over both of the above methods as it will monitor the mass of a single cell non-destructively.

Cell studies are largely performed in a saline culture, thus most applications will require in fluid cell mass sensors. The devices fabricated thus far are operable only in air or vacuum. As explained in section 3.2.1, the resonant Q factor is strongly influenced by viscous damping. Viscous damping is negligible in air and zero in vacuum. In a more viscous fluid, such as water, this damping becomes significant. The large frontal area of the resonating cantilever results in high viscous damping in fluid. The first generation device showed a structural damping Q factor at first resonance of 20.5. Calculations from section 3.2.1 show that the Q factor due to viscous damping for a 50 μm wide cantilever in water is < 9.5. Combining the influence of these two types of damping results in a Q factor of less than 6.5. This exceeds the minimum Q factor for oscillatory motion of 0.5. Given the experimental sensitivity of 1.9 kHz/ng, the minimum Q in order to resolve 0.5 ng at 15.9

kHz is:

$$Q_{min} = 8.4$$

Thus devices with reduced damping are required for in fluid use. Designs with reduced frontal area such as lateral resonators will significantly reduce the viscous damping.

While in fluid measurements of living cells were not accomplished, BHK fibroblast cells were located onto test cantilevers using the random settling technique outlined in section 3.6. Figures 7-1 and 7-2 show BHK cells attached to SiO_2 cantilevers. These scanning electron micrographs show the development of the cells 6 hours after settling onto the cantilever. The cells can be seen to be anchoring themselves to the cantilever. This is evidence of biocompatibility between the SiO_2 cantilever and the fibroblast..

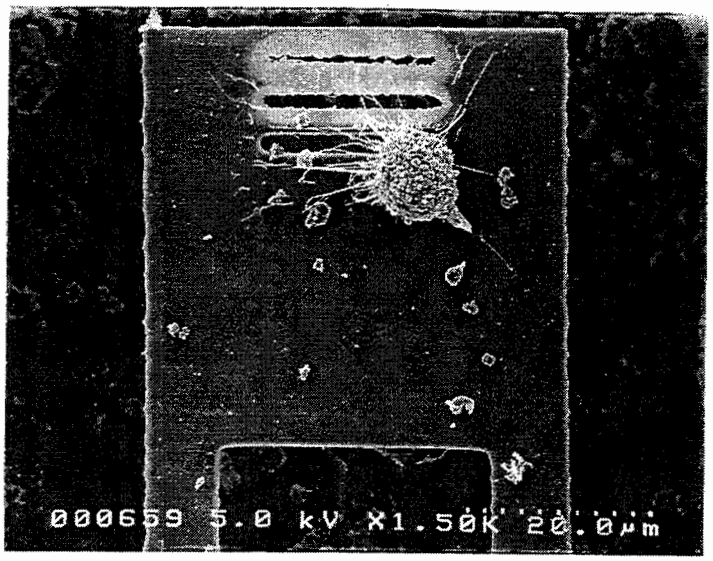

Figure 7-1: BHK Cell attached to Silicon Dioxide Cantilever

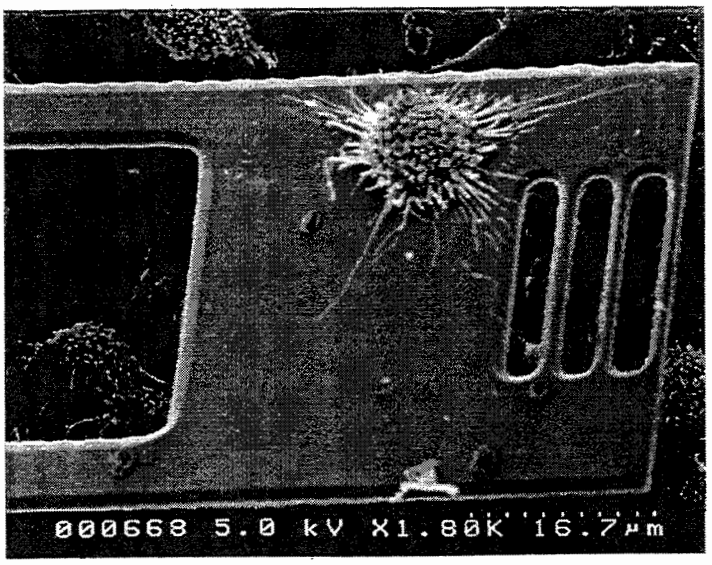

Figure 7-2: BHK Cell attached to Silicon Dioxide Cantilever

8. CONCLUSION

A novel application of micromachining has been demonstrated in this thesis. Surface micromachined silicon dioxide cantilevers were employed as resonant sensors to measure the mass of discrete objects. The mass measurement of discrete objects of diameter 10 μm and mass of less than 1 ng shows the principle of sub-nanogram discrete mass sensing. The measurement of such minute discrete objects opens many possible applications in biotechnology. The monitoring of mass fluctuations of individual living cells would be a valuable tool to bioengineers studying cell growth under various conditions.

Bulk micromachined silicon platforms were investigated as possible mass sensing candidates. Electrostatic actuation of a cantilever platform was shown using an actuating voltage of 40 V over a capacitive gap of 12 μm. Uneven etching of the bulk micromachined silicon devices resulted in a practical thickness limit of 15 μm. These relatively thick devices were judged too massive for use in small mass sensing application.

Silicon dioxide cantilever were produced using an in house process and in CMOS using CMOS compatible micromachining techniques. The cantilever was optimized to resonate in fundamental mode at 15.9 kHz. The devices were actuated externally and the resonant amplitudes were detected optically. A Q factor of 20.5 was obtained in the fundamental mode.

Polystyrene spheres were loaded individually onto the tip of a cantilever and the resonant amplitude versus frequency characteristic was obtain both with and without a load. An experimental mass sensitivity of 1.9 kHz/ng was measured. Experimental results were compared to those obtained using finite element analysis (FEA). FEA was also used to investigate the effect of mass placement on resonant frequency. For a cantilever resonating in fundamental mode, longitudinal position of the mass affects resonant frequency while lateral position has negligible effect.

Further analysis indicates that refined resonator designs can increase

sensitivity significantly. Devices with higher Q could be used to extend this application to the picogram domain. New resonator designs may reduce the effect of mass placement while designs with lower viscous damping may be used for in fluid resonance. The simple resonator presented in this work has proven the concept of sub-nanogram discrete mass sensing, opening the door to a new application of sensing the mass of even smaller and more intriguing objects.

APPENDIX A: RESONANT FREQUENCY SHIFT CALCULATIONS

This section provides an estimate of the length and width of the support arms required for the silicon dioxide cantilever described in section 5.2. Two arms support a 50 μm x 50 μm plate. The arms and plate are both 1 μm thick. The desired resonant frequency was less than 18 kHz. Due to the experimental resonator having a varying cross sectional area, the deflection profile Y(x) cannot be determined analytically. Derivation of an equation similar to (9) for the experimental configuration of two similar arms supporting a square plate is rather complicated and better suited to finite element analysis.

Equation (9) can be used for a rough estimate of the resonant frequency of the experimental device with two arms supporting a square plate. The two arms are approximated by a single cantilever with the same thickness and twice the width of one arm. The 50 μm square plate is approximated by a point mass at the end of the cantilever. This approximation ignores the bending moment at the end of the two arms produced by the mass centroid of the plate 25 μm from the end of the arms and thus yields a high estimate of fundamental resonant frequency.

As specified in section 5.2.2 the cantilever was desired to have a fundamental resonant frequency of less than 18 kHz. The two support arms are 1 μm thick and the plate has dimensions of 50 μm x 50 μm x 1 μm. The length and width of the support arms are to be determined while minimizing overall weight. To minimize weight, the width of the arms should be minimized and the length determined. For rigidity, cantilevers with arms of lengths 50 to 200 μm should use a minimum arm width of 8 μm.

Using equation (9):

$$\omega_n = \sqrt{\frac{3EI}{L^3}\left(\frac{1}{M + 0.23m}\right)} \qquad (9)$$

with:

$$I = \frac{bh^3}{12} \qquad (A.1)$$

Where: b is the combined arm width

h is the arm thickness

$$M = \rho V_{plate} \quad (A.2)$$

$$m = \rho V_{arms} \quad (A.3)$$

$$V_{plate} = (50\mu m)(50\mu m)(1\mu m) \quad (A.4)$$

$$V_{arms} = bhL \quad (A.5)$$

Where: L is the length of the arms

Along with the material properties for silicon dioxide [1]:

$$\rho = 2.5\ g/cm^3;\ E = 0.73\ E12\ dyne/cm^2$$

Substituting: $b = 16\ \mu m;\ h = 1\ \mu m;\ \omega_n = 2\pi(18000)\ Hz$

into equation (9) and solving for L results in:

$$L = 145\ \mu m$$

To ensure that the fundamental resonant frequency for the experimental device is < 18 kHz, a conservative arm length of 150 μm was selected.

APPENDIX B: FINITE ELEMENT ANALYSIS

Finite element analysis (FEA) is a mathematical method of modeling physical problems with complicated domains and boundary conditions. Physical problems with a related differential equation form such as thermal, static and dynamic structural, fluid dynamics and others can all be solved using FEA. The finite element method divides the domain into a finite number of simple sub domains which are termed finite elements [32]. The applicable boundary conditions are applied and the appropriate differential equation is solved over each element using variational techniques.

The solution over each element is a linear combination of a set of element basis functions. Each basis function has an associated node, and at the node point the basis function has unit value. Thus the solution over the element is an interpolation between nodal values. The nodes are placed at regular intervals on each element, typically at the corners of the element and for more complicated elements at the midpoints. Adjacent elements share edge nodes and thus the element solutions are connected to form a solution over the whole domain.

The differential equation in its variational form can be put into the form of a matrix equation [32]. The basis functions are chosen and the nodal values are unknown. Since the elements are connected into the domain, the element matrix equations can be combined into a global matrix equation. This equation has dimension N, where N is the number of nodes in the model. Boundary conditions are applied to the matrix equation, directly affecting the nodes along the boundary. The matrix can then be solved for the nodal values and thus for the state variable over the entire domain. The accuracy of the solution is related to the ratio of the density of nodes to the derivative of the state variable. Accurate models have high node densities in regions of large change of the state variable. Models can be refined by adding nodes until the solution converges.

This research employs the commercial finite element analysis package ANSYS version 4.4A, produced by Swanson Associates Corp., running on a Sun Sparcstation computer. This software was used to construct an element

model of resonant microstructures. This model was used to predict the resonant frequencies and mode shapes for loaded and unloaded devices were found using a modal analysis. The amplitude versus frequency response characteristic was found using the same model in a reduced dynamic analysis.

The analysis procedure using ANSYS can be divided into three sections. The first section, preprocessing, completely defines the model. This definition includes the type of analysis, material properties, model geometry, division into elements and nodes and the boundary conditions. The second section, solving, constructs the matrix equation from the model and solves it for the nodal values. This solution requires very little operator input in ANSYS. The final section, post processing, takes the raw solution data and generates graphs and contour images to make the results more meaningful to the operator.

Sections B.1 and B.2 explain the procedure used in generating the FEA models used to obtain the results in section 5.2.1.

B.1 Modal Analysis

A detailed listing of all input and output for the modal analysis is provided in appendix C.1. After entering the ANSYS program, the preprocessor "/prep7" was entered to define the model. From within the preprocessor, the "kan 2" analysis type was selected. An element of type "stif 45", a three dimensional structural brick with 8 nodes at the corners was selected. Using the "mp" command, the material properties of Young's modulus and density for silicon dioxide, as specified by Petersen [1], are associated with this element. For simplicity, the basis units of kilograms and micrometers are used. A three dimensional solid model of the cantilever is defined graphically. This particular model consists of a cantilever with overall dimensions of 200 μm long, 50 μm wide and 1 μm thick. As shown in figure B-1, the solid model consists of several volumes, each volume defined by 12 edge lines.

The elements are defined by segmenting each line manually using the line division command ("ldvs"). To keep the aspect ratio of any element below 5:1 [33], the lines are segmented into 5 μm sections. Elements and nodes are

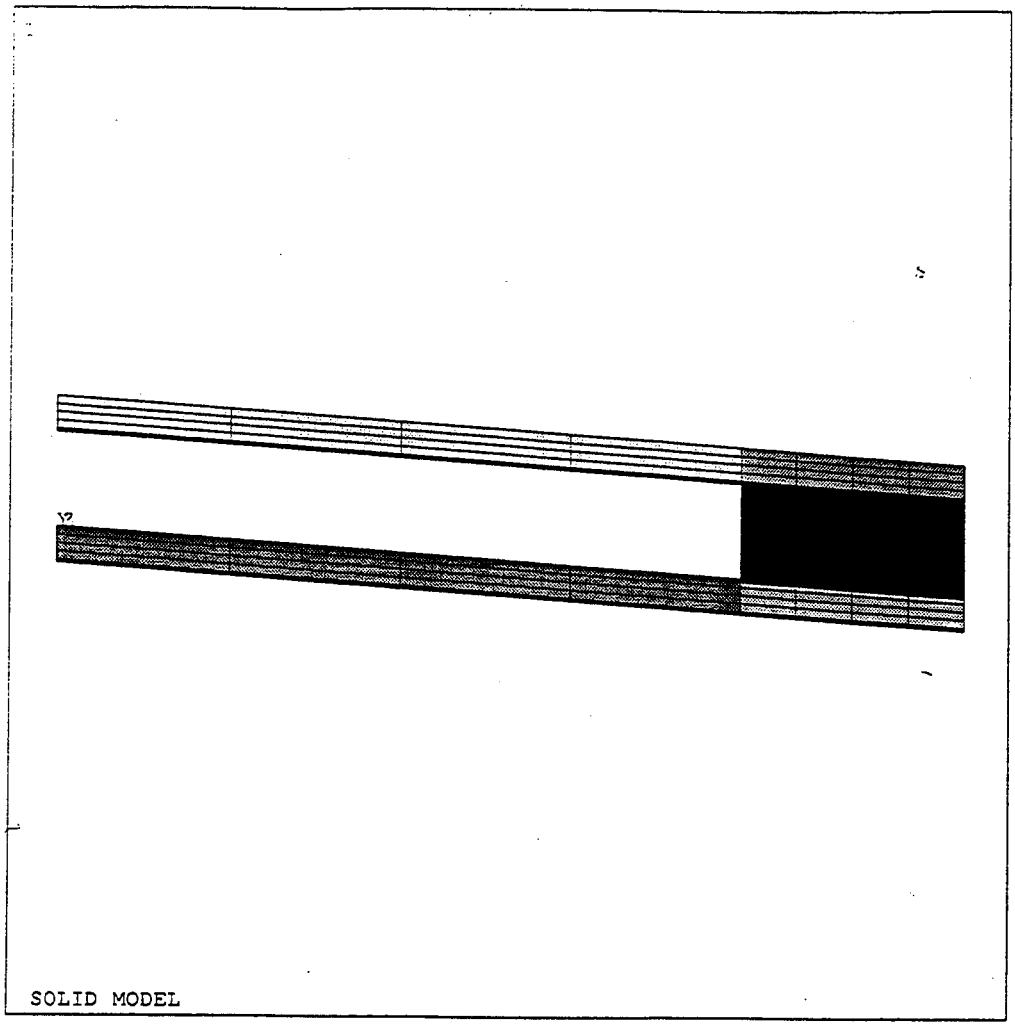

Figure B-1: FEA Solid Model

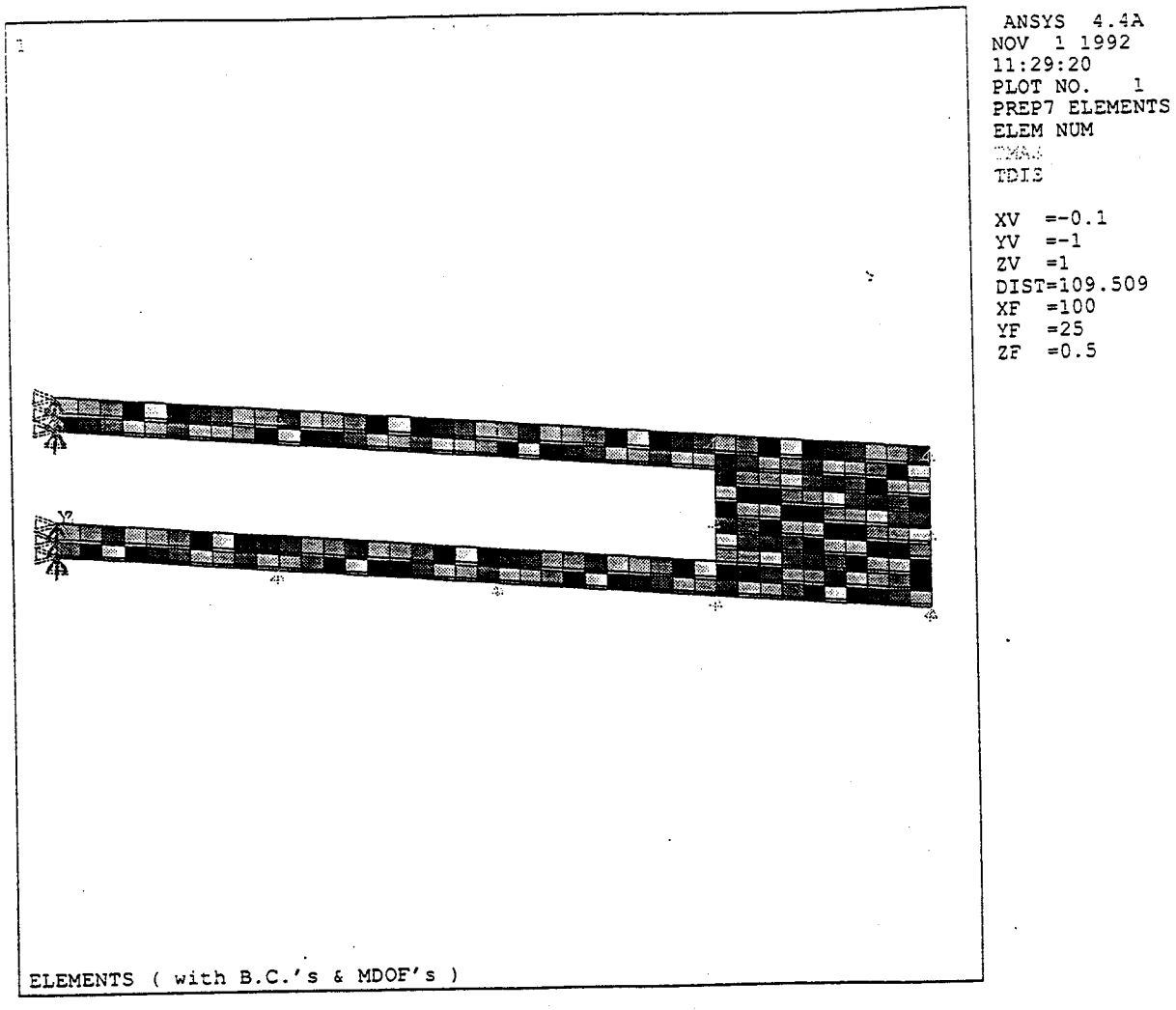

Figure B-2: FEA Elements

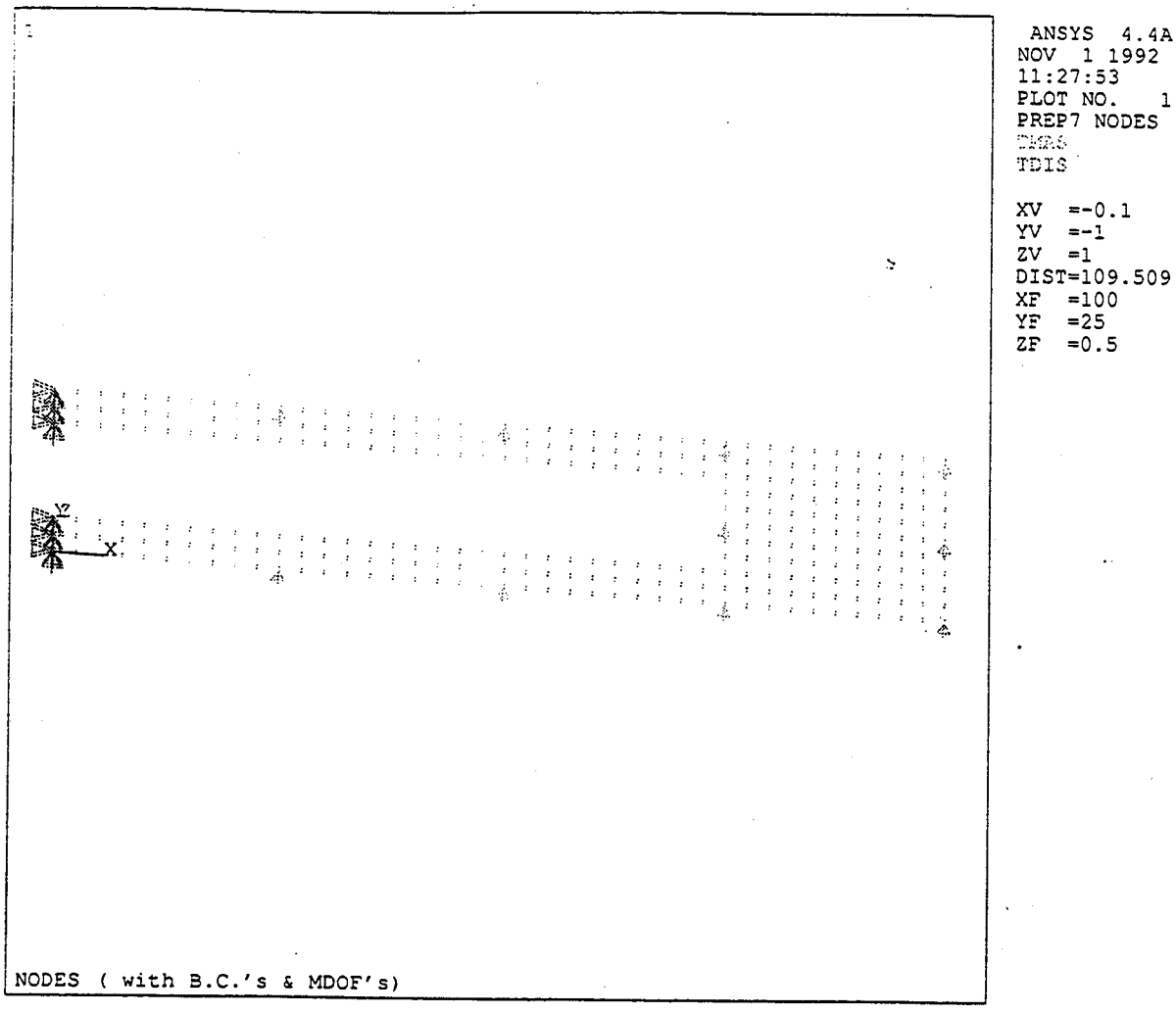

Figure B-3: FEA Nodes

generated over the solid model using the volume mesh command ("vmesh") on each volume. Figure B-2 shows the generated elements and figure B-3 shows the generated nodes.

The only boundary condition applied to this model is to clamp the base of the cantilever in three translational dimensions and three rotational dimensions. This simulates the clamping of the base of the cantilever due to its rigid connection to the substrate. This boundary condition is applied by isolating nodes along this boundary and constraining all of their degrees of freedom with the displacement ("d") command.

Mass loading was modeled using the point mass element "stif 21" located 5 μm from the tip of the cantilever. This element uses one node which is common to the structure. Thus the point mass will affect the solution of model. The point mass element is generated directly by specifying the number of the desired node in the element definition "e" command.

For determination of resonant frequencies and mode shapes, master degrees of freedom (master DOF) must be defined. A master degree of freedom is an individual degree of freedom on one node which is considered more important [33]. These master DOF's are monitored by ANSYS as it searches for resonant frequencies where these DOF's oscillate with large amplitude. Improper selection of master DOF's could result in missed resonances. A minimum of one master DOF for each resonant mode to be obtained must be provided. This research is interested in large amplitude resonances at relatively low frequencies. The thin cantilever structure is relatively inflexible in directions other than normal to its planar surface. For these reasons, 10 master DOF's were selected at equally spaced nodes in the direction normal to the planar surface.

The completed model was saved into a solution input file ("file 27") using the "afwrite" command. The solution was formed using the solver module by typing "/input,27". During the solution phase, various results are printed. The solution was post-processed using the module "/post1". The first resonant frequency data is loaded with the "set,1,1" command. The plot of mode shape shown in figure b4 is generated using the command "pldisp,2".

B.1.2 Reduced Harmonic Analysis

The listing for the reduced dynamic analysis is included in Appendix C.2. The reduced harmonic analysis "kan 6" was used to generate the amplitude frequency characteristic. The displacement of the tip of the cantilever over a range of frequencies from 14 kHz to 16 kHz was desired. This analysis used the same finite model formulated for the modal analysis. In order to obtain the mass shifted and unshifted characteristics on the same graph, a copy of the modeled cantilever with a mass load was made beside the original cantilever.

Both cantilevers were given a sinusoidal base excitation of 0.1 μm with the displacement "d" command. The experimentally determined Q of the device was placed into the model with the damping ratio "damprat" command.

The frequency range is segmented into intervals and the amplitude for all nodes at each frequency increment was computed by ANSYS. The graph in figure 5-11 used 50 increments.

The reduced harmonic analysis consists of a displacement solution pass followed by a stress solution pass. The stress pass computes stresses and displacements for each node at each frequency increment.

The post processor "/post26" was used to view the graph of the displacement versus frequency for a node on the tip of both cantilevers.

APPENDIX C: ANSYS FINITE ELEMENT ANALYSIS LISTINGS

C.1 Listing for Modal Analysis

```
THIS IS THE ANSYS(R) ENGINEERING ANALYSIS SYSTEM
COPYRIGHT(C) 1971, 1978, 1982, 1983, 1985, 1987, 1989, 1990
SWANSON ANALYSIS SYSTEMS, INC. AS AN UNPUBLISHED WORK.
PROPRIETARY DATA - UNAUTHORIZED USE, DISTRIBUTION, OR DUPLICATION
IS PROHIBITED.  ALL RIGHTS RESERVED.

IF RUNNING INTERACTIVELY, ENTER  /INTER
1
          ********** ANSYS INPUT DATA LISTING (FILE18) **********

   1  /COM,ANSYS REVISION 4.4   UP437 A 16    9.9414   11/ 1/1992
   2  /show,x11
   3  /prep7
   4  KAN,2
   5  kay,2,3
   6  kay,3,3
   7
   8  /COM, generate solid model
   9  /title MODAL ANALYSIS OF MICROMACHINED CANTILEVER
  10  k
  11  k,,150
  12  k,,200
  13  kgen,2,1,3,1,0,10
  14  kgen,2,1,6,1,0,40,0
  15  kgen,2,1,12,1,0,0,1,20
  16  v,1,2,5,4,21,22,25,24
  17  v,2,3,6,5,22,23,26,25
  18  v,5,6,9,8,25,26,29,28
  19  v,8,9,12,11,28,29,32,31
  20  v,7,8,11,10,27,28,31,30
  21
  22  /COM,define element type and material parameters
  23  et,1,45
  24  mp,EX,1,73000
  25  mp,DENS,1,.25e-14
  26
  27  /COM, mesh volumes
  28  ldvs,all,5
  29  vmesh,all
  30
  31  /COM,define boundary conditions, master DOF's
  32  nrsel,x,0
  33  d,all,all,0
  34  nall
  35  nrsel,z,0
  36  m,uz,pick
  37  KAN,2
  38  M,  187,UZ ,,,  ,  ,  ,  ,
  39  M,  250,UZ ,,,  ,  ,  ,  ,
  40  M,  379,UZ ,,,  ,  ,  ,  ,
  41  M,    2,UZ ,,,  ,  ,  ,  ,
  42  M,  265,UZ ,,,  ,  ,  ,  ,
  43  M,  381,UZ ,,,  ,  ,  ,  ,
  44  M,   22,UZ ,,,  ,  ,  ,  ,
```

```
  45 M,  463,UZ ,,,  ,  ,  ,  ,
  46 M,  473,UZ ,,,  ,  ,  ,  ,
  47 M,   12,UZ ,,,  ,  ,  ,  ,
  48 nall
  49
  50 /COM, zero mass element added 5 micron from tip
  51 /COM, to illustrate technique
  52 et,2,21
  53 r,1,0
  54 type,2
  55 e,419
  56
  57 /COM, plot nodes and elements
  58 /PBC,ALL,1
  59 /NUMBER,1
  60 /view,,-.1,1,.5
1
          ********** ANSYS INPUT DATA LISTING (FILE18) **********

  61 /title, NODES
  62 nplot
  63 /title,ELEMENTS
  64 eplot
  65
  66 /COM, save model
  67 afwr
  68 fini
  69
  70 /COM input to solver
  71 /input,27
  72 fini
  73
  74 /COM view results in postprocessor
  75 /post1
  76 /show,x11
  77 /view,,-.1,-1,.5
  78 /title fundamental mode
  79 set,1,1
  80 pldisp,2
  81
  82 /title angular harmonic
  83 set,1,3
  84 pldisp,2
  85
  86 /title torsional harmonic
  87 set,1,2
  88 pldisp,2
  89
  90 /eof
  91 /eof
 ANSYS REVISION 4.4   UP437 A 16    9.9414   11/ 1/1992
1        ANSYS - ENGINEERING ANALYSIS SYSTEM  REVISION 4.4     A 16  SIMON FRASER UNI
MAY 1,1990
    ANSYS(R)  COPYRIGHT(C) 1971, 1978, 1982, 1983, 1985, 1987, 1989, 1990  SWANSON ANALYSIS
SYSTEMS, INC. AS UNPUBLISHED WORK.
```

```
   PROPRIETARY DATA - UNAUTHORIZED USE, DISTRIBUTION OR DUPLICATION IS PROHIBI
TED.  ALL RIGHTS RESERVED.
   FOR SUPPORT CALL CHAO C CHENG     PHONE (604) 291-3820   TWX

 TITLE                                        12.8792 NOV 1,1992 CP=     2.640
**UNIVERSITY VERSION FOR EDUCATIONAL PURPOSES ONLY**

      ***** ANSYS ANALYSIS DEFINITION (PREP7) *****

ANALYSIS TYPE= 2  (MODE-FREQUENCY ANALYSIS)

EXPAND FIRST  3 MODE SHAPES (KAY(2)=  3)

PRINT THE FIRST  3 REDUCED MODE SHAPES (KAY(3)=  3)
generate solid model

NEW TITLE= MODAL ANALYSIS OF MICROMACHINED CANTILEVER


KEYPOINT   0  X,Y,Z=    0.        0.        0.    IN CSYS= 0

  KEYPOINT NUMBER =   1

KEYPOINT   0  X,Y,Z=  150.000     0.        0.    IN CSYS= 0

  KEYPOINT NUMBER =   2

KEYPOINT   0  X,Y,Z=  200.000     0.        0.    IN CSYS= 0

  KEYPOINT NUMBER =   3

GENERATE  2 TOTAL SETS OF KEYPOINTS
 SET IS FROM  1 TO  3 IN STEPS OF  1
 DX,DY,DZ=   0.     10.0      0.      CSYS= 0

GENERATE  2 TOTAL SETS OF KEYPOINTS
 SET IS FROM  1 TO  6 IN STEPS OF  1
 DX,DY,DZ=   0.     40.0      0.      CSYS= 0

GENERATE  2 TOTAL SETS OF KEYPOINTS
 SET IS FROM  1 TO 12 IN STEPS OF  1
 DX,DY,DZ=   0.      0.      1.00     CSYS= 0
 KEYPOINT INCREMENT =  20

VOLUME CONNECTING KEYPOINTS   1   2   5   4  21  22  25  24
  (GENERATED LINE SEGMENTS AND AREAS FITTED IN ACTIVE CSYS = 0)

  VOLUME NUMBER=   1

VOLUME CONNECTING KEYPOINTS   2   3   6   5  22  23  26  25
  (GENERATED LINE SEGMENTS AND AREAS FITTED IN ACTIVE CSYS = 0)

  VOLUME NUMBER=   2

VOLUME CONNECTING KEYPOINTS   5   6   9   8  25  26  29  28
```

(GENERATED LINE SEGMENTS AND AREAS FITTED IN ACTIVE CSYS = 0)

VOLUME NUMBER= 3

VOLUME CONNECTING KEYPOINTS 8 9 12 11 28 29 32 31
(GENERATED LINE SEGMENTS AND AREAS FITTED IN ACTIVE CSYS = 0)

VOLUME NUMBER= 4

VOLUME CONNECTING KEYPOINTS 7 8 11 10 27 28 31 30
(GENERATED LINE SEGMENTS AND AREAS FITTED IN ACTIVE CSYS = 0)

VOLUME NUMBER= 5
define element type and material parameters

ELEMENT TYPE 1 USES STIF 45
KEYOPT(1-9)= 0 0 0 0 0 0 0 0 0
INOPR= 0 NUMBER OF NODES= 8

ISOPAR. STRESS SOLID, 3-D

CURRENT NODAL DOF SET IS UX UY UZ
THREE-DIMENSIONAL STRUCTURE

MATERIAL 1 COEFFICIENTS OF EX VS. TEMP EQUATION
C0 = 73000.00

PROPERTY TABLE EX MAT= 1 NUM. POINTS= 2
TEMPERATURE DATA TEMPERATURE DATA
-9999.0 73000. 9999.0 73000.

MATERIAL 1 COEFFICIENTS OF DENS VS. TEMP EQUATION
C0 = 0.2500000E-14

PROPERTY TABLE DENS MAT= 1 NUM. POINTS= 2
TEMPERATURE DATA TEMPERATURE DATA
-9999.0 0.25000E-14 9999.0 0.25000E-14
mesh volumes

SET DIVISIONS ON ALL SELECTED UNMESHED LINE SEGMENTS
FOR ELEMENT SIZE = 5.0000 -- SPACING RATIO = 1.0000

GENERATE NODES AND ELEMENTS IN ALL SELECTED VOLUMES

NUMBER OF VOLUMES MESHED = 5
MAXIMUM NODE NUMBER = 602
MAXIMUM ELEMENT NUMBER = 220
define boundary conditions, master DOF's

NRSE FOR LABEL= X BETWEEN 0. AND 0. KABS= 0.
TOLERANCE= 0.100000E-05

12 NODES (OF 602 DEFINED) SELECTED BY NRSE COMMAND.

SPECIFIED DISP ALL FOR ALL SELECTED NODES

```
 VALUES=    0.       0.    ADDITIONAL DOFS=

  602 NODES (OF   602 DEFINED) SELECTED BY NALL COMMAND.

NRSE FOR LABEL= Z    BETWEEN    0.    AND    0.    KABS= 0.
 TOLERANCE= 0.100000E-05

  301 NODES (OF   602 DEFINED) SELECTED BY NRSE COMMAND.

***WARNING ***                  CP=   13.880  TIME= 12.88500
BAD M COMMAND.
NODE NUMBER MUST BE GREATER THAN ZERO.

ANALYSIS TYPE= 2  (MODE-FREQUENCY ANALYSIS)

***WARNING ***                  CP=   13.920  TIME= 12.88528
PREVIOUSLY SET KAY VALUES MAY NOT
BE VALID FOR THIS ANALYSIS TYPE.  PLEASE CHECK.
KAY 1 TO  5=   0.  3.  3.  0.  0.
KAY 6 TO 10=   0.  0.  0.  0.  0.

MASTER DOF UZ  FOR SELECTED NODES IN RANGE  187 TO  187 IN STEPS OF  1
ADDITIONAL DOFS=
NUMBER OF MASTER DOF=   1

MASTER DOF UZ  FOR SELECTED NODES IN RANGE  250 TO  250 IN STEPS OF  1
ADDITIONAL DOFS=
NUMBER OF MASTER DOF=   2

MASTER DOF UZ  FOR SELECTED NODES IN RANGE  379 TO  379 IN STEPS OF  1
ADDITIONAL DOFS=
NUMBER OF MASTER DOF=   3

MASTER DOF UZ  FOR SELECTED NODES IN RANGE    2 TO    2 IN STEPS OF  1
ADDITIONAL DOFS=
NUMBER OF MASTER DOF=   4

MASTER DOF UZ  FOR SELECTED NODES IN RANGE  265 TO  265 IN STEPS OF  1
ADDITIONAL DOFS=
NUMBER OF MASTER DOF=   5

MASTER DOF UZ  FOR SELECTED NODES IN RANGE  381 TO  381 IN STEPS OF  1
ADDITIONAL DOFS=
NUMBER OF MASTER DOF=   6

MASTER DOF UZ  FOR SELECTED NODES IN RANGE   22 TO   22 IN STEPS OF  1
ADDITIONAL DOFS=
NUMBER OF MASTER DOF=   7

MASTER DOF UZ  FOR SELECTED NODES IN RANGE  463 TO  463 IN STEPS OF  1
ADDITIONAL DOFS=
NUMBER OF MASTER DOF=   8

MASTER DOF UZ  FOR SELECTED NODES IN RANGE  473 TO  473 IN STEPS OF  1
ADDITIONAL DOFS=
```

```
NUMBER OF MASTER DOF=   9

MASTER DOF UZ  FOR SELECTED NODES IN RANGE   12 TO   12 IN STEPS OF   1
ADDITIONAL DOFS=
NUMBER OF MASTER DOF=   10

  602 NODES (OF   602 DEFINED) SELECTED BY NALL COMMAND.
 zero mass element added 5 micron from tip
 to illustrate technique

ELEMENT TYPE  2 USES STIF 21
 KEYOPT(1-9)=  0  0  0    0  0  0    0  0  0
 INOPR=  0  NUMBER OF NODES=  1

 GENERAL MASS

CURRENT NODAL DOF SET IS  UX   UY   UZ   ROTX ROTY ROTZ
 THREE-DIMENSIONAL STRUCTURE

 REAL CONSTANT SET   1  ITEMS   1 TO   6
    0.       0.       0.       0.       0.       0.

ELEMENT TYPE SET TO  2
ELEMENT  221   419
 plot nodes and elements

ALL  BOUNDARY CONDITION PLOT KEY =  1

NUMBER KEY SET TO  1  -1=NONE  0=BOTH  1=COLOR  2=NUMBER

VIEW POINT FOR WINDOW  1-0.10000     1.0000     0.50000

NEW TITLE=  NODES


NEW TITLE= ELEMENTS

 save model

*** NOTE ***
DATA CHECKED - NO FATAL ERRORS FOUND.
CHECK OUTPUT FOR POSSIBLE WARNING MESSAGES.

*** PREP7 GLOBAL STATUS ***

TITLE= ELEMENTS
ANALYSIS TYPE=   2
NUMBER OF ELEMENT TYPES=   2
  221 ELEMENTS CURRENTLY SELECTED.  MAX ELEMENT NUMBER =   221
  602 NODES CURRENTLY SELECTED.    MAX NODE NUMBER =     602
   24 KEYPOINTS CURRENTLY SELECTED. MAX KEYPOINT NUMBER =  32
   44 LINE SEG CURRENTLY SELECTED.  MAX LINE SEG NUMBER =  44
   26 AREAS CURRENTLY SELECTED.    MAX AREA NUMBER =      26
    5 VOLUMES CURRENTLY SELECTED.  MAX VOL. NUMBER =       5
MAXIMUM LINEAR PROPERTY NUMBER=   1
```

```
MAXIMUM REAL CONSTANT SET NUMBER=    1
ACTIVE COORDINATE SYSTEM=    0 (CARTESIAN)
NUMBER OF MASTER D.O.F.=   10
NUMBER OF IMPOSED DISPLACEMENTS=   36

ANALYSIS DATA WRITTEN ON FILE27

ALL CURRENT PREP7 DATA WRITTEN TO FILE16  NAME= file16.dat
 FOR POSSIBLE RESUME FROM THIS POINT


***** ROUTINE COMPLETED ***** CP =       21.070
input to solver

***** INPUT SWITCHED FROM FILE18 TO FILE27  NAME=file27.dat

NEW TITLE= ELEMENTS

1        ANSYS - ENGINEERING ANALYSIS SYSTEM  REVISION 4.4     A 16  SIMON FRASER UNI
MAY 1,1990
    ANSYS(R)  COPYRIGHT(C) 1971, 1978, 1982, 1983, 1985, 1987, 1989, 1990  SWANSON ANALYSIS
SYSTEMS, INC. AS UNPUBLISHED WORK.
    PROPRIETARY DATA - UNAUTHORIZED USE, DISTRIBUTION OR DUPLICATION IS PROHIBI
TED.  ALL RIGHTS RESERVED.
    FOR SUPPORT CALL CHAO C CHENG     PHONE (604) 291-3820   TWX

ELEMENTS                                          12.8886  NOV  1,1992 CP=    21.160
**UNIVERSITY VERSION FOR EDUCATIONAL PURPOSES ONLY**


    ***** NOTICE ***** THIS IS THE ANSYS GENERAL PURPOSE
    FINITE ELEMENT COMPUTER PROGRAM.  NEITHER SWANSON ANALYSIS
    SYSTEMS, INC. NOR THE DISTRIBUTOR SUPPLYING THIS PROGRAM
    ASSUME ANY RESPONSIBILITY FOR THE VALIDITY, ACCURACY, OR
    APPLICABILITY OF ANY RESULTS OBTAINED FROM THE ANSYS SYSTEM.
    USERS MUST VERIFY THEIR OWN RESULTS.

    ANSYS(R)  COPYRIGHT(C)  1971, 1978, 1982, 1983, 1985, 1987, 1989, 1990
    SWANSON ANALYSIS SYSTEMS, INC. AS AN UNPUBLISHED WORK.
    PROPRIETARY DATA - UNAUTHORIZED USE, DISTRIBUTION, OR DUPLICATION
    IS PROHIBITED.  ALL RIGHTS RESERVED.

    SWANSON ANALYSIS SYSTEMS,INC. IS ENDEAVORING TO MAKE THE
    ANSYS PROGRAM AS COMPLETE, ACCURATE, AND EASY TO USE AS
    POSSIBLE.  SUGGESTIONS AND COMMENTS ARE WELCOMED.  ANY
    ERRORS ENCOUNTERED IN EITHER THE DOCUMENTATION OR THE
    RESULTS SHOULD BE IMMEDIATELY BROUGHT TO OUR ATTENTION.


        ***** ANALYSIS OPTIONS *****

                    VALUE

ANALYSIS TYPE.....    2
KAY(2).....    3
```

KAY(3)..... 3
REFERENCE TEMPERATURE.... 0.00

***** ELEMENT TYPES *****

TYPE STIF DESCRIPTION KEY OPTIONS NJ INOTPR
1 2 3 4 5 6 7 8 9

NUMBER OF ELEMENT TYPES= 2

***** TABLE OF ELEMENT REAL CONSTANTS *****
NO.

NUMBER OF REAL CONSTANT SETS= 1

***** ELEMENT DEFINITIONS *****

ELEMENT NODES MAT TYPE ELEMENT REAL CONSTANTS

SWITCHED TO FIXED FORMAT INPUT

INTEGER STORAGE REQUIREMENTS FOR ELEMENT INPUT CP= 21.710 TIME= 12.88
917
FIXED DATA = 1018 TEMPORARY DATA = 1204 TOTAL= 2222
FIXED AVAIL= 1000000 TEMPORARY AVAIL= 1000000 TOTAL AVAIL= 1000000
MAXIMUM NODE NUMBER FOR AVAILABLE AUXILIARY MEMORY SIZE= 499490

NUMBER OF ELEMENTS = 221 MAXIMUM NODE NUMBER USED = 602

***** NODE DEFINITIONS *****

LOCATION ROTATION (DEGREES)

NODE X Y Z THXY THYZ THXZ
(OR R) (OR THETA) (OR PHI) (OR RT) (TZ OR TP) (RZ OR RP)

SWITCHED TO FIXED FORMAT INPUT

XMIN= 0. XMAX= 200.0 YMIN= 0. YMAX= 50.00 ZMIN= 0. ZMAX= 1.000

INTEGER STORAGE REQUIREMENTS FOR NODE INPUT CP= 22.800 TIME= 12.8894
4
FIXED DATA = 1018 TEMPORARY DATA = 7224 TOTAL= 8242

FIXED AVAIL= 1000000 TEMPORARY AVAIL= 1000000 TOTAL AVAIL= 1000000
MAXIMUM NODE NUMBER FOR AVAILABLE AUXILIARY MEMORY SIZE= 166496

***** MATERIAL PROPERTIES *****

MAXIMUM MATERIAL NUMBER= 1

***** MASTER DEGREES OF FREEDOM *****

NODE DEGREES OF FREEDOM LIST

NUMBER OF SPECIFIED MASTER D.O.F.= 10
TOTAL NUMBER OF MASTER D.O.F. = 10

INTEGER STORAGE REQUIREMENTS FOR MATERIALS, ETC. INPUT CP= 23.270 TIME= 1
2.89000
FIXED DATA = 1018 TEMPORARY DATA = 0 TOTAL= 1018
FIXED AVAIL= 1000000 TEMPORARY AVAIL= 1000000 TOTAL AVAIL= 1000000

INTEGER STORAGE REQUIREMENTS FOR LOAD DATA INPUT CP= 23.610 TIME= 12.
89028
FIXED DATA = 1302 TEMPORARY DATA = 0 TOTAL= 1302
FIXED AVAIL= 1000000 TEMPORARY AVAIL= 1000000 TOTAL AVAIL= 1000000

***** CENTROID, MASS, AND MASS MOMENTS OF INERTIA *****

CALCULATIONS ASSUME ELEMENT MASS AT ELEMENT CENTROID

TOTAL MASS = 0.13750E-10

CENTROID	MOM. OF INERTIA ABOUT ORIGIN	MOM. OF INERTIA ABOUT CENTROID
XC = 120.45	IXX = 0.1293E-07	IXX = 0.4336E-08
YC = 25.000	IYY = 0.2489E-06	IYY = 0.4943E-07
ZC = 0.50000	IZZ = 0.2619E-06	IZZ = 0.5376E-07
	IXY = -0.4141E-07	IXY = -0.1985E-22
	IYZ = -0.1719E-09	IYZ = 0.
	IZX = -0.8281E-09	IZX = 0.

ONLY THE FIRST REAL CONSTANT MASS TERM IS USED FOR THE STIF21 ELEMENTS.

*** MASS SUMMARY BY ELEMENT TYPE ***

TYPE	MASS
1	0.137500E-10

RANGE OF ELEMENT MAXIMUM STIFFNESS IN GLOBAL COORDINATES

```
MAXIMUM= 0.259238E+06  AT ELEMENT     1.
MINIMUM= 0.259238E+06  AT ELEMENT    52.

 INTEGER STORAGE REQUIREMENTS FOR ELEMENT FORMULATION          CP=   56.600 TIME
= 12.90083
FIXED DATA =   1302  TEMPORARY DATA =      0  TOTAL=   1302
FIXED AVAIL= 1000000  TEMPORARY AVAIL= 1000000  TOTAL AVAIL= 1000000

 *** ELEMENT STIFFNESS FORMULATION TIMES
 TYPE  NUMBER  STIF  TOTAL CP   AVE CP

  1     220    45    26.800    0.122
  2       1    21     0.000    0.000


TIME AT END OF ELEMENT STIFFNESS FORMULATION  CP=    56.600


MAXIMUM IN-CORE WAVE FRONT ALLOWED FOR REQUESTED MEMORY SIZE=  704.

 INTEGER STORAGE REQUIREMENTS FOR WAVE FRONT MATRIX SOLUTION     CP=   96.640 T
IME= 12.91333
FIXED DATA =   1302  TEMPORARY DATA =  27848  TOTAL=  29150
FIXED AVAIL= 1000000  TEMPORARY AVAIL= 1000000  TOTAL AVAIL= 1000000


MAXIMUM IN-CORE WAVE FRONT=   116.


   MATRIX SOLUTION TIMES
 READ IN ELEMENT STIFFNESSES  CP=        3.580


 NODAL COORD. TRANSFORMATION  CP=        0.000
 MATRIX TRIANGULARIZATION     CP=       36.050


TIME AT END OF MATRIX TRIANGULARIZATION  CP=       96.670
EQUATION SOLVER MAXIMUM PIVOT= 0.92583E+06 AT NODE  392. UZ
EQUATION SOLVER MINIMUM PIVOT=  35.743    AT NODE  419. UY


TIME AT START OF EIGENVALUE EXTRACTION  CP=     96.750


NUMBER OF MODES AVAILABLE FROM REDUCED MATRICES=  10.


EIGENVALUE EXTRACTION TIME  CP=      0.100

 INTEGER STORAGE REQUIREMENTS FOR EIGENVALUE EXTRACTION          CP=   96.960 TIM
E= 12.91389
FIXED DATA =   1302  TEMPORARY DATA =   510  TOTAL=   1812
```

```
FIXED AVAIL= 1000000  TEMPORARY AVAIL= 1000000   TOTAL AVAIL= 1000000

*** NOTE ***
SOLUTION PRINTOUT SUPPRESSED WITH NPRINT = 0

 INTEGER STORAGE REQUIREMENTS FOR BACK SUBSTITUTION          CP=  100.800 TIME= 1
2.91583
FIXED DATA =   1302  TEMPORARY DATA =   7238  TOTAL=   8540
FIXED AVAIL= 1000000  TEMPORARY AVAIL= 1000000  TOTAL AVAIL= 1000000

 INTEGER STORAGE REQUIREMENTS FOR REDUCED MODAL OUTPUT       CP=  104.010 TIM
E= 12.91694
FIXED DATA =   1302  TEMPORARY DATA =    540  TOTAL=   1842
FIXED AVAIL= 1000000  TEMPORARY AVAIL= 1000000  TOTAL AVAIL= 1000000


 *** STORAGE REQUIREMENT SUMMARY
MAXIMUM FIXED MEMORY USED   =     1302
MAXIMUM TEMPORARY MEMORY USED=    27848
MAXIMUM TOTAL MEMORY USED   =     29150
MAXIMUM TEMPORARY AVAILABLE =    998696


 *** PROBLEM STATISTICS
 NO. OF ACTIVE DEGREES OF FREEDOM =  1760
 R.M.S. WAVEFRONT SIZE =  68.0
 NUMBER OF MASTER DEGREES OF FREEDOM =  10



 *** ANSYS BINARY FILE STATISTICS
 BUFFER SIZE USED= 2048
 POST DATA WRITTEN ON FILE12

***** END OF INPUT ENCOUNTERED ON FILE27.  FILE27 REWOUND

***** INPUT FILE SWITCHED FROM FILE27 TO FILE18

1        ANSYS - ENGINEERING ANALYSIS SYSTEM  REVISION 4.4     A 16 -SIMON FRASER UNI
MAY 1,1990
    ANSYS(R)  COPYRIGHT(C) 1971, 1978, 1982, 1983, 1985, 1987, 1989, 1990  SWANSON ANALYSIS
SYSTEMS, INC. AS UNPUBLISHED WORK.
    PROPRIETARY DATA - UNAUTHORIZED USE, DISTRIBUTION OR DUPLICATION IS PROHIBI
TED.  ALL RIGHTS RESERVED.
    FOR SUPPORT CALL CHAO C CHENG     PHONE (604) 291-3820   TWX

 ELEMENTS                                          12.9175  NOV  1,1992 CP=   104.160
 **UNIVERSITY VERSION FOR EDUCATIONAL PURPOSES ONLY**


***** ANSYS SOLUTION PHASE RUN TIME ESTIMATOR *****

 COMPUTER = SUN4              NUMBER OF MASTER DOF =  10
 ANALYSIS TYPE =  2          RMS WAVE FRONT =  68
```

```
NUMBER OF ACTIVE NODES =   294  TOTAL NO. OF ITERATIONS =    3
MAX. DOF PER NODE =  6         STIFF. MATRIX SAVE KEY = 0
NUMBER OF MATRICES = 2         ELEM. MATRIX SAVE KEY = 0
NUMBER OF STRESS SOLUTIONS=  3 ROTATED NODE FRACTION= 0.000

 STIF NUMBER  FORM. TIME STRESS TIME   NAME
  21    1      0.001      0.000 GENERAL MASS
  45   220     0.168      0.043 ISOPAR. STRESS SOLID, 3-D


              FIRST    SUBSEQUENT
 ANALYSIS PHASE     ITERATION  ITERATIONS    TOTAL

ELEMENT FORMULATION      44.53      0.00     44.53
NODE ROTATION             0.00      0.00      0.00
WAVE FRONT SOLUTION      35.38      0.00     35.38
HOUSEHOLDER EIGEN CALC    0.13                 0.13
BACK SUBSTITUTION         0.87      0.87      2.60
ELEMENT STRESSES         11.40     11.40     34.19
NODAL FORCES              4.89      4.89     14.66

  TOTAL TIME (SEC)       97.19     17.15    131.49


***** ROUTINE COMPLETED ***** CP =      104.240
view results in postprocessor
1        ANSYS - ENGINEERING ANALYSIS SYSTEM  REVISION 4.4     A 16  SIMON FRASER UNI
MAY 1,1990
    ANSYS(R)  COPYRIGHT(C) 1971, 1978, 1982, 1983, 1985, 1987, 1989, 1990  SWANSON ANALYSIS
SYSTEMS, INC. AS UNPUBLISHED WORK.
    PROPRIETARY DATA - UNAUTHORIZED USE, DISTRIBUTION OR DUPLICATION IS PROHIBI
TED.  ALL RIGHTS RESERVED.
    FOR SUPPORT CALL CHAO C CHENG     PHONE (604) 291-3820   TWX

ELEMENTS                                          12.9181 NOV  1,1992 CP=   104.460
**UNIVERSITY VERSION FOR EDUCATIONAL PURPOSES ONLY**

      ***** ANSYS RESULTS INTERPRETATION (POST1) *****

VIEW POINT FOR WINDOW  1-0.10000   -1.0000    0.50000

NEW TITLE= fundamental mode


USE LOAD STEP    1  ITERATION    1  SECTION   1  FOR LOAD CASE    1



GEOMETRY STORED FOR   602  NODES   221  ELEMENTS
 TITLE= ELEMENTS

DISPLACEMENT STORED FOR  602 NODES

FOR LOAD STEP=    1  ITERATION=    1  SECTION=  1
 FREQ=  15343.7     LOAD CASE=  1
```

TITLE= ELEMENTS

PRODUCE DISPLACEMENT PLOT, KUND= 2

NEW TITLE= angular harmonic

USE LOAD STEP 1 ITERATION 3 SECTION 1 FOR LOAD CASE 1

DISPLACEMENT STORED FOR 602 NODES

FOR LOAD STEP= 1 ITERATION= 3 SECTION= 1
FREQ= 124642. LOAD CASE= 1
TITLE= angular harmonic

PRODUCE DISPLACEMENT PLOT, KUND= 2

NEW TITLE= torsional harmonic

USE LOAD STEP 1 ITERATION 2 SECTION 1 FOR LOAD CASE 1

DISPLACEMENT STORED FOR 602 NODES

FOR LOAD STEP= 1 ITERATION= 2 SECTION= 1
FREQ= 117390. LOAD CASE= 1
TITLE= ELEMENTS

PRODUCE DISPLACEMENT PLOT, KUND= 2

/EOF ENCOUNTERED ON FILE18

PREP7 AFWRITE OR SFWRITE WARNING MESSAGES = 0
NUMBER OF SOLUTION PHASE WARNING MESSAGES = 0

***** PROBLEM TERMINATED BY INDICATED ERROR(S) OR BY END OF INPUT DATA *****

***** RUN COMPLETED ***** CP= 106.0000 TIME= 12.9194

C.2 Listing for Reduced Harmonic Analysis

```
THIS IS THE ANSYS(R) ENGINEERING ANALYSIS SYSTEM
COPYRIGHT(C) 1971, 1978, 1982, 1983, 1985, 1987, 1989, 1990
SWANSON ANALYSIS SYSTEMS, INC. AS AN UNPUBLISHED WORK.
PROPRIETARY DATA - UNAUTHORIZED USE, DISTRIBUTION, OR DUPLICATION
IS PROHIBITED. ALL RIGHTS RESERVED.

IF RUNNING INTERACTIVELY, ENTER /INTER
1
          ********** ANSYS INPUT DATA LISTING (FILE18) **********

  1 /COM,ANSYS REVISION 4.4   UP437 A 16    9.9414   11/ 1/1992
  2 /show,x11
  3 /prep7
  4 KAN,6
  5
  6 /COM, generate solid model
  7 /title REDUCED HARMONIC ANALYSIS OF MICROMACHINED CANTILEVER
  8 k
  9 k,,150
 10 k,,200
 11 kgen,2,1,3,1,0,10
 12 kgen,2,1,6,1,0,40,0
 13 kgen,2,1,12,1,0,0,1,20
 14 v,1,2,5,4,21,22,25,24
 15 v,2,3,6,5,22,23,26,25
 16 v,5,6,9,8,25,26,29,28
 17 v,8,9,12,11,28,29,32,31
 18 v,7,8,11,10,27,28,31,30
 19
 20 /COM generate a second cantilever for shifted with mass curve
 21 vgen,2,1,5,1,,15
 22
 23
 24 /COM,define element type and material parameters
 25 et,1,45
 26 mp,EX,1,73000
 27 mp,DENS,1,.25e-14
 28
 29 /COM, mesh volumes
 30 ldvs,all,5
 31 vmesh,all
 32
 33 /COM,define boundary conditions, master DOF's
 34 nrsel,x,0
 35 d,all,all,0
 36
 37 /COM, define a base excitation of 0.1 micron
 38 d,all,uz,0.1
 39
 40 nall
 41 nrsel,z,0
 42 m,uz,pick
 43 M,  187,UZ ,,,  ,  ,  ,  ,
 44 M,  250,UZ ,,,  ,  ,  ,  ,
```

```
  45 M,  379,UZ ,,,  ,  ,  ,  ,
  46 M,   2,UZ ,,,  ,  ,  ,  ,
  47 M,  265,UZ ,,,  ,  ,  ,  ,
  48 M,  381,UZ ,,,  ,  ,  ,  ,
  49 M,   22,UZ ,,,  ,  ,  ,  ,
  50 M,  463,UZ ,,,  ,  ,  ,  ,
  51 M,  473,UZ ,,,  ,  ,  ,  ,
  52 M,   12,UZ ,,,  ,  ,  ,  ,
  53 nall
  54
  55 /COM, 0.59 ng mass element added 5 micron from tip
  56 /COM, of first cantilever
  57 et,2,21
  58 r,1,0
  59 type,2
  60 e,419
1
          ********** ANSYS INPUT DATA LISTING (FILE18) **********

  61
  62 /COM apply a damping ratio corresponding to Q = 14.5
  63 dmprat, 0.0345
  64
  65 kbc,1
  66 iter,5
  67
  68
  69 /COM, plot nodes and elements
  70 /PBC,ALL,1
  71 /NUMBER,1
  72 /view,,-.1,1,.5
  73 /title, NODES
  74 nplot
  75 /title,ELEMENTS
  76 eplot
  77
  78 /COM, save model
  79 afwr
  80 fini
  81
  82 /COM input to solver (displacement pass)
  83 /input,27
  84 fini
  85
  86 /COM Solving (stress pass)
  87 /stress,,,,0
  88 nstress,5
  89 iter,5
  90 harfrq,14000,16000
  91 end
  92 fini
  93
  94 /COM, view results on postprocessor
  95 /post26
  96 disp,2,419,uz,load
```

```
  97  disp,3,872,uz,nold
  98  plvar,2
  99  fini
 100  /eof
ANSYS REVISION 4.4   UP437 A 16    9.9414   11/ 1/1992
1        ANSYS - ENGINEERING ANALYSIS SYSTEM  REVISION 4.4     A 16  SIMON FRASER UNI
MAY 1,1990
   ANSYS(R)  COPYRIGHT(C) 1971, 1978, 1982, 1983, 1985, 1987, 1989, 1990  SWANSON ANALYSIS
SYSTEMS, INC. AS UNPUBLISHED WORK.
   PROPRIETARY DATA - UNAUTHORIZED USE, DISTRIBUTION OR DUPLICATION IS PROHIBI
TED.  ALL RIGHTS RESERVED.
   FOR SUPPORT CALL CHAO C CHENG     PHONE (604) 291-3820   TWX

 TITLE                                              20.7636  NOV  1,1992 CP=     2.230
**UNIVERSITY VERSION FOR EDUCATIONAL PURPOSES ONLY**

      ***** ANSYS ANALYSIS DEFINITION (PREP7) *****

ANALYSIS TYPE= 6  (REDUCED HARMONIC RESPONSE ANALYSIS)
 generate solid model

NEW TITLE= REDUCED HARMONIC ANALYSIS OF MICROMACHINED CANTILEVER


KEYPOINT   0  X,Y,Z=     0.        0.        0.    IN CSYS= 0

  KEYPOINT NUMBER =    1

KEYPOINT   0  X,Y,Z=  150.000      0.        0.    IN CSYS= 0

  KEYPOINT NUMBER =    2

KEYPOINT   0  X,Y,Z=  200.000      0.        0.    IN CSYS= 0

  KEYPOINT NUMBER =    3

GENERATE   2 TOTAL SETS OF KEYPOINTS
 SET IS FROM   1 TO   3 IN STEPS OF   1
 DX,DY,DZ=    0.      10.0       0.       CSYS= 0

GENERATE   2 TOTAL SETS OF KEYPOINTS
 SET IS FROM   1 TO   6 IN STEPS OF   1
 DX,DY,DZ=    0.      40.0       0.       CSYS= 0

GENERATE   2 TOTAL SETS OF KEYPOINTS
 SET IS FROM   1 TO  12 IN STEPS OF   1
 DX,DY,DZ=    0.       0.      1.00      CSYS= 0
 KEYPOINT INCREMENT =   20

VOLUME CONNECTING KEYPOINTS   1   2   5   4  21  22  25  24
  (GENERATED LINE SEGMENTS AND AREAS FITTED IN ACTIVE CSYS = 0)

  VOLUME NUMBER=    1
```

```
VOLUME CONNECTING KEYPOINTS   2   3   6   5  22  23  26  25
 (GENERATED LINE SEGMENTS AND AREAS FITTED IN ACTIVE CSYS =  0)

  VOLUME NUMBER=    2

VOLUME CONNECTING KEYPOINTS   5   6   9   8  25  26  29  28
 (GENERATED LINE SEGMENTS AND AREAS FITTED IN ACTIVE CSYS =  0)

  VOLUME NUMBER=    3

VOLUME CONNECTING KEYPOINTS   8   9  12  11  28  29  32  31
 (GENERATED LINE SEGMENTS AND AREAS FITTED IN ACTIVE CSYS =  0)

  VOLUME NUMBER=    4

VOLUME CONNECTING KEYPOINTS   7   8  11  10  27  28  31  30
 (GENERATED LINE SEGMENTS AND AREAS FITTED IN ACTIVE CSYS =  0)

  VOLUME NUMBER=    5
generate a second cantilever for shifted with mass curve

GENERATE   2 TOTAL SETS OF VOLUMES
 SET IS FROM   1 TO   5 IN STEPS OF   1
 DX,DY,DZ=    0.      15.0       0.       CSYS= 0
define element type and material parameters

ELEMENT TYPE  1 USES STIF 45
 KEYOPT(1-9)=  0  0  0   0  0  0   0  0  0
 INOPR=  0  NUMBER OF NODES=  8

ISOPAR. STRESS SOLID, 3-D

CURRENT NODAL DOF SET IS  UX   UY   UZ
 THREE-DIMENSIONAL STRUCTURE

 MATERIAL  1       COEFFICIENTS OF EX  VS. TEMP EQUATION
 C0 =  73000.00

PROPERTY TABLE EX   MAT=  1 NUM. POINTS= 2
  TEMPERATURE    DATA  TEMPERATURE    DATA
  -9999.0    73000.    9999.0    73000.

 MATERIAL  1       COEFFICIENTS OF DENS VS. TEMP EQUATION
 C0 =  0.2500000E-14

PROPERTY TABLE DENS  MAT=  1 NUM. POINTS= 2
  TEMPERATURE    DATA  TEMPERATURE    DATA
  -9999.0    0.25000E-14 9999.0    0.25000E-14
 mesh volumes

SET DIVISIONS ON ALL SELECTED UNMESHED LINE SEGMENTS
   FOR ELEMENT SIZE =  5.0000    -- SPACING RATIO =    1.0000

GENERATE NODES AND ELEMENTS  IN  ALL  SELECTED VOLUMES
```

```
NUMBER OF VOLUMES MESHED  =   10
MAXIMUM NODE NUMBER       =  1204
MAXIMUM ELEMENT NUMBER    =  440
define boundary conditions, master DOF's

NRSE FOR LABEL= X   BETWEEN    0.    AND    0.    KABS= 0.
 TOLERANCE= 0.100000E-05

  24 NODES (OF  1204  DEFINED) SELECTED BY NRSE  COMMAND.

SPECIFIED DISP ALL  FOR ALL SELECTED NODES
 VALUES=    0.       0.    ADDITIONAL DOFS=
 define a base excitation of 0.1 micron

SPECIFIED DISP UZ  FOR ALL SELECTED NODES
 VALUES= 0.10000       0.    ADDITIONAL DOFS=

 1204 NODES (OF  1204  DEFINED) SELECTED BY NALL  COMMAND.

NRSE FOR LABEL= Z   BETWEEN    0.    AND    0.    KABS= 0.
 TOLERANCE= 0.100000E-05

  602 NODES (OF  1204  DEFINED) SELECTED BY NRSE  COMMAND.

***WARNING ***                  CP=   16.750  TIME= 20.77000
BAD M COMMAND.
NODE NUMBER MUST BE GREATER THAN ZERO.

MASTER DOF UZ  FOR SELECTED NODES IN RANGE  187 TO  187 IN STEPS OF  1
ADDITIONAL DOFS=
NUMBER OF MASTER DOF=   1

MASTER DOF UZ  FOR SELECTED NODES IN RANGE  250 TO  250 IN STEPS OF  1
ADDITIONAL DOFS=
NUMBER OF MASTER DOF=   2

MASTER DOF UZ  FOR SELECTED NODES IN RANGE  379 TO  379 IN STEPS OF  1
ADDITIONAL DOFS=
NUMBER OF MASTER DOF=   3

MASTER DOF UZ  FOR SELECTED NODES IN RANGE   2 TO   2 IN STEPS OF  1
ADDITIONAL DOFS=
NUMBER OF MASTER DOF=   4

MASTER DOF UZ  FOR SELECTED NODES IN RANGE  265 TO  265 IN STEPS OF  1
ADDITIONAL DOFS=
NUMBER OF MASTER DOF=   5

MASTER DOF UZ  FOR SELECTED NODES IN RANGE  381 TO  381 IN STEPS OF  1
ADDITIONAL DOFS=
NUMBER OF MASTER DOF=   6

MASTER DOF UZ  FOR SELECTED NODES IN RANGE   22 TO   22 IN STEPS OF  1
ADDITIONAL DOFS=
NUMBER OF MASTER DOF=   7
```

```
MASTER DOF UZ  FOR SELECTED NODES IN RANGE  463 TO  463 IN STEPS OF  1
ADDITIONAL DOFS=
NUMBER OF MASTER DOF=  8

MASTER DOF UZ  FOR SELECTED NODES IN RANGE  473 TO  473 IN STEPS OF  1
ADDITIONAL DOFS=
NUMBER OF MASTER DOF=  9

MASTER DOF UZ  FOR SELECTED NODES IN RANGE  12 TO  12 IN STEPS OF  1
ADDITIONAL DOFS=
NUMBER OF MASTER DOF=  10

 1204 NODES (OF  1204  DEFINED) SELECTED BY NALL COMMAND.
6.59 ng mass element added 5 micron from tip
of first cantilever

ELEMENT TYPE  2 USES STIF 21
 KEYOPT(1-9)=  0 0 0   0 0 0   0 0 0
 INOPR=  0 NUMBER OF NODES=  1

GENERAL MASS

CURRENT NODAL DOF SET IS  UX   UY   UZ   ROTX ROTY ROTZ
 THREE-DIMENSIONAL STRUCTURE

 REAL CONSTANT SET  1  ITEMS  1 TO  6
    0.       0.       0.       0.       0.       0.

ELEMENT TYPE SET TO  2
ELEMENT  441   419
apply a damping ratio corresponding to Q = 14.5

DAMPING RATIO =     0.0345

STEP BOUNDARY CONDITION KEY= 1

NITTER=    5  NPRINT= 99900  NPOST=    5

ALL PRINT CONTROLS RESET TO 99900
 ALL POST DATA FILE CONTROLS RESET TO   5
plot nodes and elements

ALL  BOUNDARY CONDITION PLOT KEY =  1

NUMBER KEY SET TO  1  -1=NONE  0=BOTH  1=COLOR  2=NUMBER

VIEW POINT FOR WINDOW  1-0.10000     1.0000     0.50000

NEW TITLE=  NODES


NEW TITLE= ELEMENTS

save model
```

```
*** NOTE ***
DATA CHECKED - NO FATAL ERRORS FOUND.
CHECK OUTPUT FOR POSSIBLE WARNING MESSAGES.

*** PREP7 GLOBAL STATUS ***

TITLE= ELEMENTS
ANALYSIS TYPE=    6
NUMBER OF ELEMENT TYPES=    2
  441 ELEMENTS CURRENTLY SELECTED.  MAX ELEMENT NUMBER =   441
 1204 NODES CURRENTLY SELECTED.     MAX NODE NUMBER =    1204
   48 KEYPOINTS CURRENTLY SELECTED. MAX KEYPOINT NUMBER =   48
   88 LINE SEG CURRENTLY SELECTED.  MAX LINE SEG NUMBER =   88
   52 AREAS CURRENTLY SELECTED.     MAX AREA NUMBER =      52
   10 VOLUMES CURRENTLY SELECTED.   MAX VOL. NUMBER =      10
MAXIMUM LINEAR PROPERTY NUMBER=    1
MAXIMUM REAL CONSTANT SET NUMBER=    1
ACTIVE COORDINATE SYSTEM=    0 (CARTESIAN)
NUMBER OF MASTER D.O.F.=   10
NUMBER OF IMPOSED DISPLACEMENTS=   72

ANALYSIS DATA WRITTEN ON FILE27

ALL CURRENT PREP7 DATA WRITTEN TO FILE16  NAME= file16.dat
 FOR POSSIBLE RESUME FROM THIS POINT


***** ROUTINE COMPLETED ***** CP =       27.610
input to solver (displacement pass)

***** INPUT SWITCHED FROM FILE18 TO FILE27  NAME=file27.dat

NEW TITLE= ELEMENTS

1        ANSYS - ENGINEERING ANALYSIS SYSTEM  REVISION 4.4     A 16  SIMON FRASER UNI
MAY 1,1990
    ANSYS(R)  COPYRIGHT(C) 1971, 1978, 1982, 1983, 1985, 1987, 1989, 1990  SWANSON ANALYSIS
SYSTEMS, INC. AS UNPUBLISHED WORK.
    PROPRIETARY DATA - UNAUTHORIZED USE, DISTRIBUTION OR DUPLICATION IS PROHIBI
TED.  ALL RIGHTS RESERVED.
    FOR SUPPORT CALL CHAO C CHENG     PHONE (604) 291-3820   TWX

ELEMENTS                                          20.7744  NOV  1,1992 CP=    27.660
**UNIVERSITY VERSION FOR EDUCATIONAL PURPOSES ONLY**


    ***** NOTICE ***** THIS IS THE ANSYS GENERAL PURPOSE
    FINITE ELEMENT COMPUTER PROGRAM.  NEITHER SWANSON ANALYSIS
    SYSTEMS, INC. NOR THE DISTRIBUTOR SUPPLYING THIS PROGRAM
    ASSUME ANY RESPONSIBILITY FOR THE VALIDITY, ACCURACY, OR
    APPLICABILITY OF ANY RESULTS OBTAINED FROM THE ANSYS SYSTEM.
    USERS MUST VERIFY THEIR OWN RESULTS.

    ANSYS(R)  COPYRIGHT(C)  1971, 1978, 1982, 1983, 1985, 1987, 1989, 1990
```

SWANSON ANALYSIS SYSTEMS, INC. AS AN UNPUBLISHED WORK.
PROPRIETARY DATA - UNAUTHORIZED USE, DISTRIBUTION, OR DUPLICATION
IS PROHIBITED. ALL RIGHTS RESERVED.

SWANSON ANALYSIS SYSTEMS,INC. IS ENDEAVORING TO MAKE THE
ANSYS PROGRAM AS COMPLETE, ACCURATE, AND EASY TO USE AS
POSSIBLE. SUGGESTIONS AND COMMENTS ARE WELCOMED. ANY
ERRORS ENCOUNTERED IN EITHER THE DOCUMENTATION OR THE
RESULTS SHOULD BE IMMEDIATELY BROUGHT TO OUR ATTENTION.

***** ANALYSIS OPTIONS *****

VALUE

ANALYSIS TYPE 6
REFERENCE TEMPERATURE 0.00

***** ELEMENT TYPES *****

TYPE STIF DESCRIPTION KEY OPTIONS NJ INOTPR
1 2 3 4 5 6 7 8 9

NUMBER OF ELEMENT TYPES= 2

***** TABLE OF ELEMENT REAL CONSTANTS *****
NO.

NUMBER OF REAL CONSTANT SETS= 1

***** ELEMENT DEFINITIONS *****

ELEMENT NODES MAT TYPE ELEMENT REAL CONSTANTS

SWITCHED TO FIXED FORMAT INPUT

INTEGER STORAGE REQUIREMENTS FOR ELEMENT INPUT CP= 28.480 TIME= 20.77
500
FIXED DATA = 1018 TEMPORARY DATA = 2408 TOTAL= 3426
FIXED AVAIL= 1000000 TEMPORARY AVAIL= 1000000 TOTAL AVAIL= 1000000
MAXIMUM NODE NUMBER FOR AVAILABLE AUXILIARY MEMORY SIZE= 499490

NUMBER OF ELEMENTS = 441 MAXIMUM NODE NUMBER USED = 1204

***** NODE DEFINITIONS *****

NODE	X (OR R)	Y (OR THETA)	Z (OR PHI)	THXY (OR RT)	THYZ (TZ OR TP)	THXZ (RZ OR RP)
	LOCATION			ROTATION (DEGREES)		

SWITCHED TO FIXED FORMAT INPUT

XMIN= 0. XMAX= 200.0 YMIN= 0. YMAX= 65.00 ZMIN= 0. ZMAX= 1.000

INTEGER STORAGE REQUIREMENTS FOR NODE INPUT CP= 30.280 TIME= 20.7758
3
FIXED DATA = 1018 TEMPORARY DATA = 14448 TOTAL= 15466
FIXED AVAIL= 1000000 TEMPORARY AVAIL= 1000000 TOTAL AVAIL= 1000000
MAXIMUM NODE NUMBER FOR AVAILABLE AUXILIARY MEMORY SIZE= 166496

***** MATERIAL PROPERTIES *****

MAXIMUM MATERIAL NUMBER= 1

***** MASTER DEGREES OF FREEDOM *****

NODE DEGREES OF FREEDOM LIST

NUMBER OF SPECIFIED MASTER D.O.F.= 10
TOTAL NUMBER OF MASTER D.O.F. = 10

INTEGER STORAGE REQUIREMENTS FOR MATERIALS, ETC. INPUT CP= 30.880 TIME= 2
0.77639
FIXED DATA = 1018 TEMPORARY DATA = 0 TOTAL= 1018
FIXED AVAIL= 1000000 TEMPORARY AVAIL= 1000000 TOTAL AVAIL= 1000000

INTEGER STORAGE REQUIREMENTS FOR LOAD DATA INPUT CP= 31.290 TIME= 20.
77667
FIXED DATA = 2564 TEMPORARY DATA = 0 TOTAL= 2564
FIXED AVAIL= 1000000 TEMPORARY AVAIL= 1000000 TOTAL AVAIL= 1000000

***** CENTROID, MASS, AND MASS MOMENTS OF INERTIA *****

CALCULATIONS ASSUME ELEMENT MASS AT ELEMENT CENTROID

TOTAL MASS = 0.27500E-10

CENTROID	MOM. OF INERTIA ABOUT ORIGIN	MOM. OF INERTIA ABOUT CENTROID

```
XC =  120.45      IXX =  0.3927E-07    IXX =  0.1022E-07
YC =  32.500      IYY =  0.4979E-06    IYY =  0.9885E-07
ZC =  0.50000     IZZ =  0.5371E-06    IZZ =  0.1091E-06
                  IXY = -0.1077E-06    IXY =  0.2382E-21
                  IYZ = -0.4469E-09    IYZ =  0.
                  IZX = -0.1656E-08    IZX =  0.
ONLY THE FIRST REAL CONSTANT MASS TERM IS USED FOR THE STIF21  ELEMENTS.


*** MASS SUMMARY BY ELEMENT TYPE ***

TYPE     MASS
  1  0.275000E-10

RANGE OF ELEMENT MAXIMUM STIFFNESS IN GLOBAL COORDINATES


MAXIMUM= 0.259238E+06  AT ELEMENT     1.
MINIMUM= 0.259238E+06  AT ELEMENT     52.

 INTEGER STORAGE REQUIREMENTS FOR ELEMENT FORMULATION          CP=   84.800  TIME
= 20.79361
FIXED DATA =   2564  TEMPORARY DATA =      0  TOTAL=   2564
FIXED AVAIL= 1000000  TEMPORARY AVAIL= 1000000   TOTAL AVAIL= 1000000

 *** ELEMENT STIFFNESS FORMULATION TIMES
 TYPE  NUMBER  STIF  TOTAL CP   AVE CP

  1    440    45    43.770    0.099
  2      1    21     0.000    0.000


TIME AT END OF ELEMENT STIFFNESS FORMULATION  CP=     84.800


MAXIMUM IN-CORE WAVE FRONT ALLOWED FOR REQUESTED MEMORY SIZE=  574.

 INTEGER STORAGE REQUIREMENTS FOR WAVE FRONT MATRIX SOLUTION     CP=  174.290
TIME= 20.82222
FIXED DATA =   2564  TEMPORARY DATA =  47628  TOTAL=   50192
FIXED AVAIL= 1000000  TEMPORARY AVAIL= 1000000   TOTAL AVAIL= 1000000


MAXIMUM IN-CORE WAVE FRONT=   124.


   MATRIX SOLUTION TIMES
 READ IN ELEMENT STIFFNESSES  CP=        6.240


 NODAL COORD. TRANSFORMATION  CP=        0.000
 MATRIX TRIANGULARIZATION     CP=       82.760


TIME AT END OF MATRIX TRIANGULARIZATION  CP=       174.370
```

```
EQUATION SOLVER MAXIMUM PIVOT= 0.92583E+06 AT NODE  392. UZ
EQUATION SOLVER MINIMUM PIVOT= 0.11516     AT NODE  1146. UZ


TIME AT START OF HARMIC  CP=    174.400


TIME AT START OF FREQUENCIES  CP=    174.440

***** END OF INPUT ENCOUNTERED ON FILE27.  FILE27 REWOUND

***** INPUT FILE SWITCHED FROM FILE27 TO FILE18


 INTEGER STORAGE REQUIREMENTS FOR REDUCED HARMONIC RESPONSE      CP=  174.560
TIME= 20.82278
FIXED DATA =   2564  TEMPORARY DATA =    808  TOTAL=   3372
FIXED AVAIL= 1000000  TEMPORARY AVAIL= 1000000  TOTAL AVAIL= 1000000


 *** STORAGE REQUIREMENT SUMMARY
MAXIMUM FIXED MEMORY USED   =      2564
MAXIMUM TEMPORARY MEMORY USED=     47628
MAXIMUM TOTAL MEMORY USED   =      50192
MAXIMUM TEMPORARY AVAILABLE =     997436


 *** PROBLEM STATISTICS
 NO. OF ACTIVE DEGREES OF FREEDOM =  3530
 R.M.S. WAVEFRONT SIZE =  71.4
 NUMBER OF MASTER DEGREES OF FREEDOM =  10



 *** ANSYS BINARY FILE STATISTICS
 BUFFER SIZE USED= 2048
 ELEMENT MATRICES WRITTEN ON FILE02  (      4216976 BYTES)
 TRIANGULARIZED MATRIX WRITTEN ON FILE11  (      1923444 BYTES)
 REDUCED DISPLACEMENTS WRITTEN ON FILE10
1        ANSYS - ENGINEERING ANALYSIS SYSTEM  REVISION 4.4     A 16  SIMON FRASER UNI
MAY 1,1990
    ANSYS(R)  COPYRIGHT(C) 1971, 1978, 1982, 1983, 1985, 1987, 1989, 1990  SWANSON ANALYSIS
SYSTEMS, INC. AS UNPUBLISHED WORK.
    PROPRIETARY DATA - UNAUTHORIZED USE, DISTRIBUTION OR DUPLICATION IS PROHIBI
TED.  ALL RIGHTS RESERVED.
    FOR SUPPORT CALL CHAO C CHENG     PHONE (604) 291-3820   TWX

ELEMENTS                                          20.8231  NOV  1,1992 CP=   174.590
**UNIVERSITY VERSION FOR EDUCATIONAL PURPOSES ONLY**


***** ANSYS SOLUTION PHASE RUN TIME ESTIMATOR *****

COMPUTER = SUN4              NUMBER OF MASTER DOF =  10
```

```
ANALYSIS TYPE = 6          RMS WAVE FRONT = 72
NUMBER OF ACTIVE NODES = 589  TOTAL NO. OF ITERATIONS = 5
MAX. DOF PER NODE = 6       STIFF. MATRIX SAVE KEY = 0
NUMBER OF MATRICES = 3      ELEM. MATRIX SAVE KEY = 0
NUMBER OF STRESS SOLUTIONS= 5  ROTATED NODE FRACTION= 0.000

 STIF NUMBER  FORM. TIME  STRESS TIME  NAME
  21    1      0.001       0.000  GENERAL MASS
  45   440     0.168       0.043  ISOPAR. STRESS SOLID, 3-D


                FIRST    SUBSEQUENT
 ANALYSIS PHASE    ITERATION  ITERATIONS    TOTAL

ELEMENT FORMULATION      89.06      0.00     89.06
NODE ROTATION             0.00      0.00      0.00
WAVE FRONT SOLUTION     132.44      0.00    132.44
FREQUENCY EVALUATIONS     0.00      0.00      0.02
BACK SUBSTITUTION         1.84      1.84      9.20
ELEMENT STRESSES         22.80     22.80    113.98
NODAL FORCES             14.66     14.66     73.29

  TOTAL TIME (SEC)      260.79     39.30    417.97


***** ROUTINE COMPLETED ***** CP =      174.640
Solving (stress pass)
1        ANSYS - ENGINEERING ANALYSIS SYSTEM  REVISION 4.4     A 16  SIMON FRASER UNI
MAY 1,1990
   ANSYS(R)  COPYRIGHT(C) 1971, 1978, 1982, 1983, 1985, 1987, 1989, 1990  SWANSON ANALYSIS
SYSTEMS, INC. AS UNPUBLISHED WORK.
   PROPRIETARY DATA - UNAUTHORIZED USE, DISTRIBUTION OR DUPLICATION IS PROHIBI
TED.  ALL RIGHTS RESERVED.
   FOR SUPPORT CALL CHAO C CHENG     PHONE (604) 291-3820   TWX

                                          20.8231 NOV  1,1992 CP=   174.700
**UNIVERSITY VERSION FOR EDUCATIONAL PURPOSES ONLY**

***** ANSYS STRESS PASS *****


RUN MODE IS /EXEC

*** LOAD STEP  1  OPTIONS SPECIFICATIONS

NUMBER OF STRESS PASS CALCULATIONS=   5

PRINTOUT SUPPRESSED BY NPRINT =   0

 INTEGER STORAGE REQUIREMENTS FOR LOAD DATA INPUT          CP=  174.840  TIME= 20.
82333
FIXED DATA =  2566  TEMPORARY DATA =     0  TOTAL=  2566
FIXED AVAIL= 1000000  TEMPORARY AVAIL= 1000000  TOTAL AVAIL= 1000000

 INTEGER STORAGE REQUIREMENTS FOR HARMONIC STRESSES        CP=  178.890  TIME= 2
```

```
0.82833
FIXED DATA =   2566  TEMPORARY DATA =     0  TOTAL=   2566
FIXED AVAIL= 1000000  TEMPORARY AVAIL= 1000000  TOTAL AVAIL= 1000000


 *** STORAGE REQUIREMENT SUMMARY
MAXIMUM FIXED MEMORY USED   =     2566
MAXIMUM TEMPORARY MEMORY USED=       0
MAXIMUM TOTAL MEMORY USED   =     2566
MAXIMUM TEMPORARY AVAILABLE =   997432


 *** ANSYS BINARY FILE STATISTICS
BUFFER SIZE USED= 2048
POST DATA WRITTEN ON FILE12


***** ROUTINE COMPLETED ***** CP =      179.120
 view results on postprocessor
1        ANSYS - ENGINEERING ANALYSIS SYSTEM  REVISION 4.4     A 16  SIMON FRASER UNI
MAY 1,1990
   ANSYS(R)  COPYRIGHT(C) 1971, 1978, 1982, 1983, 1985, 1987, 1989, 1990  SWANSON ANALYSIS
SYSTEMS, INC. AS UNPUBLISHED WORK.
   PROPRIETARY DATA - UNAUTHORIZED USE, DISTRIBUTION OR DUPLICATION IS PROHIBI
TED.  ALL RIGHTS RESERVED.
   FOR SUPPORT CALL CHAO C CHENG     PHONE (604) 291-3820   TWX

ELEMENTS                                          20.8294 NOV  1,1992 CP=   179.290
**UNIVERSITY VERSION FOR EDUCATIONAL PURPOSES ONLY**


      ***** GENERAL GRAPH POSTPROCESSOR (POST26) *****

ALL POST26 SPECIFICATIONS ARE RESET TO INITIAL DEFAULTS

VARIABLE  2 IS  419 UZ

VARIABLE  3 IS  872 UZ

STORAGE COMPLETE FOR     1 DATA POINTS

   SUMMARY OF VARIABLES STORED THIS STEP AND EXTREME VALUES
VARI TYPE  IDENTIFIERS  NAME  MINIMUM   AT TIME   MAXIMUM   AT TIME



***** ROUTINE COMPLETED ***** CP =      179.710

/EOF ENCOUNTERED ON FILE18


PREP7 AFWRITE OR SFWRITE WARNING MESSAGES =  0
NUMBER OF SOLUTION PHASE WARNING MESSAGES =  0
```

LIST OF REFERENCES

[1] K. E. Petersen. "Silicon as a Mechanical Material" Proc. IEEE 70,5 (May 1982): 420-457.

[2] .B. Angell, S.C. Terry and P.W. Barth. "Silicon Micromechanical Devices" Scientific American (April 1983): 44-55.

[3] M. Esashi, S Shoji and A. Nakano. "Normally Closed Microvalve and Micropump Fabricated on a Silicon Wafer" Sensors and Actuators 20 (1989): 163-169.

[4] L.S. Fan, Y.C. Tai and R.S. Muller. "IC- Processed Electrostatic Micromotors" Sensors and Actuators 20 (1989): 41-47.

[5] R. Gannon. "Micromachine Magic" Popular Science (March 1989): 88-92.

[6] L.M. Roylance and J.B. Angell. "A Batch-Fabricated Silicon Accelerometer" IEEE Trans. Electron Devices ED-26,12 (December 1979): 1911-1917.

[7] M.D. Ward and D.A. Buttry. " In Situ Interfacial Mass Detection with Piezoelectric Transducers" Science 249 (August 1990): 1000-1007.

[8] R.A. Buser and N.F. De Rooij. "Resonant Silicon Structures" Sensors and Actuators 17 (1989): 145-154.

[9] T.S.J. Lammerink, and W. Wlodarski. "Integrated Thermally Excited Resonant Diaphragm Pressure Sensor" Proc. Intr. Conf. Solid State Sensors and Actuators (Philadelphia: 1985): 97.

[10] P. Hauptmann. "Resonant Sensors and Applications" Sensors and Actuators 25-27 (1991): 371-377.

[11] R.C. Jaeger, Introduction to Microelectron Fabrication, vol. 5 of Modular Series on Solid State Devices, ed. G.W. Neudeck and R.F. Pierret, New York: Addison-Wesley Publishing Co., 1988.

[12] H. Seidel, L. Csepregi, A. Heuberger, and H. Baumgartel. "Anisotropic Etching of Crystalline Silicon in Alkaline Solutions" J. Electrochem. Soc. 137,11 (November 1990): 3612-3623.

[13] M. Parameswaran. Microelectronic and Micromechanical Sensors and Actuators in CMOS Technology - a Novel Scheme Towards Regularization and Integration, PhD. Thesis, University of Alberta, Canada, (1990).

[14] R.T. Howe and R.S. Muller. "Resonant-Microbridge Vapor Sensor" IEEE Trans. Elect. Devices ED-33,4 (April 1986): 499-506.

[15] W.F. Stokey. "Vibration of System having Distributed Mass and Elasticity" Chap. in Shock and Vibration, 3d ed., ed. C.M. Harris, New York: McGraw-Hill Book Co., 1988.

[16] W.T. Thomson. Theory of Vibration with Applications, 2d ed., Englewood Cliffs: Prentice-Hall Inc., 1981.

[17] W.J. Smith. Modern Optical Engineering New York: McGraw-Hill Book Co., 1966.

[18] R.D. Blevins, Flow-Induced Vibration, 2d ed., New York: Van Nostrand Reinhold, 1990.

[19] M. Parameswaran, L.J. Ristic, K. Chau, A.M. Robinson and W. Allegretto. "CMOS Electrothermal Microactuators" 3rd IEEE Workshop on Electro Micromechanical Systems (February 1990):128-131.

[20] D. Moser, O. Brand, and H. Baltes. "A CMOS Compatible Thermally Excited Silicon Oxide Beam Resonator with Aluminium Mirror" Proc. 1991 Intl. Conf . Solid-State Sensors and Actuators (San Francisco 1991):547-550.

[21] H. Bezzaoui and E. Voges. "Integrated Optics Combined with Micromechanics on Silicon" Sensors and Actuators 29 (1991): 219-223.

[22] F. Rudolf, A. Jornod and P. Bencze. "Silicon Microaccelerometer" Proc. 4th Intl. Conf. Solid State Sensors and Actuators (1987): 395-398.

[23] J.T. Suminto. "A Simple High Performance Piezoresistive Accelerometer" Proc. 1991 Intl. Conf . Solid-State Sensors and Actuators (San Francisco 1991):104-107.

[24] E.S. Kim, J.R. Kim, and R.S. Muller. "Improved IC-Compatible Piezoelectric Microphone and CMOS Process" Proc. 1991 Intl. Conf . Solid-State Sensors and Actuators (San Francisco 1991):270-273.

[25] E. Hecht. Optics 2d ed., Reading: Addison-Wesley Publishing Co., 1987.

[26] S. Prescesky, M. Parameswaran, M. Weber, M. Syrzycki and M.R. Gothe. "CMOS-Silicon Bonding: A hybrid Approach for the Fabrication of Integrated Micromechanical Transducers" Proc. 4th Intl. Forum Asic and Transducer Technology (Leuven: May 1991): 117-128.

[27] X. Wu and W.H. Ko. "A Study of Compensating Corner Undercutting in Anisotropic Etching of (100) Silicon", Proc. 4th Intl. Conf. Solid State Sensors and Actuators (1987): 126-129.

[28] F.P. Beer and E.R. Johnston. Mechanics of Materials New York: McGraw-Hill Book Co., 1981.

[29] M. Parameswaram, S. Prescesky and A. Rawicz, "Micromachining Technology for Sub-Nanogram Discrete Mass Resonant Sensors", Proc. 6th Canadian Semiconductor Technology Conference (Ottawa: August 1992)

[30] K.K. Frame and W. Hu. "Cell Volume Measurement as an Estimation of Mammalian Cell Biomass" Biotechnology and Bioengineering, 36 (1990): 191-197.

[31] D.G. Kilburn, P. Fitzpatrick, B.C. Blake-Coleman, D.J. Clarke and J.B. Griffiths. "On-Line Monitoring of Cell Mass in Mammalian Cell Cultures by Acoustic Densitometry" Biotechnology and Bioengineering, 33 (1989): 1379-1384.

[32] E.B. Becker, G.F. Carey and J.T. Oden, Finite Elements an Introduction Volume 1 Englewood Cliffs: Prentice-Hall Inc., 1981.

[33] P.C. Kohnke, ed. ANSYS Engineering Analysis System Theoretical Manual Houston, Penn.: Swanson Analysis Systems Inc., 1989.